Universidade de São Paulo
Instituto de Física

Viscosidade de cisalhamento anisotrópica e comportamento crítico dos modos quasinormais não-hidrodinâmicos em plasmas fortemente acoplados

Maicon Zaniboni Siqueira

Orientador: Prof. Dr. Jorge José Leite Noronha Junior.

Tese de doutorado apresentada ao Instituto de Física da Universidade de São Paulo para obtenção do título de Doutor em Ciências.

Banca Examinadora:

Prof. Dr. Jorge José Leite Noronha Junior (IFUSP)
Prof. Dr. Fernando Silveira Navarra (IFUSP)
Prof. Dr. Carlos Molina Mendes (IFUSP)
Prof. Dr. Donato Giorgio Torrieri (IFGW)
Prof. Dr. Marcelo Santos Guimarães (IFUERJ)

São Paulo
2017

FICHA CATALOGRÁFICA
Preparada pelo Serviço de Biblioteca e Informação
do Instituto de Física da Universidade de São Paulo

Siqueira, Maicon Zaniboni

Viscosidade de cisalhamento anisotrópica e comportamento crítico dos modos quasinormais não hidrodinâmicos em plasmas fortemente acoplados. São Paulo, 2017.

Tese (Doutorado) – Universidade de São Paulo. Instituto de Física. Depto. Física Experimental.

Orientador(a): Prof. Dr. Jorge José Leite Noronha Junior
Área de Concentração: Física das Partículas Elementares e Campos

Unitermos: 1.Teoria quântica de campo; 2.Cromodinâmica quântica; 3.Colisões de íons pesados relativísticos; 4. Supersimetria; 5.Supergravidade .

USP/IF/SBI-066/2017

University of São Paulo
Institute of Physics

Anisotropic shear viscosity and critical behavior of non-hydrodynamic quasinormal modes in strongly coupled plasmas

Maicon Zaniboni Siqueira

Adviser: Prof. Dr. Jorge José Leite Noronha Junior.

Doctoral thesis presented to the Instituto de Física da Universidade de São Paulo as a requisite to the title of Doctor of Science.

Thesis Committee:

Prof. Dr. Jorge José Leite Noronha Junior (IFUSP)
Prof. Dr. Fernando Silveira Navarra (IFUSP)
Prof. Dr. Carlos Molina Mendes (IFUSP)
Prof. Dr. Donato Giorgio Torrieri (IFGW)
Prof. Dr. Marcelo Santos Guimarães (IFUERJ)

São Paulo
2017

Agradecimentos

Primeiramente, agradeço à minha família pelo amor e suporte. Em especial agradeço à minha mãe, Maria Zaniboni, que com todo seu carinho e amizade teve papel fundamental ao me aconselhar e me apoiar em tempos difíceis. Meu pai, Mario Siqueira, e meu irmão, Mailson Zaniboni, com amizade e bom humor alegram meus dias. E o meu amado felino, Linus, recebe seus agradecimentos, pois desde que apareceu em minha vida melhorou muito meu humor com seu jeitinho meigo e suas brincadeiras.

Agradeço ao meu orientador, Jorge Noronha, pelo profissionalismo e paciência com minhas dificuldades. Sobre seus ombros enxerguei como realmente funciona o mundo acadêmico da física.

Agradeço aos meus colaboradores e amigos Renato Critelli, Rômulo Rougemont, e Stefano Finazzo.

Agradeço aos amigos do Insituto de Física dos quais a amizade não permaneceu apenas no instituto: Riis Rhavia, Rafael Rodrigues (amigo de longa data), Gilson Ronchi, e Natasha Aguero. Aos amigos do GRHAFITE: Luiz de Oliveira, Bruno Moreira, Jorgivan Dias, Diego Spiering, André Giannini, David Fogaça, e Samuel Sanches. E agradeço aos professores desse grupo, pois mostraram suas diferentes perspectivas e opiniões sobre os mais variados assuntos na física: Fernando Navarra, Renato Higa, Marina Nielsen, Manoel Robilotta, e Alberto Martinez.

Um agradecimento especial aos amigos que conheci na saudosa Unicamp que ainda continuam comigo ao longo desses anos todos com muitas partidas de tabuleiro.

Agradeço aos professores que compuseram minha Banca Examinadora apontando correções e fazendo comentários pertinentes.

Por fim agradeço ao suporte financeiro dado pela CAPES de 2012 à 2016. E ao meu pai pelo *paitrocínio* fornecido de 2016 à 2017.

Resumo

Nessa tese usamos a dualidade holográfica calibre/gravidade para estudar dois aspectos diferentes de plasmas não-Abelianos fortemente acoplados. No primeiro tópico estudamos os efeitos de campos magnéticos (Abelianos) intensos sobre o coeficientes de transporte de um plasma não-Abeliano fortemente acoplado. Devido à anisotropia espacial criada pelo campo magnético, o tensor de viscosidade mais geral de um plasma magnetizado deve possuir 5 coeficientes de viscosidade de cisalhamento e 2 de viscosidade volumétrica. Usamos a correspondência holográfica para um plasma $\mathcal{N} = 4$ Supersimétrico de Yang-Mills (SYM) fortemente acoplado para calcular a viscosidade de cisalhamento perpendicular ao campo magnético e a viscosidade de cisalhamento paralela ao campo. Na presença do campo magnético, a viscosidade de cisalhamento perpendicular ao campo satura o limite viscoso de Kovtun-Son-Starinets enquanto que na direção paralela ao campo o limite é violado.

O segundo tópico investigado nessa tese é motivado pelo estudo do comportamento próximo ao equilíbrio de plasmas não-Abelianos fortemente interagentes que exibem um ponto crítico em seus diagramas de fase. Focamos no espectro dos modos quasinormais não-hidrodinâmicos de um plasma $\mathcal{N} = 4$ SYM fortemente acoplado na presença de um potencial químico, que exibe um ponto crítico no equilíbrio. Exceto próximo ao ponto crítico, observamos que ao aumentar o potencial químico geralmente se intensifica a taxa de amortecimento dos modos quasinormais, que levam à redução dos tempos de equilibração característicos do plasma dual fortemente acoplado. Entretanto, aproximando-se do ponto crítico o tempo de equilibração típico aumenta embora sua derivada em relação ao potencial químico diverge com um expoente igual à $-1/2$. Encontramos também um modo não-hidrodinâmico puramente imaginário no canal de difusão vetorial com potencial químico não-nulo que dita o tempo de equilibração neste canal próximo do ponto crítico.

Palavras-chave: dualidade calibre-gravidade, coeficientes de transporte anisotrópicos, ponto crítico, modos quasinormais.

Abstract

In this thesis we use the holographic gauge/gravity duality to study two different aspects of strongly coupled non-Abelian plasmas. In the first topic we study the effects of strong (Abelian) magnetic fields on the transport coefficients of a strongly coupled non-Abelian plasma. Due to the spatial anisotropy created by the magnetic field, the most general viscosity tensor of a magnetized plasma has 5 shear viscosity coefficients and 2 bulk viscosities. We use the holographic correspondence for a strongly coupled $\mathcal{N} = 4$ Supersymmetric Yang-Mills (SYM) plasma to evaluate the shear viscosity perpendicular to the magnetic field and the shear viscosity parallel to the field. In the presence of a magnetic field, the shear viscosity perpendicular to the field saturates the Kovtun-Son-Starinets viscosity bound while in the direction parallel to the field the bound is violated.

The second topic investigated in this thesis is motivated by the study of the near equilibrium behavior of strongly interacting non-Abelian plasmas that display a critical point in their phase diagram. We focus on the spectra of non-hydrodynamic quasinormal modes of a strongly coupled $\mathcal{N} = 4$ SYM plasma in the presence of a chemical potential, which displays a critical point in equilibrium. Except close to the critical point, we observe that by increasing the chemical potential one generally increases the damping rate of the quasinormal modes, which leads to a reduction of the characteristic equilibration times in the dual strongly coupled plasma. However, as one approaches the critical point the typical equilibration time increases though its derivative with respect to the chemical potential diverges with an exponent equal to $-1/2$. We also find a purely imaginary non-hydrodynamical mode in the vector diffusion channel at nonzero chemical potential which dictates the equilibration time in this channel near the critical point.

Keywords: gauge-gravity duality, anisotropic transport coefficients, critical point, quasinormal modes.

List of Figures

List of Tables

Contents

Part I

Motivation

1 Introduction

The new state of matter formed in ultra-relativistic heavy ion collisions (STAR, 2005; PHENIX, 2005; BRAHMS, 2005; PHOBOS, 2005) behaves as a strongly coupled Quark-Gluon Plasma (QGP) (GYULASSY; MCLERRAN, 2005). Perhaps one of its most striking features is its apparent near "perfect" fluid behavior inferred from comparisons of relativistic hydrodynamic calculations to heavy ion data (for a recent review see Heinz and Snellings (2013)). In fact, the experimental data can be reasonably described[1] using very small values of the shear viscosity to entropy density ratio, $\eta/s \sim 0.2$ (HEINZ; SNELLINGS, 2013), which is of the order of the ratio $\eta/s = 1/(4\pi)$ (POLICASTRO; SON; STARINETS, 2001; BUCHEL; LIU, 2004; KOVTUN; SON; STARINETS, 2005) found in a large class of strongly coupled non-Abelian plasmas using the gauge/gravity duality (MALDACENA, 1999; GUBSER; KLEBANOV; POLYAKOV, 1998; WITTEN, 1998a) (see Casalderrey-Solana et al. (2014) for a review that includes applications to heavy ion collisions). Such a small η/s is not really compatible with standard weak coupling QCD results (ARNOLD; MOORE; YAFFE, 2000; ARNOLD; MOORE; YAFFE, 2003) and other mechanisms/models have been tried over the years to explain this ratio (DANIELEWICZ; GYULASSY, 1985; ASAKAWA; BASS; MULLER, 2006; MEYER, 2007; XU; GREINER, 2008; HIDAKA; PISARSKI, 2008; NORONHA-HOSTLER; NORONHA; GREINER, 2009; NORONHA-HOSTLER; NORONHA; GREINER, 2012; ASAKAWA; BASS; MüLLER, 2013; OZVENCHUK et al., 2013). In this aspect, the gauge/gravity duality remains as one of the leading non-perturbative tools suited for calculations of real time properties of strongly coupled non-Abelian plasmas. In this thesis we study how strong magnetic fields and also the presence of a critical point can affect the near equilibrium properties of strongly coupled systems that can be seen as "toy models" for the QGP formed in heavy ion collisions.

Several works have emphasized in recent years that non-central heavy ion collisions (where the ions do not collide "head-on") are not only characterized by a sizable anisotropic flow but also by the presence of very strong electromagnetic fields formed at the early stages of the collisions (KHARZEEV; MCLERRAN; WARRINGA, 2008; FUKUSHIMA; KHARZEEV; WARRINGA, 2008; SKOKOV; ILLARIONOV; TONEEV, 2009; TUCHIN, 2013; DENG; HUANG, 2012; BLOCZYNSKI et al., 2013). This has created a lot of interest on the effects of strong electromagnetic fields in strongly interacting QCD matter (KHARZEEV et al., 2013) and, recently, lattice calculations with physical quark

[1] There are other effects, not included in the analysis of Heinz and Snellings (2013), which can affect the effective value of η/s in the QGP. For instance, there are many transport coefficients in viscous relativistic hydrodynamics (DENICOL et al., 2012) and very little is known about their values and their effects on the anisotropic flow. In fact, it has been recently found that the inclusion of bulk viscosity directly affects estimates of η/s in the QGP (NORONHA-HOSTLER et al., 2013; NORONHA-HOSTLER; NORONHA; GRASSI, 2014; RYU et al., 2015).

masses have determined how a strong external magnetic field changes the thermodynamic properties of the QGP (BALI et al., 2012; BALI et al., 2014). If the magnetic field is still large enough at the time that elliptic flow is building up, it is natural to also consider the effects of strong magnetic fields on the subsequent hydrodynamic expansion of the QGP.

The presence of a magnetic field alters the near equilibrium behavior of charged fluids. For instance, the magnetic field breaks the spatial SO(3) rotational symmetry to a SO(2) invariance about the magnetic field axis and this type of magnetic field-induced anisotropic relativistic hydrodynamics has more transport coefficients than the spatially isotropic case (to distinguish the dynamics along the magnetic field direction from that in the plane orthogonal to the field). In fact, this means that the number of independent transport coefficients in the shear viscosity tensor η_{ijkl} increases from 1 (in the isotropic case) to 5 in the presence of the magnetic field while there are 2 bulk viscosity coefficients (HUANG; SEDRAKIAN; RISCHKE, 2011; LIFSHITZ; PITAEVSKII, 1981; LANDAU et al., 1986; TUCHIN, 2012).

Since one no longer has SO(3) invariance, one may expect that some of the different shear viscosities could violate the universal result $\eta/s = 1/(4\pi)$ valid for isotropic Einstein geometries (BUCHEL; LIU, 2004; KOVTUN; SON; STARINETS, 2005), which would then constitute an example of the violation of the viscosity bound that is of direct relevance to heavy ion collisions. Previous examples involving the violation of the viscosity bound include: anisotropic deformations of $\mathcal{N} = 4$ Super-Yang-Mills (SYM) theory due to a z-dependent axion profile (MATEOS; TRANCANELLI, 2011) computed in Rebhan and Steineder (2012) where $\eta_{\parallel}/s < 1/(4\pi)$ along the direction of anisotropy; anisotropic holographic superfluids with bulk SU(2) non-Abelian fields which present universality deviation for $\eta_{\parallel}/s$ (NATSUUME; OHTA, 2010; ERDMENGER; KERNER; ZELLER, 2011; ERDMENGER; FERNANDEZ; ZELLER, 2013); and a dilaton-driven anisotropic calculation recently shown in Jain et al. (2015). However, we note that the first examples of viscosity bound violation were found in (spatially isotropic) theories with higher order derivatives in the gravity dual action (KATS; PETROV, 2009; BRIGANTE et al., 2008b; BRIGANTE et al., 2008a; BUCHEL; MYERS; SINHA, 2009).

In chapter 4 we evaluate two components of the shear viscosity tensor, namely $\eta_{\perp} \equiv \eta_{xyxy}$ and $\eta_{\parallel} \equiv \eta_{xzxz} = \eta_{yzyz}$, in a strongly coupled non-Abelian plasma in the presence of an external magnetic field using the gauge/gravity duality (other two shear coefficients are identically zero for the theory considered here). These calculations are done using the membrane paradigm (IQBAL; LIU, 2009; THORNE; PRICE; MACDONALD, 1986). The holographic model we consider is simple Einstein gravity (with negative cosmological constant) coupled with a Maxwell field, which corresponds to strongly coupled $\mathcal{N} = 4$ SYM subjected to an external constant and homogeneous magnetic field (D'HOKER; KRAUS, 2010a; D'HOKER; KRAUS, 2009; D'HOKER; KRAUS, 2010b). We examine the

role played by the anisotropy introduced by the external field searching for a violation of the viscosity bound in $\eta_{\parallel}/s$. A study of the behavior of $\eta_{\parallel}/s$ is also of phenomenological interest for the modeling of the strongly coupled QGP under strong magnetic fields.

Another important aspect of the QGP formed in heavy ion collisions involves the possibility of finding effects from a critical point in the QCD phase diagram. Even if there is indeed a critical point in the phase diagram, it is important to remark that the system formed in heavy ion collisions is not in thermodynamic equilibrium — non-equilibrium effects, induced by viscosities, affect the evolution of the system. Therefore, it is interesting to investigate the out-of-equilibrium properties of strongly coupled plasmas that display a critical point when in equilibrium. In this thesis, we use the gauge/gravity duality to initiate the study of this topic via the investigation of the behavior of Quasinormal Modes (QNM's), which are exponentially damped collective excitations (VISHVESHWARA, 1970; DAVIS et al., 1971) that define the characteristic behavior of fluctuations of black holes and black branes (for reviews, see Nollert (1999), Kokkotas and Schmidt (1999), Berti, Cardoso and Starinets (2009), Konoplya and Zhidenko (2011)). The spectra of QNM's collectively describe the linear part of the decaying fluctuations of a disturbed black hole, a phenomenon known as "quasinormal ringing", which is analogous to the decaying sound emitted by a brass bell when struck by a mallet (KAC, 1966). For this reason, QNM's are important in astrophysical and cosmological observations since they describe the ringdown of possible black hole remnants of binary stars and black hole mergers, which were pivotal to the direct detection of gravitational waves in 2016 (LIGO; VIRGO, 2016b; LIGO; VIRGO, 2016a).

In the context of the holographic gauge/gravity duality (MALDACENA, 1999; GUBSER; KLEBANOV; POLYAKOV, 1998; WITTEN, 1998a; WITTEN, 1998b), QNM's associated with the fluctuations of a given bulk field are related to the poles of the retarded Green's function of the dual operator in the quantum field theory (STARINETS, 2002; KOVTUN; STARINETS, 2005). These poles describe hydrodynamic and non-hydrodynamic dispersion relations with which one can not only compute hydrodynamic transport coefficients but also derive upper bounds for characteristic equilibration times of the dual plasma (HOROWITZ; HUBENY, 2000). Additionally, non-hydrodynamic modes (which correspond to collective excitations whose frequency remains nonzero even in homogeneous situations) play an important role in the fate of the hydrodynamic gradient series, as demonstrated by studies in holography (HELLER; JANIK; WITASZCZYK, 2013; BUCHEL; HELLER; NORONHA, 2016) and also in kinetic theory (FLORKOWSKI; RYBLEWSKI; SPALIńSKI, 2016; DENICOL; NORONHA, 2016; HELLER; KURKELA; SPALINSKI, 2016).

Previous works (ALANEN et al., 2011; JANIK; JANKOWSKI; SOLTANPANAHI, 2016a; JANIK; JANKOWSKI; SOLTANPANAHI, 2016b) have dealt with QNM's in

bottom-up Einstein-dilaton constructions (GUBSER; NELLORE, 2008; GUBSER et al., 2008; GÜRSOY et al., 2011; FINAZZO et al., 2015) exhibiting different kinds of phase transitions at zero chemical potential. Additionally, Ref. Buchel, Heller and Myers (2015) investigated the QNM's associated with scalar operators in a top-down $\mathcal{N} = 2^*$ non-conformal plasma also at zero chemical potential. On the other hand, in Rougemont et al. (2016) the QNM's of an external scalar perturbation were investigated in a bottom-up, QCD-like Einstein-Maxwell-dilaton model at finite baryon density. In general, through the holographic correspondence, any question regarding the thermalization process in a given strongly coupled gauge theory necessarily involves a study of the QNM's of its gravity dual. These modes describe different timescales in the gauge theory and, close to a critical point, one may expect that the QNM's of the corresponding gravity dual display critical behavior.

In fact, near a critical point, thermodynamical quantities typically display divergences which enable the definition of critical exponents. Static properties such as single time correlation functions and linear response coefficients to time-independent perturbations display critical behavior which are determined by the underlying equilibrium distribution. However, critical behavior is also observed in many dynamical quantities such as the transport coefficients, which depend on the properties of multi-time correlations functions and are not determined by the information contained in the equilibrium distribution. In fact, while static thermodynamical properties of several different physical systems may be grouped into a few different (static) universality classes, dynamical properties associated with slowly varying hydrodynamical fluctuations of a system near criticality do not fit into this static classification scheme, as discussed in detail in Hohenberg and Halperin (1977) nearly 40 years ago. The dynamic universality classes reviewed in Hohenberg and Halperin (1977) require the study of hydrodynamic modes, i.e., collective excitations whose frequency vanishes in the case of homogeneous disturbances. While these modes dominate the long time behavior of the system (since they are associated with conserved currents) and can be used to study how transport coefficients (such as the shear viscosity) behave near a critical point, there is much more information about dynamical critical phenomena in multi-time correlation functions that cannot be obtained from their zero frequency limit.

In chapter 5 we initiate the investigation of the critical behavior displayed by non-hydrodynamic modes in strongly coupled gauge theories with gravity duals. This novel type of critical phenomena determines the behavior of different characteristic equilibration times of the system at zero wavenumber and, since these QNM's are not directly associated with conserved currents, their behavior at criticality does not follow from the analysis made in Ref. Hohenberg and Halperin (1977). In this thesis, as the first exploration in this new arena, we compute QNM's for an external scalar perturbation and also for the diffusion channel associated with a vector perturbation in the so-called 1-R charge black

hole (1RCBH) model (GUBSER, 1999; BEHRNDT; CVETIC; SABRA, 1999; KRAUS; LARSEN; TRIVEDI, 1999; CAI; SOH, 1999; CVETIC; GUBSER, 1999a; CVETIC; GUBSER, 1999b). This is an analytical top-down construction obtained from $(4+1)$-dimensional maximally supersymmetric gauged supergravity, which is holographically dual to a strongly coupled $\mathcal{N}=4$ SYM plasma in flat $(3+1)$ dimensions with a finite chemical potential under a U(1) subgroup of the global SU(4) symmetry of R-charges. This theory is conformal and its phase diagram is a function of a single dimensionless ratio μ/T, where μ and T are the U(1) R-charge chemical potential and temperature of the black brane background, respectively. The model has a very simple phase diagram with a critical point at $\mu/T=\pi/\sqrt{2}$ and its static critical exponents were computed in Maeda, Natsuume and Okamura (2008) and Buchel (2010). Also, the fact that the R-charge conductivity remains finite at the critical point (MAEDA; NATSUUME; OKAMURA, 2008) shows that this model belongs to the type B dynamical universality class (HOHENBERG; HALPERIN, 1977) and the anomalous static critical exponent was found to vanish in Buchel (2010). Thus, this model is of mean-field type (BUCHEL, 2010), which was later argued (NATSUUME; OKAMURA, 2011) to be a general consequence of the underlying large N_c approximation.

This simple model provides a useful arena for investigating dynamical phenomena in a strongly coupled plasma at finite temperature and density, even though it does not possess the full set of physical properties (such as chiral symmetry) displayed by the real world quark-gluon plasma (QGP) (ROUGEMONT, 2016). In fact, such a model may be useful for discovering new dynamical phenomena associated with critical endpoints in strongly coupled non-Abelian plasmas which could be further investigated in more realistic models of the QGP such as Rougemont et al. (2016), Rougemont, Noronha and Noronha-Hostler (2015), with a view towards applications to the ongoing beam energy scan program at RHIC. Other studies of critical phenomena in holography include Refs. Buchel (2009), Buchel and Pagnutti (2010), Buchel and Pagnutti (2011), DeWolfe, Gubser and Rosen (2011a), Cai, He and Li (2012).

As we are going to show in chapter 5, the real and imaginary parts of non-hydrodynamical modes in the external scalar and vector diffusion channels display an infinite slope at the critical point of the phase diagram of the 1RCBH model. This is true also for higher order QNM's, showing that high frequency modes are also sensitive to the presence of the critical point. In particular, from the imaginary part of the QNM's it is possible to extract the behavior of different characteristic equilibration times in the finite density plasma at criticality (at zero wavenumber) and define a dynamical critical exponent associated with their derivatives with respect to the dimensionless ratio μ/T. We find the same critical exponent $1/2$ for all the equilibration times investigated in the different channels.

By increasing the chemical potential one generally increases the damping of the quasinormal black brane oscillations which, consequently, leads to a reduction of the characteristic equilibration times of the dual plasma. However, as the critical point is approached these equilibration times increase and they acquire an infinite slope. When $\mu/T \sim 2$ is taken towards its critical value (given by $\pi/\sqrt{2}$), a purely imaginary, non-hydrodynamical mode appears in the vector diffusion channel at nonzero chemical potential and zero wavenumber which defines the critical behavior of the equilibration time in this channel (we remark that such a mode was also found in Ref. Janiszewski and Kaminski (2016) in the context of a $(4+1)$-dimensional Einstein-Maxwell model without a chemical potential, though in the presence of a magnetic field).

This thesis is organized as follows. In the introductory part in chapter 2, we briefly review some properties of quantum chromodynamics and the relevant features displayed by the quark-gluon plasma that served as motivation for this thesis. We also include in section 2.4 a discussion about linear response theory to illustrate in a simple manner how Kubo-like formulas for transport coefficients may be obtained. Since there are by now many authoritative books about the gauge/gravity duality and its applications, see for instance Nastase (2015), Ammon and Erdmenger (2015), in this thesis we decided to focus on the work we have done using the duality and provide to the reader only a quick introduction to this topic in chapter 3. As mentioned above, the main results of this thesis are shown in chapter 4 and chapter 5. We finish this work in chapter 6 with our conclusions and outlook. We use natural units where $\hbar = c = k_B = 1$ and a mostly plus metric signature.

2 Basic aspects about quantum chromodynamics, the quark-gluon plasma, and linear response theory

2.1 Standard Model

After several decades of observation and theoretical investigations, the different stages of the evolution of the Universe can be understood using the standard model of cosmology (WEINBERG, 2008). This is a mathematical formulation of the Big Bang model in which the Universe has a cosmological constant, and is the simplest model that reasonably accounts for the cosmic microwave background, the Big Bang nucleosynthesis, and the large-scale structure in the distribution of galaxies which are accelerated moving away from each other. The observations collected over years were able to quantify the energy content of the Universe (WMAP, 2013) see Figure 1, which shows that only 4.6% is constituted of ordinary matter composed of protons, neutrons, and electrons. This small fraction of the Universe has many properties which today are mathematically understood using the Standard Model of Particle Physics (PESKIN; SCHROEDER, 1995).

Figure 1 – Energy content of the Universe: only 4.6% is ordinary matter (e.g. protons, neutrons and electrons), a greater fraction, 24% of the universe, is constituted by dark matter which interacts only gravitationally and the biggest fraction, 71.4%, is called dark energy, which is the source for the accelerated expansion of the universe.

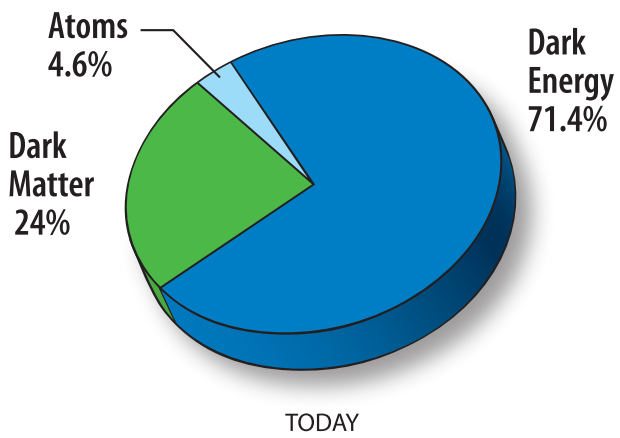

Source – NASA/WMAP Science Team (2013).

The Standard Model of Particle Physics describes the fundamental forces in nature

(except for gravity), which can be understood via the interactions between all elementary particles modeled mathematically by quantum field theory. These elementary particles are, in principle, indivisible and may be classified in two groups concerning their statistical properties. The first group of particles defines the so-called fermions (a name coined by Paul Dirac from the surname of physicist Enrico Fermi), which display Fermi-Dirac statistics and also obey the Pauli exclusion principle (the fermions in the Standard Model have spin 1/2). The second group has Bose-Einstein statistics, being called bosons (a name also coined by Paul Dirac from the surname of physicist Satyendra Nath Bose) and have spin 0 or 1 depending on the type of boson.

The fundamental forces in nature are the electromagnetic force, the weak force, and the strong force[1]. Fermions in the Standard Model are classified in two sectors according to its interaction via the strong force. Leptons belong to one of these sectors and do not interact via the strong force but they interact via the weak and electromagnetic forces. There are 6 types of leptons: electron (e), muon (μ), tau (τ), electron neutrino (ν_e), muon neutrino (ν_μ), and tau neutrino (ν_τ). On the other sector one finds the quarks and they interact via the strong force (and, since they carry also electric charge, they also interact via the electromagnetic force). There are 6 types (so-called flavors) of quarks: up (u), down (d), charm (c), strange (s), top (t), and bottom (b).

Furthermore, to complete the list of particles in the Standard Model, one finds the gauge bosons, sometimes called "force carriers", and also the Higgs particle (scalar boson). Gauge bosons have spin 1 and there are 3 types of gauge bosons[2]: the carrier of the strong force, the gluon (g), the electromagnetic force carrier, the photon (γ), and the carriers of the weak force, $W^{\pm}$ and Z bosons. The Higgs boson is the only particle with spin 0 in the Standard Model (assuming that this particle is indeed fundamental, not being composed of other yet unknown particles). The respective masses, spins, and electrical charges of the fermions and bosons are shown in Figure 2a while in Figure 2b we see the possible interactions between the elementary particles.

The quark sector and the gluons share an intrinsic property that other particles do not, they possess the so-called color charge (PESKIN; SCHROEDER, 1995). This property can be, by analogy with the electric charge in electromagnetism, either "positive" in which one just refers to it as color or "negative", namely anticolor. In the Standard Model, there are three possible colors: red, green, and blue; and, thus, three possible anticolors: antired, antigreen, and antiblue. Each quark carries only one color, and a gluon carries, simultaneously, both a color and a different anticolor. Besides that, quantum field theory predicts the existence of an antiparticle for each particle in the Standard Model, that is, a similar picture of Figure 2a where the the masses and spins are the same but

[1] The gravitational force, described by General Relativity (CARROLL, 2004), is not included in the Standard Model.

[2] It is expected that carrier of the gravitational force, the graviton, is a gauge boson with spin 2.

Figure 2 – Standard Model of Particle Physics: the 12 fundamental fermions (quarks and leptons), 4 fundamental gauge bosons and 1 scalar boson (Higgs boson). The values currently depicted in (a) are from Ref. Particle Data Group (2012) (see also the PDG website: <http://pdg.lbl.gov/>). A diagram summarizing the interactions between elementary particles according to the Standard Model are shown in (b). Dark circles/ovals represent types of particles (bosons are circles and fermions are ovals) and the blue arcs represent the possible interactions among them.

(a) Mass, spin, and charge.

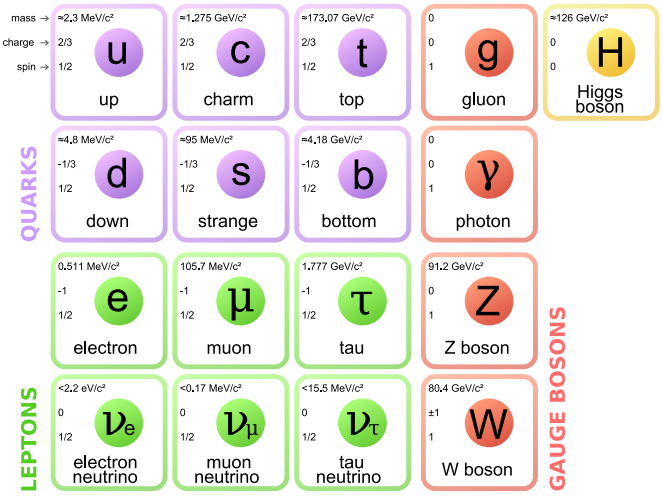

Source Wikipedia (2013).

(b) Interactions.

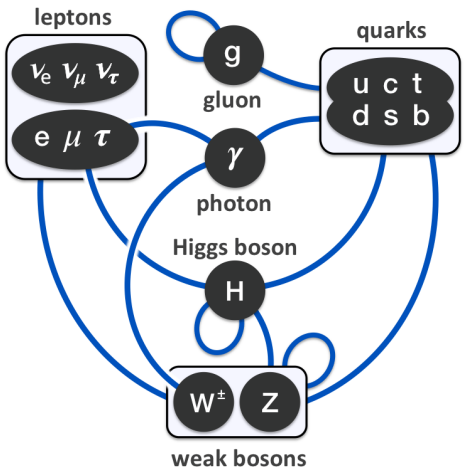

Source Wikipedia (2014).

with opposite electric charge and color charge. Then the antiparticle of a quark with given color is called an antiquark which possesses anticolor.

Elementary particles are subject to *color confinement* (PESKIN; SCHROEDER, 1995), a non-perturbative phenomenon that dictates that any observable must be "colorless", a feature achieved when either all three different colors (or all three different anticolors) are included, or when a color and the same anticolor are present[3]. The consequence of color confinement is the binding, via the strong force, of a color charged particle together with other color charged particles yielding a colorless object, which physically means one cannot observe a free quark nor a free gluon.

These clumps of color charged particles are called hadrons: subatomic particles formed by quarks and antiquarks held together, primarily, by the strong force via the exchange of gluons. Hadrons are classified according to their *baryonic* quantum number $\mathcal{B} = \frac{1}{3}(n_{\mathrm{q}} - n_{\bar{\mathrm{q}}})$, where n_{q} is the number of quarks present in this hadron and $n_{\bar{\mathrm{q}}}$ is the number of antiquarks. The baryonic number must be an integer and also a conserved quantum number when a reaction between hadrons happens. If $\mathcal{B} = 0$ the hadron is called a meson. One way to achieve this is, for instance, by binding a quark and an antiquark

[3] Elementary particles with no color charge are, by definition, colorless, e.g., the electron.

in such a way that the system becomes colorless, e.g., the pion. Another way involves binding two quarks and two antiquarks forming a hadron called tetraquark which, again, is constrained to be colorless. If $\mathcal{B} = 1$ the bound state of quarks and gluons is simply called a baryon (for instance, the proton and the neutron). It is possible also to form other more exotic states if one adds to these three quarks a colorless combination of a quark and an antiquark, which gives a baryon called the pentaquark, e.g. P_c^+. If $\mathcal{B} = -1$ we have an antibaryon, which can be constructed by exchanging quarks with antiquarks (and vice-versa) from a given baryon.

After this brief introduction to the Standard Model, we now discuss in more detail below some of the important features of QCD.

2.2 Quantum Chromodynamics

Consider a non-Abelian gauge theory with symmetry group $\mathrm{SU}(N_c)$, where N_c is the number of colors, and N_f different fermionic flavors in the fundamental representation. The gauge invariant Lagrangian density is (PESKIN; SCHROEDER, 1995)

$$\mathcal{L} = \sum_{f=1}^{N_f} \bar{\psi}_{f,i}(i\not{D}_{ij} - m_f\delta_{ij})\psi_{f,j} - \frac{1}{4}G^a_{\mu\nu}G^{a\mu\nu}, \tag{2.1}$$

where δ_{ij} is the Kronecker delta in color space, and the latin and greek indices are summed implicitly following Einstein's summation convention, except for the index f where the summation is explicit. In this Lagrangian there are N_f flavors and $N_c^2 - 1$ types of gluons. A quark with flavor f has mass m_f and carries a color i from a total of N_c colors. The quarks with these specific features are represented by a quark spinor field, $\psi_{f,i}$. Each type of gluon is labeled by a, from the total set of $N_c^2 - 1$ possibilities, and the gluon field transforms in the adjoint representation of $\mathrm{SU}(N_c)$. Gluons are represented by the gluon field A^a_μ which is related to the gluon rank-2 field strength tensor,

$$G^a_{\mu\nu} = \partial_\mu A^a_\nu - \partial_\nu A^a_\mu + g f^{abc} A^b_\mu A^c_\nu, \tag{2.2}$$

where the greek indices indicate tensorial notation for a four-dimensional spacetime. The coupling constant of this theory is g which, along with the quark masses m_f, is subject to renormalization (PESKIN; SCHROEDER, 1995). Moreover, the quantities f^{abc} are the structure constants of $\mathrm{SU}(N_c)$ satisfying $[T^a, T^b] = if^{abc}T^c$. Finally, the interaction between quarks and gluons is described by the covariant derivative (we use Feynman's slash notation, $\not{D} = \gamma^\mu D_\mu$ where γ^μ are the so-called gamma matrices) defined as

$$D_\mu = \partial_\mu + igT^a A^a_\mu. \tag{2.3}$$

The local gauge invariance in Equation 2.1 has the symmetry group $\mathrm{SU}(N_c)$, where any element, $V(x)$, of this group in the fundamental representation can be written as

$V(x) = \exp(ig\alpha^a(x)T^a)$ for $\alpha^a(x)$ defined in 4-dimensional spacetime. Let the quark field with all color components be defined as

$$\psi_f = \begin{pmatrix} \psi_{f,1} \\ \psi_{f,2} \\ \vdots \\ \psi_{f,N_c} \end{pmatrix}, \tag{2.4}$$

then if we take the gauged quark field to be $\psi'_f = V\psi_f$ and substitute it in the operator $\bar{\psi}_f\psi_f$, it remains invariant, i.e. $\bar{\psi}'_f\psi'_f = \bar{\psi}_f\psi_f$. Also from the covariant derivative in Equation 2.3, one concludes that after a gauge transformation the gluon field satisfies

$$A'^a_\mu T^a = V\left(A^a_\mu T^a + \frac{i}{g}\partial_\mu\right)V^\dagger. \tag{2.5}$$

Besides the local symmetry group $\mathrm{SU}(N_c)$, Equation 2.1 also has a U(1) global symmetry, $V = \exp(i\alpha)$ where α is a global phase. The conserved charge resulting from this U(1) symmetry is the baryonic number $\mathcal{B}$, which was discussed above. Also, if we take $m_f = 0$ for all flavors, we obtain new symmetries, the global axial U(1) symmetry given by $V = \exp(i\gamma_5\alpha)$, and the global chiral symmetry $\mathrm{SU_L}(N_f)\times\mathrm{SU_R}(N_f)$, where the subscripts L and R stand for left-handed and right-handed fermions, respectively. In the former, each group acts on the respective chiral quark field separately.

When $N_c = 3$ and $N_f = 6$ this theory is called QCD, which is the quantum field theory that mathematically describes the fundamental strong force that governs the dynamics of quarks and gluons in the Standard Model as described before. Color confinement, as discussed previously, is believed to be a consequence of QCD, although no mathematical proof of that exists yet.

Furthermore, the coupling constant g of QCD, present in the covariant derivative and in the gluon field strength tensor, is subject to renormalization (PESKIN; SCHROEDER, 1995). This roughly means that in this quantum field theory the coupling depends on the scale of the process that is being investigated. For $N_c = 3$ and $N_f = 3$ (massless) quarks one finds the following expression at 1-loop order

$$g(\mu) = \frac{(4\pi)^3}{7}\frac{1}{\ln(\frac{\mu^2}{\Lambda^2})}, \tag{2.6}$$

where μ is an energy scale and $\Lambda \sim 200$ MeV (comparable to the mass of a pion) indicates the typical energy scale for strong interactions. This shows that the beta function in QCD is $\beta(g) = \mu dg/\mu < 0$, the hallmark of asymptotic freedom (see (PESKIN; SCHROEDER, 1995)). However, note that the formula for the running of the coupling shown above is only valid when $\mu \gg \Lambda$. When this is not the case and the renormalization scale μ is taken to be close to Λ, the coupling constant becomes large. This defines the non-perturbative

regime of the theory within which the physics of color confinement and spontaneous chiral symmetry breaking take place. In this strong coupling regime, weak coupling perturbation theory methods are not applicable and other non-perturbative techniques, such as lattice QCD (GATTRINGER; LANG, 2010), must be employed.

On the other hand, for a comparison, in Quantum Electrodynamics (QED) the beta function is positive, which means that the electromagnetic coupling constant becomes large when evaluated at large energy scales - the opposite of the strong coupling constant. In practice, for any energy that we can probe directly in current particle physics collider experiments the QED coupling constant remains sufficiently small and perturbation theory may be used.

2.3 Quark-gluon plasma

Microseconds after the Big Bang (WEINBERG, 2008), the Universe was filled with an exotic state of matter called the quark-gluon plasma. In this type of matter, quarks and gluons are not confined into hadrons and they can become the main degrees of freedom. Nowadays, the QGP is being recreated in ultrarelativistic heavy ion collisions that take place at the Relativistic Heavy Ion Collider (RHIC) at the Brookhaven National Laboratory in NY, USA, and also at the Large Hadron Collider (LHC) at CERN in Geneva.

In the proton-proton collisions at the LHC each proton beam carries around 10^{11} protons being squeezed down to 64 µm (in comparison, the human hair is 50 µm thick) at the interaction point in order to increase the chances of collision (CERN, 2008). Although there is an enormously number of protons, only an average of 20 collisions happens per crossing. The remaining intact protons continue circulating the LHC ring when the two beams meet each other again at the interaction point and this process repeats again and so on, being able to last for 10 to 20 hours. Since these protons are ultra-relativistic[4], i.e. accelerated to high energies around 7 TeV, then, at the start of a fill with nominal current, they obtain peak crossing rates of 40 MHz, which means that around 6×10^8 collisions occur per second (bypassing the small number of collisions per crossing). On the other hand, in collisions among heavy nuclei many interactions happen and the system produced is much more involved than that formed in typical proton-proton collisions.

Such processes involving ultrarelativistic heavy ion collisions produce a QGP defined at high temperature and (relatively small) baryon density. By comparisons of heavy ion collision data and hydrodynamic simulations (HEINZ; SNELLINGS, 2013), one may obtain that the temperatures achieved in these collisions can be as large as ~ 300 MeV, which corresponds to $\sim 4 \times 10^{12}$ K. After the initial collisions among heavy ions take place, the

[4] Around 99.999999% of the speed of light.

hot and dense deconfined matter composed of quarks and gluons expands and cools down. When the temperature is similar to the pion mass $T \sim 140$ MeV (HEINZ, 2004), the system eventually hadronizes forming a hadron gas which will evolve in space and time until its interactions cease (due to the very large mean free path) and the final hadrons are measured by the particle detectors.

Figure 3 – QCD phase diagram

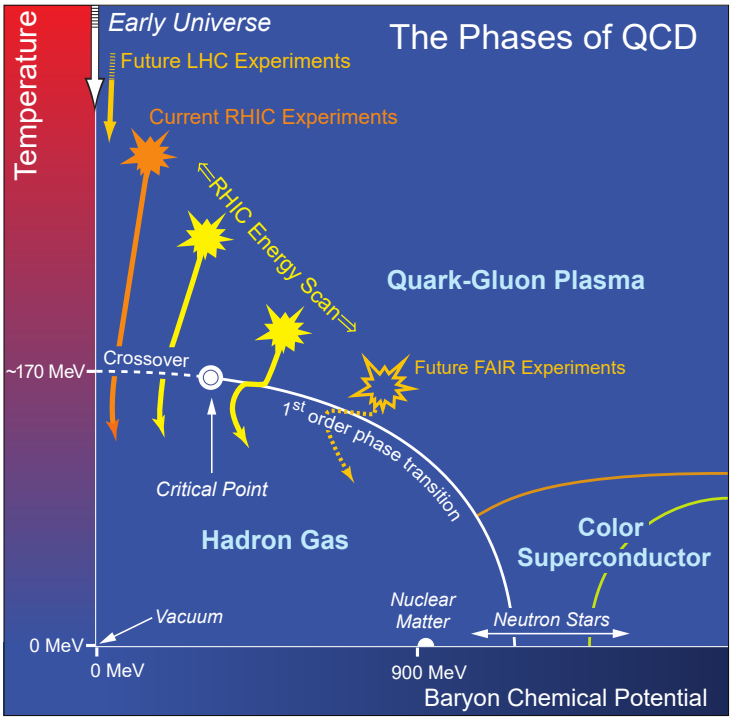

Source – DOE/NSF NSAC (2007, p. 46).

In Figure 3 we see a cartoon of the different phases of QCD phase diagram in the T and baryon chemical potential plane. There are basically three main phases, the QGP phase, the hadronic phase, and the color superconducting phase (RISCHKE, 2004). The QGP phase occurs at high temperatures while normal nuclear matter can be found within the hadron phase. The color superconducting phase only occurs at very large baryon densities and small temperatures and it may be relevant for the physics of compact stars (RISCHKE, 2004). One can see that this phase diagram includes a critical endpoint, which defines the end of a first-order transition line towards a crossover at small chemical potential. The only part of this phase diagram that has been directly confirmed by ab initio QCD calculations on the lattice is the crossover region (AOKI et al., 2006). In this region, there is no real phase transition and the thermodynamic quantities vary rapidly but smoothly as shown in Figure 4. One can see that the entropy density found on the lattice changes smoothly from the low temperature hadronic phase to a high temperature QGP phase but no latent heat (characteristic of a 1st order phase transition) is found.

At first, due to the asymptotic freedom property of QCD, it was hoped that the

Figure 4 – Normalized entropy density, s/T^3, evaluated by lattice QCD with $N_f = 2+1$, as a function of the temperature T, asymptotically approaching the non-interacting (Stefan-Boltzmann) limit indicated in the graph by an arrow for large T.

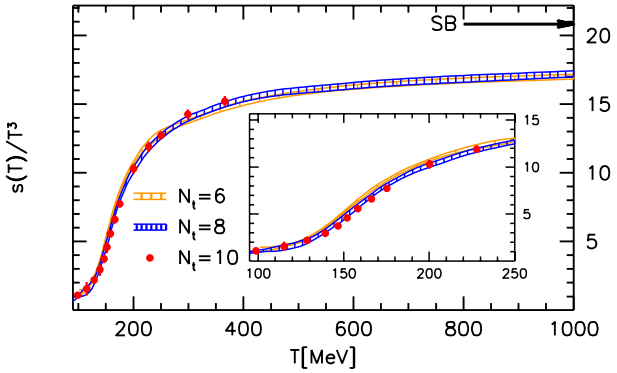

Source – Borsányi et al. (2010, p. 17).

QGP formed in heavy ion collisions could be described using weak coupling techniques. This turned out to not be the case. For instance, one can see in Figure 4 that for the typical temperatures produced in heavy ion collisions, between 100 and 400 MeV, the entropy density of the plasma is very different than its non-interacting limit (given by a simple gas of free quarks and gluons). This already suggests that the QGP formed in heavy ion collisions is in the strong coupling regime of QCD.

Another important development was the finding that the QGP behaves as a nearly perfect fluid (for a recent review see (HEINZ; SNELLINGS, 2013)) in which the ratio between the shear viscosity, η, and the entropy density, s, is in the ballpark of $1/(4\pi)$, the value for this ratio obtained by (POLICASTRO; SON; STARINETS, 2001; BUCHEL; LIU, 2004; KOVTUN; SON; STARINETS, 2005) in a large class of strongly coupled non-Abelian plasmas using the gauge/gravity duality (MALDACENA, 1999; GUBSER; KLEBANOV; POLYAKOV, 1998; WITTEN, 1998a) (see (CASALDERREY-SOLANA et al., 2014) for references that include applications of these ideas to heavy ion collisions). If the QGP were weakly coupled, such as dilute gas of quarks and gluons as naively suggested by asymptotic freedom arguments, η/s would be at least an order of magnitude larger, as shown by (ARNOLD; MOORE; YAFFE, 2000; ARNOLD; MOORE; YAFFE, 2003). Rather, the QGP behaves as a strongly coupled plasma. As will be shown later in this thesis, η is a transport coefficient that measures the near equilibrium properties of the system and is defined by a Kubo formula that involves a real time correlator. Therefore, this quantity cannot be computed yet on the lattice (where only Euclidean correlators can be done) (MEYER, 2011) and other type of strong coupling techniques must be used.

In this thesis, we will use the fact that holography generally gives a very small value for the η/s ratio, which is compatible with current estimates for the QGP coming from heavy ion collisions, to motivate the application of gauge/gravity ideas to understand some

key aspects of the near equilibrium behavior of the QGP. For the sake of completeness, in the next section we will review the general concepts behind linear response theory, which is used to define the transport coefficients discussed in this thesis.

2.4 Review about linear response theory

In this section we review the basic ideas behind linear response theory (KAPUSTA; GALE, 2011). We describe how an output obtained from an ensemble may vary in time when a small external force perturbs the system. If we isolate an ensemble from the rest of the universe and give to it enough time to relax and achieve thermodynamical equilibrium, then the time-independent Hamiltonian in the Schrödinger picture describing this system will be H_0. Consider that an external force starts acting on the ensemble at time $t = t_0$ in such a way that the source of this force, which is a time-dependent source field $J(t, \mathbf{x})$, couples to one of the several operators that may be used to characterize this system. The so-called "external Hamiltonian" describing such an interaction is the time-dependent operator $H_{\text{ext}}(t)$, which is also in Schrödinger picture and is constrained to $H_{\text{ext}}(t < t_0) = 0$. Therefore, by the superposition principle, the Hamiltonian describing this system for times $t \geq t_0$ is

$$H(t) = H_0 + H_{\text{ext}}(t). \tag{2.7}$$

Knowing the above form of the Hamiltonian, the next step to achieve our goal is to solve the Schrödinger equation of motion for the time evolution operator $U(t, t_0)$,

$$\frac{\partial U(t, t_0)}{\partial t} = -iH(t)U(t, t_0), \tag{2.8}$$

where the initial condition is $U(t_0, t_0) = 1$. Unfortunately, there is no general exact solution for the equation above (unlike the simple case where the Hamiltonian is time-independent). So we limit ourselves to consider small perturbations of the system, which is actually our objective since the beginning of this section.

Let $H_{\text{ext}}(t) = \lambda H_1(t)$ where $\lambda > 0$ is the coupling constant taken to be sufficiently small so perturbation theory may be used[5], and $H_1(t)$ does not depend on λ. The Hamiltonian now takes the exact form

$$H(t) = H_0 + \lambda H_1(t). \tag{2.9}$$

Since λ is small, we can expand $U(t, t_0)$ in a power series for a defined set of values in λ that makes the convergence of this series valid, then

$$U(t, t_0) = \sum_{n=0}^{\infty} \lambda^n U_n(t, t_0). \tag{2.10}$$

[5] What really defines mathematically the smallness of the coupling constant is the radius of convergence of the power series expansion around $\lambda = 0$ for the time evolution operator. Therefore, for simplicity, we simply admit that λ satisfies the condition of convergence and proceed with the computations.

The initial condition for the evolution operator constrains each coefficient of this power series to

$$U_0(t_0, t_0) = 1, \text{ and } U_{n\geq 1}(t_0, t_0) = 0. \tag{2.11}$$

Substituting Equation 2.9 and Equation 2.10 into Schrödinger's equation of motion given by Equation 2.8, we obtain

$$\sum_{n=0}^{\infty} \lambda^n \frac{\partial U_n(t, t_0)}{\partial t} = -iH_0 U_0(t, t_0) - i \sum_{n=1}^{\infty} \lambda^n \Big(H_1(t) U_{n-1}(t, t_0) + H_0 U_n(t, t_0) \Big). \tag{2.12}$$

From now on terms with λ^2 and higher will be neglected (even if we know their explicit form), which is the greatest virtue of perturbation theory: to be able to truncate our power series expansion at a chosen order without losing most of the predictive power. Equating the coefficients order by order in λ for the series in Equation 2.12 we obtain the following equations of motion

$$\begin{aligned} \frac{\partial U_0(t, t_0)}{\partial t} &= -iH_0 U_0(t, t_0), \\ \frac{\partial U_1(t, t_0)}{\partial t} &= -iH_1(t) U_0(t, t_0) - iH_0 U_1(t, t_0). \end{aligned} \tag{2.13}$$

The zeroth-order equation above is well-known and its solution is

$$U_0(t, t_0) = e^{-iH_0(t-t_0)}, \tag{2.14}$$

and one can readily check that $U_0(t_0, t_0) = 1$. The first-order equation has the same structure of the zeroth-order one but with a remainder function, $-iH_1(t)U_0(t, t_0)$. Its solution is exact and pretty similar to the one-dimensional case,

$$U_1(t, t_0) = -ie^{-iH_0(t-t_0)} \int_{t_0}^{t} \mathrm{d}t' e^{iH_0(t'-t_0)} H_1(t') e^{-iH_0(t'-t_0)}, \tag{2.15}$$

where $U_1(t_0, t_0) = 0$. For simplicity, we use the Heisenberg picture defined using the unperturbed system for $H_1(t)$, then

$$U_1(t, t_0) = -ie^{-iH_0(t-t_0)} \int_{t_0}^{t} \mathrm{d}t' H_1^{\mathrm{H}}(t'), \tag{2.16}$$

where $H_1^{\mathrm{H}}(t) = e^{iH_0(t-t_0)} H_1(t) e^{-iH_0(t-t_0)}$.

The next step is to obtain the time evolution for the density matrix, ρ, of the ensemble under the influence of a small external force,

$$\rho(t) = U(t, t_0)\rho(t_0)U^{\dagger}(t, t_0). \tag{2.17}$$

We can also expand $\rho(t)$ in a power series to find

$$\rho(t) = \sum_{n=0}^{\infty} \lambda^n \rho_n(t), \tag{2.18}$$

where the coefficient of each power is

$$\rho_0(t_0) = \rho(t_0), \text{ and } \rho_{n\geq 1}(t_0) = 0. \tag{2.19}$$

Now we substitute Equation 2.10 and Equation 2.18 into Equation 2.17 and equate the coefficients order by order in λ to obtain

$$\begin{aligned} \rho_0(t) &= U_0(t,t_0)\rho(t_0)U_0^\dagger(t,t_0), \\ \rho_1(t) &= U_0(t,t_0)\rho(t_0)U_1^\dagger(t,t_0) + U_1(t,t_0)\rho(t_0)U_0^\dagger(t,t_0), \end{aligned} \tag{2.20}$$

where higher order coefficients are neglected as we said before. Substituting Equation 2.14 and Equation 2.16 into Equation 2.20 we obtain

$$\begin{aligned} \rho_0(t) &= e^{-iH_0(t-t_0)}\rho(t_0)e^{iH_0(t-t_0)}, \\ \rho_1(t) &= ie^{-iH_0(t-t_0)}\int_{t_0}^{t} \mathrm{d}t'[\rho(t_0), H_1^{\mathrm{H}}(t')]e^{iH_0(t-t_0)}. \end{aligned} \tag{2.21}$$

Density matrices have in their definition a set of enumerable states and in our case we consider thermal states,

$$\rho(t) = C\exp\left[-\beta\left(H(t) - \sum_i \mu_i N_i\right)\right], \tag{2.22}$$

where β is inversely proportional to the temperature of the system, the subscript i indicates the type of conserved charge in question, μ_i is the chemical potential, N_i is number operator, and C is a normalization constant. The eigenstates of this matrix are thermal states of the form $|E_k(t), \{n_i(t)\}\rangle$, where $E_k(t)$ is the eigenvalue (energy) of the Hamiltonian $H(t)$, and $n_i(t)$ is the eigenvalue (number of particles of type i) of the operator N_i. As we have said above these eigenstates are enumerable and therefore they support a well-defined trace operation. From Equation 2.17 we obtain a constant of motion,

$$\begin{aligned} \mathrm{Tr}\,\rho(t) &= \mathrm{Tr}\,U(t,t_0)\rho(t_0)U^\dagger(t,t_0), \\ &= \mathrm{Tr}\,\rho(t_0)U^\dagger(t,t_0)U(t,t_0), \\ &= \mathrm{Tr}\,\rho(t_0), \end{aligned} \tag{2.23}$$

where both the cyclic property of the trace and also the unitary property of the evolution operator, i.e. $U^\dagger(t,t_0)U(t,t_0) = 1$, were used. Here we are free to choose the normalization condition $\mathrm{Tr}\,\rho(t_0) = 1$, thus

$$C = \frac{1}{\mathrm{Tr}\exp\left[-\beta\left(H(t) - \sum_i \mu_i N_i\right)\right]}. \tag{2.24}$$

After this last step we are ready to compute outputs at different times and compare them to the unperturbed system, which allows us to obtain the effects of the external force.

Let the observable $A(t,\mathbf{x})$ be a time-dependent field operator in Schrödinger picture, then its average over a statistical ensemble at a given time, t, and given point in space, $\mathbf{x}$, is

$$\langle A(t,\mathbf{x})\rangle = \frac{\operatorname{Tr}\rho(t)A(t,\mathbf{x})}{\operatorname{Tr}\rho(t)}. \tag{2.25}$$

We can make an expansion in power series for this statistical average too,

$$\langle A(t,\mathbf{x})\rangle = \sum_{n=0}^{\infty}\lambda^n\langle A(t,\mathbf{x})\rangle_n, \tag{2.26}$$

where the constrains are

$$\langle A(t_0,\mathbf{x})\rangle_0 = \langle A(t_0,\mathbf{x})\rangle, \text{ and } \langle A(t_0,\mathbf{x})\rangle_{n\geq 1} = 0. \tag{2.27}$$

The term $\langle A(t,\mathbf{x})\rangle_0$ is the statistical average over the unperturbed ensemble, and we will use this term to compute

$$\delta\langle A(t,\mathbf{x})\rangle \equiv \langle A(t,\mathbf{x})\rangle - \langle A(t,\mathbf{x})\rangle_0. \tag{2.28}$$

Substituting Equation 2.18 and Equation 2.26 into Equation 2.25, and equating the coefficients order by order in λ we obtain

$$\begin{aligned}\langle A(t,\mathbf{x})\rangle_1 &= \operatorname{Tr}\rho_1(t)A(t,\mathbf{x}),\\ &= i\operatorname{Tr}e^{-iH_0(t-t_0)}\int_{t_0}^{t}\mathrm{d}t'[\rho(t_0),H_1^{\mathrm{H}}(t')]e^{iH_0(t-t_0)}A(t,\mathbf{x}),\\ &= i\int_{t_0}^{t}\mathrm{d}t'\operatorname{Tr}\rho(t_0)[H_1^{\mathrm{H}}(t'),A^{\mathrm{H}}(t,\mathbf{x})],\end{aligned} \tag{2.29}$$

where we have used again the Heisenberg picture for the field observable cited above, $A^{\mathrm{H}}(t,\mathbf{x}) = e^{iH_0(t-t_0)}A(t,\mathbf{x})e^{-iH_0(t-t_0)}$, and we also used the cyclic property of trace operation for the evolution operator and the commutator. The zeroth-order is not explicitly computed since Equation 2.28 does not require it. Higher orders in λ in Equation 2.28 are truncated yielding an approximation at the first order. Then we finally obtain the equation we were looking for in this section

$$\delta\langle A(t,\mathbf{x})\rangle = i\int_{t_0}^{t}\operatorname{Tr}\rho(t_0)[H_{\mathrm{ext}}^{\mathrm{H}}(t'),A^{\mathrm{H}}(t,\mathbf{x})] + \text{higher order corrections}, \tag{2.30}$$

where we used the external Hamiltonian definition given in the beginning of this section but in Heisenberg picture. The Equation 2.30 is at the core of linear response theory.

2.4.1 Scalar field source

As a simple application of this idea, let us suppose that the external small force is generated by a time-dependent scalar source field $J(t,\mathbf{x})$ (not an operator). This source

couples to an observable $A(t, \mathbf{x})$, which is defined in the unperturbed system. The external Hamiltonian in Heisenberg picture takes the form

$$H^{\mathrm{H}}_{\mathrm{ext}}(t) = \int \mathrm{d}^3x J(t, \mathbf{x}) A^{\mathrm{H}}(t, \mathbf{x}), \tag{2.31}$$

where $J(t_0, \mathbf{x}) = 0$. We are interested in computing the linear response effect on the observable due to the external source. Therefore, using Equation 2.30, we obtain

$$\delta\langle A(t, \mathbf{x})\rangle \sim -i \int_{t_0}^{t} \mathrm{d}t' \int \mathrm{d}^3x' J(t', \mathbf{x}') \,\mathrm{Tr}\, \rho(t_0)[A^{\mathrm{H}}(t, \mathbf{x}), A^{\mathrm{H}}(t', \mathbf{x}')]. \tag{2.32}$$

At this point, it is useful to work with Green's functions because they satisfy well-known properties known already from quantum field theory (PESKIN; SCHROEDER, 1995). We can identify the retarded Green's function in the equation above since $t' \in [t_0, t]$ for all the integration interval and then

$$iG_R(t, \mathbf{x}; t', \mathbf{x}') = \Theta(t - t') \,\mathrm{Tr}\, \rho(t_0)[A^{\mathrm{H}}(t, \mathbf{x}), A^{\mathrm{H}}(t', \mathbf{x}')], \tag{2.33}$$

where Θ is the Heaviside step function. If we extend the lower limit of the integral in Equation 2.32 to $-\infty$ (which does not affect the result), then this equation becomes

$$\delta\langle A(x)\rangle = \int \mathrm{d}^4x' J(x') G_R(x; x'), \tag{2.34}$$

where $x = (t, \mathbf{x})$. One of the properties of Green's function in QFT for systems in thermal equilibrium, such as the one in Equation 2.33, is that[6] $G_R(x; x') = G_R(x - x')$, i.e., translation invariance. Each function in Equation 2.34 is substituted by their Fourier transform as follows,

$$\begin{aligned} J(x') &= \int \frac{\mathrm{d}^4k}{(2\pi)^4} e^{ik\cdot x'} \tilde{J}(k), \\ G_R(x - x') &= \int \frac{\mathrm{d}^4k'}{(2\pi)^4} e^{ik'\cdot(x - x')} \tilde{G}_R(k'), \\ \delta\langle A(x)\rangle &= \int \frac{\mathrm{d}^4k}{(2\pi)^4} e^{ik\cdot x} \delta\langle \tilde{A}(k)\rangle, \end{aligned} \tag{2.35}$$

where $k^\mu = (\omega, \mathbf{k})$ is the momentum. Then, we use the integral representation for the delta function,

$$(2\pi)^4 \delta(k - k') = \int \mathrm{d}^4x' e^{i(k - k')\cdot x'}, \tag{2.36}$$

and, by comparing both sides of the resulting equation, one obtains the linear response relation

$$\delta\langle \tilde{A}(k)\rangle = \tilde{J}(k) \tilde{G}_R(k). \tag{2.37}$$

This equation allows one to determine the linear effects coming from the presence of the source on the system. As a matter of fact, transport coefficients may be computed using this expression, as shown below.

[6] This would not be true for a solid or crystal.

2.4.2 Transport coefficient

We now assume that the statistical ensemble describing the correlator has a simpler limit known from a physical model, which in this case is hydrodynamics. More specifically, we consider the long-wavelength/long time hydrodynamic limit, i.e. which corresponds to $\mathbf{k} \to 0$ and then $\omega \to 0$ in Equation 2.37. In this limit, one obtains an Ohm's law-like expression

$$\delta\langle A\rangle \sim \chi \partial_t J, \tag{2.38}$$

where χ is the transport coefficient (a real number) of this hydrodynamical model. Applying the Fourier transform on $J(x)$, just the way we have done in Equation 2.35, then taking $\mathbf{k} \to 0$ we obtain the approximate expression

$$\delta\langle \tilde{A}(\omega, \mathbf{0})\rangle \sim -i\omega\chi \tilde{J}(\omega, \mathbf{0}). \tag{2.39}$$

It is important to remember the equation above is valid only for small frequencies. Therefore, when comparing this equation to Equation 2.37, we are able to relate the retarded Green's function with the transport coefficient via the so-called Kubo formula (RAMALLO, 2015),

$$\chi = -\lim_{\omega\to 0} \frac{\operatorname{Im} \tilde{G}_R(\omega, \mathbf{0})}{\omega}. \tag{2.40}$$

In chapter 4 we will come back to linear response theory and the calculation of transport coefficients in a strongly coupled anisotropic plasma. In that case, we will show how to define the shear viscosity (in its isotropic limit) via a Kubo formula involving the retarded correlator of the energy-momentum tensor.

3 Gauge/gravity duality

As mentioned before in this thesis, there are many review articles and books such as (NASTASE, 2015; AMMON; ERDMENGER, 2015; KIRITSIS, 2007), about the gauge/gravity duality. Therefore, we refer the reader to those references for detailed discussions about the duality and its derivation from string theory. In fact, in this thesis we only consider the duality at finite temperature and density and, thus, important aspects about the duality in the vacuum will not be discussed. In this chapter, for the sake of completeness, we are going to heuristically motivate the gauge/gravity duality by focusing on the aspects involving the Anti-de Sitter/Conformal Field Theory (AdS/CFT) correspondence. In this specific case, the string side of this duality refers to type IIB string theory on $AdS_5 \times S^5$ while the gauge theory side refers to an $\mathcal{N} = 4$ SYM plasma in four spacetime dimensions. After reviewing some basic mathematical concepts involved in the description of AdS spacetime (HAWKING; ELLIS, 2011), we briefly explain the correspondence and show some of its applications related to the thermodynamics of black holes in an asymptotically AdS spacetime, which is very different from the properties of black holes defined in asymptotically flat spacetimes.

3.1 Embedding mathematical structures

Lets begin this introductory section talking about a sphere, a well-known structure, which is a set where each one of its elements is a list of three real numbers (x, y, z) satisfying the equation $x^2 + y^2 + z^2 = r^2$, where r is the so-called radius, a real number. Despite that three numbers are needed to describe each element of this sphere, only two of them are said to be independent and the third dependent one must satisfy an equation. Also, these two independent numbers are bounded to a domain, otherwise the third number could be complex. Thus, this sphere is a two-dimensional structure since we need only two (bounded) independent variables.

Now we want to define distances on this sphere. We usually imagine a two-dimensional surface embedded in an abstract three-dimensional Euclidean space where the distance from the origin of this space to any point on the surface of the sphere is the same for all points on this sphere (which is, historically, the geometrical definition of a sphere). In fact, any geometrical structure we are able to imagine/visualize are always embedded in an abstract three-dimensional flat space which follows Euclidean postulates[1]. Then any point in this space can be described by a set of coordinates (e.g. Cartesian coordinates), so the geometrical structure is embedded. If we extend analytically the number of dimensions of this flat space to d, then higher dimensional (up to $d - 1$) geometrical structures can be embedded. Each point in this higher dimensional Euclidean space is identified by

[1] This embedding fact is a rough way to refer to the more general *Nash embedding theorems*.

d real numbers (building up the entire space with, for example, the set $\mathbb{R}^d$ if one uses Cartesian coordinates). And the distance between two infinitesimally close points in this d-dimensional Euclidean space is defined by the line element,

$$\mathrm{d}s^2 = \sum_{i=1}^{d} (\mathrm{d}X^i)^2, \tag{3.1}$$

where $\mathrm{d}s^2 \geq 0$, and the Cartesian set of coordinates $\{X^i\}$ was used with $|\mathrm{d}X^i| \ll 1$ for all i. Lets get back to the sphere above and embed it in this $d = 3$ dimensions Euclidean space. In order to embed it, we need a correspondence between the coordinates of the Euclidean space, $\{X^i\}$, and the coordinates of the sphere (also called variables), $\{x^i\}$, i.e. the correspondence follows a map[2] $X^i = f^i(x^1, x^2, \ldots, x^d)$. It is very common to choose the simple one, $X^i = x^i$, which makes structures, such as spheres, to be uniquely defined by their geometrical counterpart (i.e. if one knows the line element then the rest follows in a straightforward manner), and it is also easy to read coordinates and variables at the same time with this correspondence. Some mappings are, in fact, the same because of the symmetries of Euclidean space: rotations and translations. So taking the common choice for the sphere we have: $X^1 = x$, $X^2 = y$ and $X^3 = z$, where one should apply the sphere equation and substitute this correspondence into Equation 3.1. Instead, we will use a simpler set of coordinates to this case, the spherical coordinates: $X^1 = x = r\sin\theta\cos\phi$, $X^2 = y = r\sin\theta\sin\phi$, and $X^3 = z = r\cos\theta$, where $\theta \in [0, \pi]$ and $\phi \in [0, 2\pi]$. This set automatically satisfies the equation for the sphere, and yields the following line element $\mathrm{d}s^2 = r^2\mathrm{d}\Omega_2^2 = r^2\mathrm{d}\theta^2 + r^2\sin^2\theta\mathrm{d}\phi^2$.

Besides the embedding Euclidean space $\mathbb{R}^d$, there is the Minkowski space-time $\mathbb{R}^{p,q}$, where its line element is defined to be

$$\mathrm{d}s^2 = \sum_{i=1}^{p} (\mathrm{d}X^i)^2 - \sum_{i=1}^{q} (\mathrm{d}Y^i)^2, \tag{3.2}$$

where two sets of Cartesian coordinates were used, $\{X^i\}$ and $\{Y^i\}$. By convention, X^i are called spatial-coordinates and Y^i are time-coordinates. The spatial line element is defined as $\sum_{i=1}^{p}(\mathrm{d}X^i)^2$ and the time line element is $\sum_{i=1}^{q}(\mathrm{d}Y^i)^2$ (notice there is no minus sign in this latter definition). If $\mathrm{d}s^2 > 0$ we have a space-like distance, if $\mathrm{d}s^2 < 0$ a time-like distance, and $\mathrm{d}s^2 = 0$ a light-like distance. Because one can have $\mathrm{d}s^2 < 0$ then there is no coordinate transformation that takes Equation 3.2 into Equation 3.1 for any $d = p + q$ (even if we try to embed a Minkowski space-time into a higher dimensional Euclidean space will not work), implying that Minkowski space-time is a non-Euclidean space, thus one cannot imagine/visualize geometrical structures in this space-time. When evaluating the average of an observable over a statistical ensemble described by QFT (which is in a Minkowski space-time), one can use the so-called Wick rotation $Y^j \to iX^{p+j}$ where $X^{p+j} \in \mathbb{R}$, so the value of the averaged observable may be evaluated in an Euclidean space.

[2] These maps are not diffeomorphisms so the geometrical structure generated may not be the same when using two different maps.

The presence of time coordinates makes the corresponding map between Minkowski coordinates and the variables describing a structure not straightforward to identify as was done in the Euclidean case. To clarify this statement we give the following example, suppose we want to embed the sphere above into a Minkowski space-time $\mathbb{R}^{2,1}$, then using spherical coordinates and the same correspondence done for Euclidean case but with $Y^1 = z$, we obtain $\mathrm{d}s^2 = r^2\cos(2\theta)\mathrm{d}\theta^2 + r^2\sin^2\theta\mathrm{d}\phi^2$. Instead, if one chooses $Y^1 = x$ then the line element will be different (and this is not a problem). This happens because the sphere equation is invariant under O(3) and the Minkowski space-time with the same number of dimensions has only O(2). For a general Minkowski space-time, there are more symmetry groups than Euclidean space, it preserves symmetry by rotation in both of its Euclidean subspaces separately (i.e. the one generated by spatial-coordinates, and the other generated by time-coordinates), it preserves translation, and boosts (a type of symmetry that mixes spatial-coordinates and time-coordinates).

3.1.1 Anti-de Sitter geometry

One can find a structure which is invariant under the same symmetry group that Minkowski space-time is and use a simple map for correspondence. This structure is the $(p+q-1)$-dimensional (conjugate) hyperboloid which is a set that satisfies the following equation[3]

$$\sum_{i=1}^{p}(x^i)^2 - \sum_{i=1}^{q}(y^i)^2 = \pm L^2, \tag{3.3}$$

where L is a constant positive number. The structure with minus sign on the right hand side is the conjugate hyperboloid, while the one with plus sign is just a hyperboloid. If one embeds a $(p+q-1)$-dimensional hyperboloid into a Minkowski $\mathbb{R}^{p,q}$ with the correspondence $X^i = x^i$ and $Y^i = y^i$ and substitutes Equation 3.3 with positive sign into Equation 3.2, then one obtains the so-called *de Sitter space*. The resulting line element is not diagonal with these coordinates which makes analytical properties difficult to obtain. To circumvent this obstacle, we introduce the so-called static coordinates, $y^1 = \sqrt{L^2 - r^2}\sinh(t/L)$, $x^1 = \sqrt{L^2 - r^2}\cosh(t/L)$, and $x^i = rz^i$ for $i \in \{2, 3, \ldots, p\}$. One can check these coordinates satisfy Equation 3.3 with $r \in [0, L]$ noticing that coordinates $\{z^i\}$ must satisfy a $(p-2)$-dimensional sphere, i.e. $\sum_{i=2}^{p}(z^i)^2 = 1$. Using the static coordinates one obtains

$$\mathrm{d}s^2 = -\left(1 - \frac{r^2}{L^2}\right)\mathrm{d}t^2 + \left(1 - \frac{r^2}{L^2}\right)^{-1}\mathrm{d}r^2 + r^2\mathrm{d}\Omega^2_{p-2}, \tag{3.4}$$

[3] Mathematicians prefer to define an inner product in Minkowski space-time that is an analytical extension of the usual inner product of vectors in Euclidean space, and then make the correspondence between a $(d-1)$-dimensional sphere embedded in an Euclidean space $\mathbb{R}^d$ with a $(d-1=p+q-1)$-dimensional conjugate hyperboloid embedded in a Minkowski space-time $\mathbb{R}^{p,q}$. The latter one is sometimes referred as *quasi-spheres* because it satisfies similar properties as the sphere.

where $\mathrm{d}\Omega_{p-2}^2$ is the line element of a $(p-2)$-sphere of unit radius. In this geometry, L receives the name *cosmological horizon* (since $r \leq L$).

Now we get to the point we are interested in as we will embed a $(p+q-1)$-dimensional conjugate hyperboloid into a Minkowski $\mathbb{R}^{p,q}$ with the mapping $X^i = x^i$ and $Y^i = y^i$ and substitute Equation 3.3 with negative sign into Equation 3.2 to obtain the so-called *Anti-de Sitter space* (AdS). These coordinates suffer from the same difficulty as the ones in the hyperboloid case and, then, this time we focus on a slightly different case: the $(p+2-1)$-dimensional conjugate hyperboloid and introduce the so-called Poincaré coordinates,

$$\begin{aligned} y^1 &= \frac{r}{2}\left(\frac{L^2}{r^2} + \frac{\vec{z}^2 - t^2}{L^2} + 1\right), \\ y^2 &= \frac{r}{L}t, \\ x^1 &= \frac{r}{2}\left(\frac{L^2}{r^2} + \frac{\vec{z}^2 - t^2}{L^2} - 1\right), \\ x^i &= \frac{r}{L}z^i, \text{ for } i \in \{2, 3, \ldots, p\}, \end{aligned} \tag{3.5}$$

where $z_i \in \mathbb{R}$, $\vec{z}^2 = \sum_{i=2}^{p}(z^i)^2$, and $r \in \mathbb{R}_{>0}$. Here, despite the similar notation used in de Sitter coordinates, neither $\{z^i\}$ are constrained to a sphere nor r is the radius of a sphere. The line element then takes the simple form

$$\mathrm{d}s^2 = -\frac{r^2}{L^2}\mathrm{d}t^2 + \frac{L^2}{r^2}\mathrm{d}r^2 + \frac{r^2}{L^2}\mathrm{dE}_{p-1}^2, \tag{3.6}$$

where dE_{p-1}^2 is the line element of a $(p-1)$-Euclidean space. In this geometry, L is called the *AdS radius*, and in the context of the gauge/gravity duality r is *holographic coordinate*. When $r \to +\infty$ the line element tends to a conformal flat space, the Minkowski space-time $\mathbb{R}^{p-1,1}$. It is important to note, however, that this patch of coordinates does not cover all AdS space. To do so, one uses *global coordinates* (HAWKING; ELLIS, 2011), which define an analytical extension of Equation 3.4 where the cosmological horizon L^2 is replaced with the AdS radius $-L^2$.

Now that some of the mathematical properties of AdS space-time have been discussed, we briefly discuss in the next section the main arguments behind the gauge/gravity duality.

3.2 AdS/CFT correspondence

In string theory, the elementary objects are one-dimensional structures called strings (instead point-like particles). Strings are classified according to their boundary conditions and they could be either open or closed strings and their oscillations are described by fields. Open strings' ends are attached to p-dimensional hypersurfaces called branes and the

motion of these strings on this brane satisfies Dirichlet boundary conditions and, therefore, these special branes are so-called D-branes, or Dp-branes (KIRITSIS, 2007). Just like particles scatter in quantum field theory, strings also scatter in string theory but a more complete understanding of this is only achieved in the perturbative regime because string theory still currently lacks a full formalism valid also in the non-perturbative regime. The Euclidean action of D-branes is proportional to the tension (KIRITSIS, 2007)

$$T_p = \frac{1}{g_s \ell_s (2\pi \ell_s)^p}, \tag{3.7}$$

where g_s is the string coupling constant, and ℓ_s is the string length. When $g_s \to 0$, quantities such as the partition function of these objects ($Z = \int \mathcal{D}[\dots] e^{-T_p \int [\dots]}$) cannot be computed perturbatively. This statement ensures that D-branes are non-perturbative objects in string theory with open strings coupled to it behaving as fluctuations. On the other hand, one could still consider a low-energy limit when $\ell_s \to 0$. Another important aspect in string theory is that it is possible to associate a charge to each end of the open string and, since these ends are attached to a D-brane, then these charges also live on the D-brane. In the low-energy limit one can consider N_c D-branes stacked together because the open strings connecting each brane have $\ell_s \to 0$ and, therefore, the conserved charge living on them imposes a symmetry $U(N_c)$ to the fields on D-branes. This is the string theory way to define a gauge theory on the world volume of D-branes.

Unlike bosonic string theory that describes only bosonic strings, superstring theory models fermions and bosons by adding supersymmetry, which means fermions and bosons can be swapped in such a way the predictions of the theory remain invariant. There are five types of superstring theories, all of them are related to each other in a non-trivial way and they are conjectured to be the limiting cases of a more general theory, the so-called M-theory (for references see (KIRITSIS, 2007)). One of these superstring theories is called type IIB superstring theory, where each field associated to an open string fluctuates on a ten-dimensional bulk space-time while their ends are attached to the boundary of this space-time featured by a stack of N_c coincident D3-branes (notice $p = 3$ on this case, and $\ell_s \to 0$). With the low energy limit considered, the fluctuations on these D3-branes are described by a four-dimensional gauge theory SU(N_c), the so-called $\mathcal{N} = 4$ SYM, where the number 4 stands for the number of supersymmetries and N_c the number of colors interpreted in the same way as in QCD, for example. SYM is a classical conformal field theory that remains conformal even after quantization with the beta function vanishing at all orders in perturbation theory. Outside the low-energy limit, the total action of the theory is a sum of three terms: the action of the fields oscillating around closed strings created from open strings inside the bulk of space-time, the action of the fields vibrating on D-branes at the boundary of space-time, and the action describing the interaction between branes and closed strings. However, in the low energy limit the action for the interaction term vanishes, and, therefore, $\mathcal{N} = 4$ SYM completely describes the fields at

the boundary while free type IIB supergravity describes the fields in the bulk.

Still in the low energy limit but also with $g_s \to 0$, the metric for type IIB supergravity acquires the form

$$\mathrm{d}s^2 = \left(1 + \frac{L^4}{r^4}\right)^{-1/2} (-\mathrm{d}t^2 + \mathrm{dE}_3^2) + \left(1 + \frac{L^4}{r^4}\right)^{1/2} (\mathrm{d}r^2 + r^2 \mathrm{d}\Omega_5^2). \tag{3.8}$$

The AdS radius is related to string theory via the following equation

$$L^4 = \ell_s^4 M, \tag{3.9}$$

where $M = g_s N_c$ is the mass of a black hole. Along with the line element, there is an electromagnetic tensor sourced by an electric charge $Q = g_s N_c$ on the D-brane. Since $Q = M$, this solution is considered extremal (no temperature) and the event horizon is localized at $r = 0$, which is also the singularity of a black hole. Thus, near the horizon the metric for type IIB supergravity takes the form

$$\mathrm{d}s^2 = -\frac{r^2}{L^2}\mathrm{d}t^2 + \frac{L^2}{r^2}\mathrm{d}r^2 + \frac{r^2}{L^2}\mathrm{dE}_3^2 + L^2 \mathrm{d}\Omega_5^2, \tag{3.10}$$

which, according to Equation 3.6, is the product $\mathrm{AdS}_5 \times \mathrm{S}^5$, where both structures have the same radius L. Notice that this metric has the same form of the AdS-Schwarzchild metric shown later in Equation 3.16 if one takes $d = 4$ and $r \to \infty$.

For our purposes in this thesis, the AdS/CFT correspondence states that fluctuations at the event horizon of an extreme black brane of type IIB supergravity on $\mathrm{AdS}_5 \times \mathrm{S}^5$ background have corresponding fluctuations defined in $\mathcal{N} = 4$ SYM. In order to be a valid correspondence, the low-energy limit, $\ell_s \to 0$, is achieved when compared to the macroscopic scale of the geometry into which strings are embedded, which means

$$\frac{\ell_s}{L} \ll 1 \implies N_c g_s \gg 1. \tag{3.11}$$

The string coupling is related to the gauge coupling constant, $g_s = g_{\mathrm{YM}}^2$, and therefore $g_{\mathrm{YM}} \to 0$. Despite the gauge coupling constant being small, this does not mean that we can apply perturbation theory. In fact, in the large $N_c \to \infty$ case we consider one needs to analyze the 't Hooft coupling, which is defined as $\lambda = N_c g_{\mathrm{YM}}^2$, and by Equation 3.11 we obtain $\lambda \gg 1$. Then, the gauge theory on D3-branes described by $\mathcal{N} = 4$ SYM is in its non-perturbative, strongly coupled regime.

Lets summarize what we have discussed so far. While the fields on the gravity/string side are treated perturbatively (the classical regime, where the string coupling is small, $g_s \to 0$), the corresponding fields on the gauge side are treated non-perturbatively (strongly coupling, $\lambda \to \infty$). This shows why holography can be so useful to study the properties of strongly coupled gauge theories. Problems in strongly coupled theories, which cannot even be properly defined (or computed) using standard techniques such as the shear viscosity,

can be readily computed using classical gravity. Furthermore, the Maldacena's conjecture, or gauge/gravity duality, in its stronger form states that the reverse is also true, i.e. when the fields on the gravity side are treated non-perturbatively (within quantum gravity where the coupling is strong $g_s \to \infty$), the corresponding fields on the gauge theory are treated perturbatively (weak 't Hooft coupling, $\lambda \to 0$). These results are better visualized in Table 1.

Table 1 – Holographic dictionary.

Boundary QFT				Bulk Gravity
Operator	$\mathcal{O}(x)$	$\longleftrightarrow$	$\Phi(x,r)$	Field
Spin	$s_{\mathcal{O}}$	$\longleftrightarrow$	s_{Φ}	Spin
Global Charge	$q_{\mathcal{O}}$	$\longleftrightarrow$	q_{Φ}	Gauge Charge
Scaling dimension	$\Delta_{\mathcal{O}}$	$\longleftrightarrow$	m_{Φ}	Mass
Source	$J(x)$	$\longleftrightarrow$	$\Phi(x,r)\|_{\partial}$	Boundary Value (B.V.)
Expectation Value	$\langle\mathcal{O}\rangle$	$\longleftrightarrow$	$\Pi_{\Phi}(x,r)\|_{\partial}$	B.V. of Radial Momentum
Global Symmetry Group	G	$\longleftrightarrow$	G	Gauge Symmetry Group
Source for Global Current	$\mathcal{A}_{\mu}(x)$	$\longleftrightarrow$	$A_{\mu}(x,r)\|_{\partial}$	B.V. of Gauge Field
Expectation Current	$\langle\mathcal{J}^{\mu}(x)\rangle$	$\longleftrightarrow$	$\Pi^{\mu}_{A}(x,r)\|_{\partial}$	B.V. of Momentum
Stress Tensor	$T_{\mu\nu}(x)$	$\longleftrightarrow$	$g_{\mu\nu}(x,r)$	Spacetime Metric
Source for Stress-Energy	$h_{\mu\nu}(x)$	$\longleftrightarrow$	$g_{\mu\nu}\|_{\partial}$	B.V. of Metric
Expected Stress-Eenrgy	$\langle T_{\mu\nu}(x)\rangle$	$\longleftrightarrow$	$\Pi_{g,\mu\nu}(x,r)\|_{\partial}$	B.V. of Momentum
# of Degrees of Freedom per Spacetime Point	N^2	$\longleftrightarrow$	$(\frac{L}{\ell_p})^{d-1}$	Radius of Curvature in Planck Units
Characteristic Strength of Interactions	λ	$\longleftrightarrow$	$(\frac{L}{\ell_s})^{d}$	Radius of Curvature in String Units
QFT Partition Function with Sources $J_i(x)$	$Z_{\mathrm{QFT}_d}[J_i]$	$\longleftrightarrow$	$Z_{\mathrm{QG}_{d+1}}[\Phi_i[J_i]]$	QG Partition Function in AdS with $\Phi_i\|_{\partial} = J_i$
QFT Partition Function at Strong Coupling	$Z^{\lambda,N\gg1}_{\mathrm{QFT}_d}[J_i]$	$\longleftrightarrow$	$e^{-I_{\mathrm{GR}_{d+1}}[\Phi_i[J_i]]}$	Classical GR Action in Ads with $\Phi_i\|_{\partial} = J_i$
QFT n-point Functions at Strong Coupling	$\langle\mathcal{O}_1\ldots\mathcal{O}_n\rangle$	$\longleftrightarrow$	$\frac{\delta^n I_{\mathrm{GR}_{d+1}}[\Phi_i[J_i]]}{\delta J_1\ldots\delta J_n}\|_{J_i=0}$	Classical Derivatives of the On-Shell Classical GR Action
Thermodynamic State		$\longleftrightarrow$		Black Hole
Temperature	T	$\longleftrightarrow$	T_H	Hawking Temperature
Chemical Potential	μ	$\longleftrightarrow$	Q	Charge of Black Hole
Free Energy	F	$\longleftrightarrow$	$I_{\mathrm{GR}}\|_{\text{on-shell}}$	On-Shell Bulk Action
Entropy	S	$\longleftrightarrow$	A_H	Area of Horizon

Source – Adams et al. (2012).

After quickly reviewing the holographic correspondence, we can now state some basic results related to the thermodynamics of black holes and their implications to the properties of strongly coupled gauge theory plasmas.

3.2.1 AdS-Schwarzschild geometry

Alternatively to the geometrical definition given before, it is useful to remember that one may obtain either de Sitter or Anti-de Sitter space-time from the vacuum solution

of Einstein's field equations with a cosmological constant,

$$S = \frac{1}{2\kappa}\int \mathrm{d}^{d+1}x\sqrt{-g}\left(R \pm \frac{d(d-1)}{L^2}\right), \tag{3.12}$$

where d is the Minkowski dimensions and the extra 1 refers to the holographic coordinate r (such as the ones in Equation 3.4 and Equation 3.6). The action with a plus sign refers to de Sitter geometry, while the negative sign to the Anti-de Sitter spacetime. Both have constant scalar curvature proportional to the cosmological constant. Since this action is a functional of the metric, using the principle of least action one obtains the Einstein field equations (without matter fields),

$$R_{\mu\nu} = \pm\frac{d}{L^2}g_{\mu\nu}. \tag{3.13}$$

It is possible to obtain a spherically symmetric solution by introducing a spherical black hole in both spaces, analogously to the well-known $(d+1)$-Schwarzschild solution (i.e. no cosmological constant),

$$\mathrm{d}s^2 = -\left(1 - \frac{2M}{r^{d-2}}\right)\mathrm{d}t^2 + \left(1 - \frac{2M}{r^{d-2}}\right)^{-1}\mathrm{d}r^2 + r^2\mathrm{d}\Omega_{d-1}^2, \tag{3.14}$$

where one finds a singular solution at $r = 0$ of mass M [4]. Therefore, one obtains

$$\mathrm{d}s^2 = -\left(1 - \frac{2M}{r^{d-2}} \pm \frac{r^2}{L^2}\right)\mathrm{d}t^2 + \left(1 - \frac{2M}{r^{d-2}} \pm \frac{r^2}{L^2}\right)^{-1}\mathrm{d}r^2 + r^2\mathrm{d}\Omega_{d-1}^2, \tag{3.15}$$

where the minus sign refers to the *spherical de Sitter-Schwarzschild metric* while the plus sign refers to the *spherical AdS-Schwarzschild metric*.

It is also possible to obtain a solution that preserves both rotation and translation symmetry. This solution has a planar event horizon rather than the usual spherical one. Then in a Poincaré patch (see Equation 3.6) for a $(d+1)$-dimensional solution the metric takes the form

$$\mathrm{d}s^2 = -\left(\pm\frac{r^2}{L^2} \mp \frac{2M}{r^{d-2}}\right)\mathrm{d}t^2 + \left(\pm\frac{r^2}{L^2} \mp \frac{2M}{r^{d-2}}\right)^{-1}\mathrm{d}r^2 + \frac{r^2}{L^2}\mathrm{dE}_{d-1}^2, \tag{3.16}$$

where the upper sign solution is the *planar AdS-Schwarzschild* while the lower one is the *planar dS-Schwarzschild*. The solution in Equation 3.16 describes black holes with an event horizon, r_H, if it is asymptotically Anit-de Sitter (or a cosmological horizon if it is asymptotically de Sitter) given by the outer most positive root of $1/g_{rr} = 0$.

[4] Here in this section we are using a system of units where any quantity is expressed as powers of length. In a space-time with four dimensions the mass of a black hole has then units of [length], and in $d+1$ dimensions this mass has unit of [length]$^{d-2}$, where this deviation from standard units follows from the gravitational constant G_{d+1}.

3.3 Thermodynamics of black holes

Let a stationary isotropic black hole be described by diagonal metric normalized at the boundary,

$$\mathrm{d}s^2 = -f(r)\mathrm{d}t^2 + \frac{\mathrm{d}r^2}{g(r)} + g_{ii}(r)(\mathrm{d}x^i)^2, \tag{3.17}$$

where the event horizon, $r = r_H$, is the outer most positive root of $g(r) = 0$, hence $f(r_H) = 0$ too. For $r > r_H$ all functions above are positive. The normalization imposed means that for $r \to \infty$ the metric components are asymptotically Minkowski with $f(r) = g(r) = g_{ii} \sim 1$, or asymptotically AdS with $f(r) = g(r) = g_{ii} \sim r^2/L^2$. Using Euclidean time $t \to it_E$ (along with Wick rotation) near the event horizon, the line element approaches

$$\mathrm{d}s^2 \sim (r - r_H)f'(r_H)\mathrm{d}t_E^2 + \frac{\mathrm{d}r^2}{(r - r_H)g'(r_H)} + g_{ii}(r_H)(\mathrm{d}x^i)^2. \tag{3.18}$$

Using polar coordinates, $\rho = 2\sqrt{(r - r_H)/g'(r_H)}$ and $\phi = \sqrt{f'(r_H)g'(r_H)}\, t_E/2$, the metric takes the form

$$\mathrm{d}s^2 \sim \mathrm{d}\rho^2 + \rho^2\mathrm{d}\phi^2 + g_{ii}(r_H)(\mathrm{d}x^i)^2. \tag{3.19}$$

In order to make this metric continuous (without a conical singularity) one needs to impose a periodical structure with $\phi \to \phi + 2\pi$, which is equivalent to $t_E \to t_E + \frac{1}{T}$, where

$$T = \frac{\sqrt{f'(r_H)g'(r_H)}}{4\pi}. \tag{3.20}$$

This is the Hawking temperature for a black hole (KIRITSIS, 2007).

With this formula we are able to compute the temperature for Equation 3.14, and Equation 3.16. In the following we show the thermodynamical properties of a spherical black hole and a planar one.

a) Schwarzschild metric,

$$T = \frac{d-2}{4\pi} r_H^{-1}; \tag{3.21}$$

b) planar AdS-Schwarzschild metric,

$$T = \frac{d}{4\pi L^2} r_H. \tag{3.22}$$

Now we proceed to compute the entropy s of a black hole, which according to the Bekenstein-Hawking formula is proportional to the volume of the remaining space in Equation 3.18 around the horizon (i.e. the space constructed by keeping fixed t_E and $r = r_H$),

$$s = \frac{2\pi}{\kappa} \int \mathrm{d}^{d-1}x \sqrt{\det\left(g_{ii}(r_H)\right)}. \tag{3.23}$$

Therefore, as was done for the temperature, we obtain the entropy for

a) Schwarzschild metric,

$$s = \frac{2\pi^{\frac{d+1}{2}}}{\kappa\Gamma\left(\frac{d+1}{2}\right)} r_H^{d-1}; \tag{3.24}$$

b) planar AdS-Schwarzschild

$$s = \frac{2\pi V}{\kappa L^{d-1}} r_H^{d-1}. \tag{3.25}$$

Note the appearance of V in the latter case , which is the (infinite) volume of $(d-1)$-Euclidean space, the same spatial volume of the asymptotic ($r \to \infty$) conformal Minkowski space-time[5]. One can divide both sides of this equation by V to obtain the entropy density for the gauge theory "living" at the boundary of this space.

Relating the entropy to the temperature the above equations take the form

a) Schwarzschild

$$s \propto \frac{1}{T^{d-1}}; \tag{3.26}$$

b) planar AdS-Schwarzschild

$$s \propto T^{d-1}. \tag{3.27}$$

Besides the geometrical difference between the horizons of the above two metrics, there is also a great difference between the thermodynamic expressions. By the second law of thermodynamics, black hole entropy must increase (or remains fixed) over time, thus while the former black hole above has its temperature decreasing over time (i.e. it loses mass), the latter one has its temperature fixed over time[6]. Alternatively, one can see this feature on the heat capacity at constant volume,

$$C_V = T\left(\frac{\partial s}{\partial T}\right)_V, \tag{3.28}$$

where $C_V < 0$ for Schwarzschild while $C_V > 0$ for AdS-Schwarzschild case. This means that the first black hole loses heat by evaporation over time, while the second defines a thermal bath. The explanation for this phenomenon relies on the fact that, in global coordinates, AdS space-time is cylindrically bounded in the r direction and, then, light rays traveling on this direction go to infinity and return to the emitting source in finite time (AdS space works as a box). This feature is important because one can introduce a black hole in asymptotic AdS geometry and prevent it from evaporating because the

[5] This volume is infinite because this black hole has an infinite planar surface while the former one has a spherical horizon which has a finite area.

[6] The temperature could in principle increase with increasing entropy, but it does not since the system is isolated and there is no matter source field to feed this black hole.

environment outside the black hole event horizon is saturated with its own radiation (detailed balance occurs). Thus, while evaporation is the final fate for black holes in asymptotic Minkowski geometry such as the Schwarzschild black hole, black holes in AdS spacetimes correspond to well-defined systems in thermodynamical equilibrium.

Besides temperature, black holes can also have conserved charges. In this case, within the context of the holographic duality, charged black holes describe states in the strongly coupled gauge theories in the presence of a chemical potential. The possibility that black holes in higher order dimensional spacetimes may be used as models of strongly coupled plasmas at finite temperature and density has led to several applications over the years, both in condensed matter physics (ZAANEN et al., 2015) and also in the physics of the QGP formed in heavy ion collisions (CASALDERREY-SOLANA et al., 2014).

In the next chapters we will show how the gauge/gravity duality can be used to understand some new features displayed by strongly coupled anisotropic plasmas in the presence of a magnetic field and also how the correspondence can shed light on the near equilibrium properties of strongly coupled fluids that display a critical point.

3.4 Membrane Paradigm

In this section we show how the transport coefficient χ evaluated in Equation 2.40 for a thermodynamical state in QFT can be computed in a bulk gravity theory, more specifically using thermodynamical variables obtained from a black hole which are evaluated at a vanishingly close distance from the event horizon. The key idea here is to consider perturbations on the event horizon behaving as a thin membrane that is mathematically described as hydrodynamical systems (or nonequilibrium statical mechanics) so we can extract transport coefficients. This is the so-called Membrane Paradigm (THORNE; PRICE; MACDONALD, 1986) which is a semi-classical model used to understand quantum mechanics effects for the exterior of black holes (see Figure 5 for an intuitive picture). This approach was used to model the Hawking radiation effect predicted by quantum mechanics.

First lets consider the action of a massless scalar field $\phi(t, \mathbf{x}, r)$ in the bulk of a $(d+1)$-dimensional spacetime (where r stands for the holographic coordinate),

$$S = -\frac{1}{2}\int \mathrm{d}^{d+1}x\sqrt{-g}\frac{\partial_\mu\phi\partial^\mu\phi}{q(r)}, \tag{3.29}$$

where $q(r)$ is the effective coupling and depends only on r. According to the holographic dictionary (see Table 1), the field ϕ on the bulk gravity side is related to an operator $\mathcal{O}$ at the boundary QFT. At the boundary of spacetime this field becomes a source $J(x)$ for a corresponding QFT, more specifically (RAMALLO, 2015)

$$J(x) = \lim_{r\to\infty} r^{d-\Delta}\phi(x, r), \tag{3.30}$$

Figure 5 – Intuitive picture of the Membrane Paradigm being used as a tool for AdS/CFT correspondence: A perturbation on the event horizon of a black hole corresponds to a perturbation on the CFT living at the boundary of the spacetime. Both perturbations behave as hydrodynamical systems.

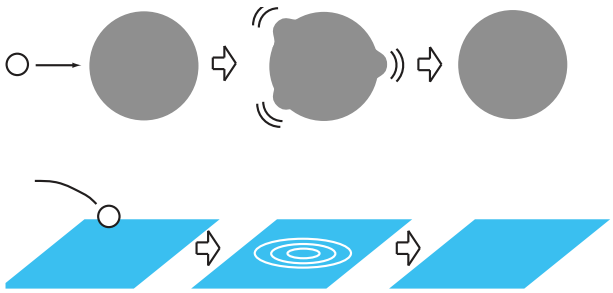

Source – Natsuume (2015, p. 5).

where Δ is the scaling dimension which is related to the mass of the field by

$$\Delta = \frac{d}{2} + \sqrt{\left(\frac{d}{2}\right)^2 + m^2 L^2}. \tag{3.31}$$

And this source affects the QFT partition function, consequently the expectation value for the corresponding operator $\mathcal{O}$ as follows

$$\langle \mathcal{O}(x) \rangle = \lim_{r \to \infty} r^{\Delta - d} \Pi, \tag{3.32}$$

where is Π the radial canonical momentum,

$$\Pi(t, \mathbf{x}, r) = -\frac{\partial \mathcal{L}}{\partial(\partial_r \phi)}, \tag{3.33}$$

where $\mathcal{L}$ is the Lagrangian density of the action. Since we are considering the massless case, all relations above simplify. If one consider the field ϕ as a perturbation, then the relation Equation 2.38 applies in the hydrodynamical limit ($\mathbf{k} \to 0$) obtaining the Kubo formula

$$\chi = \lim_{\omega \to 0} \lim_{\mathbf{k} \to \mathbf{0}} \lim_{r \to \infty} \frac{\tilde{\Pi}}{i\omega\tilde{\phi}}, \tag{3.34}$$

where the Fourier transform were applied for both Π and ϕ as

$$\begin{aligned} \tilde{\phi}(\omega, \mathbf{k}, r) &= \int \frac{\mathrm{d}\omega \mathrm{d}^{d-1}x}{(2\pi)^d} e^{i(\omega t - \mathbf{k}\cdot\mathbf{x})} \phi(t, \mathbf{x}, r), \\ \tilde{\Pi}(\omega, \mathbf{k}, r) &= \int \frac{\mathrm{d}\omega \mathrm{d}^{d-1}x}{(2\pi)^d} e^{i(\omega t - \mathbf{k}\cdot\mathbf{x})} \Pi(t, \mathbf{x}, r). \end{aligned} \tag{3.35}$$

The transport coefficient χ describes the perturbation of QFT theory living at the boundary. However we can show this same transport coefficient describes the perturbation on the event horizon of the black hole.

3.4.1 Isotropic case

The last assumption can be shown for the very special case where we have a diagonal metric that only depends on the holographic coordinate and is isotropic,

$$\mathrm{d}s^2 = g_{tt}(r)\mathrm{d}t^2 + g_{rr}(r)\mathrm{d}r^2 + g_{zz}(r)\sum_{i=1}^{d-1}(\mathrm{d}x^i)^2. \tag{3.36}$$

Lets define a function that closely resembles the transport coefficient for every slice of constant r but outside the hydrodynamical limit, i.e.

$$\rho(r) = \frac{\tilde{\Pi}}{i\omega\tilde{\phi}}. \tag{3.37}$$

The transport coefficient function for every slice of constant r is just the hydrodynamical limit in a linear response theory,

$$\chi(r) = \lim_{\omega\to 0}\lim_{\mathbf{k}\to\mathbf{0}}\rho(r). \tag{3.38}$$

We want to show that $\chi(r)$ does not depend on r.

From the radial momentum definition we obtain

$$\Pi = \frac{\sqrt{-g}}{q}g^{rr}\partial_r\phi. \tag{3.39}$$

The equation of motion for a massless scalar field takes the form

$$\partial_\mu\left(\frac{\sqrt{-g}}{q}g^{\mu\nu}\partial_\nu\phi\right) = 0, \tag{3.40}$$

which after some substitutions we obtain

$$\partial_r\Pi + \frac{\sqrt{-g}}{q}\left(g^{tt}\partial_t^2 + g^{zz}\sum_{i=1}^{d-1}\partial_i^2\right)\phi = 0. \tag{3.41}$$

Since only ϕ and Π are functions of $(t, \mathbf{x})$, then we can simply take Fourier transform of the equation of motion,

$$\frac{\mathrm{d}\tilde{\Pi}}{\mathrm{d}r} = \frac{\sqrt{-g}}{q}\left(g^{tt}\omega^2 + g^{zz}k^2\right)\tilde{\phi}, \tag{3.42}$$

where $k^2 = \mathbf{k}\cdot\mathbf{k}$. Also from Equation 3.39 we obtain

$$\tilde{\Pi} = \frac{\sqrt{-g}}{q}g^{rr}\frac{\mathrm{d}\tilde{\phi}}{\mathrm{d}r}. \tag{3.43}$$

Now we want to transport the function $\rho(r)$ defined in Equation 3.37 from the boundary, along the holographic coordinate, to the event horizon via a differential equation

and then apply the hydrodynamical limit in the linear response. Then we take Equation 3.37 and Equation 3.43, and put $\mathrm{d}\tilde{\phi}/\mathrm{d}r$ in terms of $\rho(r)$ and $\tilde{\phi}(r)$,

$$\frac{\mathrm{d}\tilde{\phi}}{\mathrm{d}r} = i\omega\frac{qg_{rr}}{\sqrt{-g}}\rho\tilde{\phi}. \tag{3.44}$$

Therefore, we are able to do the same thing with $\mathrm{d}\tilde{\Pi}/\mathrm{d}r$ starting from Equation 3.37,

$$\begin{aligned}\frac{\mathrm{d}\tilde{\Pi}}{\mathrm{d}r} &= i\omega\frac{\mathrm{d}(\tilde{\phi}\rho)}{\mathrm{d}r}, \\ &= i\omega\tilde{\phi}\left(i\omega\frac{qg_{rr}}{\sqrt{-g}}\rho^2 + \frac{\mathrm{d}\rho}{\mathrm{d}r}\right).\end{aligned} \tag{3.45}$$

Now we substitute this equation into the equation of motion and obtain the so-called *flow equation*,

$$\frac{\mathrm{d}\rho}{\mathrm{d}r} = -i\omega\left[\frac{qg_{rr}}{\sqrt{-g}}\rho^2 + \frac{\sqrt{-g}}{q}\left(g^{tt} + g^{zz}\frac{k^2}{\omega^2}\right)\right]. \tag{3.46}$$

Applying the hydrodynamical limit (i.e. the ordered limit $\lim_{\omega\to 0}\lim_{\mathbf{k}\to\mathbf{0}}$) on both sides of the above equation we obtain

$$\frac{\mathrm{d}\chi(r)}{\mathrm{d}r} = 0, \tag{3.47}$$

which means that

$$\chi = \lim_{r\to\infty}\chi(r) = \lim_{r\to r_H}\chi(r). \tag{3.48}$$

Thus we have show the initial hypothesis.

We do not need to solve the Equation 3.46 for every value of r. We just need to solve it near the horizon r_H. More specifically, near the horizon the function ρ can be exactly expanded into an infinite series,

$$\rho(r) = \rho_H + \rho'_H(r - r_H) + \mathcal{O}((r - r_H)^2), \tag{3.49}$$

where the subscript H is used to indicate that the given function is evaluated at the horizon. The metric components also admit such an expansion,

$$\begin{aligned} g_{tt}(r) &= (g_{tt})'_H(r - r_H) + \mathcal{O}((r - r_H)^2), \text{ where } (g_{tt})'_H < 0, \\ g_{rr}(r) &= \frac{(r - r_H)^{-1}}{(g^{rr})'_H} + \mathcal{O}((r - r_H)^0), \\ g_{zz}(r) &= (g_{zz})_H + \mathcal{O}((r - r_H)^1), \end{aligned} \tag{3.50}$$

With this trick we expand the flow equation (Equation 3.46) around the horizon to obtain

$$i\omega\left(\frac{q_H}{\sqrt{-g_H}(g^{rr})'_H}\rho_H^2 + \frac{\sqrt{-g_H}}{q_H(g_{tt})'_H}\right)(r - r_H)^{-1} + \mathcal{O}((r - r_H)^0) = 0 \tag{3.51}$$

The above equation indicates it needs to be zero for every order in $(r - r_H)^n$. Then the function ρ at the horizon takes the form

$$\rho_H = \pm \frac{1}{q_H} \sqrt{\frac{g_H (g^{rr})'_H}{(g_{tt})'_H}}. \tag{3.52}$$

Notice there is no dependence on the momentum $\mathbf{k}$, neither on ω. Intuitively, one should choose the solution with positive sign, since typical transport coefficients (e.g. diffusion coefficient, heat transport coefficient, mass transport coefficient, shear viscosity, and electrical conductivity) are all positive. But the choice of the sign also brings important physics, and we will do this by analyzing the wave-function ϕ. Let $\tilde{\phi}(r) = (r - r_H)^\alpha f(r)$, where f_H is finite and nonzero, then we can apply the same procedure we used in the flow equation to solve Equation 3.37 for $\tilde{\phi}$ (remember to use Equation 3.43 for $\tilde{\Pi}$). So expanding around the horizon the equation Equation 3.37, we obtain

$$\frac{f(r_H)}{\sqrt{-g_H}(g^{rr})'_H} \left(-i\omega \rho_H q_H + \alpha \sqrt{-g_H} (g^{rr})'_H \right) (r - r_H)^{-1} + \mathcal{O}((r - r_H)^0) = 0. \tag{3.53}$$

Again order by order each coefficient of $(r - r_H)^n$ is zero. So α must take the value

$$\alpha = \pm \frac{i\omega}{\sqrt{-(g^{rr})'_H (g_{tt})'_H}}. \tag{3.54}$$

Therefore, $\phi(t, \mathbf{x}, r)$ is

$$\phi_\pm = e^{i\omega(\pm bu - t) + i\mathbf{k}\cdot\mathbf{x}} f_\pm(r), \tag{3.55}$$

where

$$u = \ln(r - r_H), \text{ and } b = \frac{1}{\sqrt{-(g^{rr})'_H (g_{tt})'_H}}. \tag{3.56}$$

To analyze the speed of a wave function, one has to keep track a given point on this wave as time goes by. By definition a wave function has constant speed v if, initially, at a given point u_0 and instant t_0 the wave has amplitude ϕ_0, and at a posterior instant t and position $u_0 + v(t - t_0)$ it has the same amplitude ϕ_0. If we let $v = \mathrm{d}u/\mathrm{d}t$ and keep $\mathbf{x}$ fixed, and use the definition of wave-function speed at the event horizon,

$$\left(\frac{\mathrm{d}\phi_\pm}{\mathrm{d}t} \right)_H = 0, \tag{3.57}$$

we obtain after some computations that

$$v_\pm(r_H) = \mp \frac{1}{b}. \tag{3.58}$$

Clearly, the plus sign solution (i.e. v_-) refers to a wave outgoing the horizon since r is increasing with time t, and the minus sign solution (i.e. v_+) refers to a wave infalling

at the horizon since r diminishes with increasing time. We take the negative sign solution, which is ϕ_+ because this solution is related to causality since a classical black hole does not radiate (i.e. no Hawking radiation). Another reason is that at the boundary QFT one relates this solution with the retarded Green function. Therefore, as we predicted we take the positive ρ_H and now, as the membrane paradigm takes place, this is related to the transport coefficient of the thin membrane hovering over the horizon,

$$\begin{aligned}\chi &= \lim_{\omega\to 0}\lim_{\mathbf{k}\to\mathbf{0}} \rho_H \\ &= \frac{1}{q_H}\sqrt{\frac{g_H (g^{rr})'_H}{(g_{tt})'_H}}.\end{aligned} \tag{3.59}$$

Since we are considering a planar black hole (i.e. not a spherical one), we can rewrite the above equation as

$$\chi = \frac{1}{q_H}\frac{A}{V}, \tag{3.60}$$

where A is the are of the event horizon and V is the spatial volume. We can go further and relate these geometrical quantities with the thermodynamics of this black hole (which corresponds to the membrane), the entropy density is

$$s = \frac{A}{4G_{d+1}V}, \tag{3.61}$$

therefore

$$\frac{\chi}{s} = \frac{4G_{d+1}}{q_H}. \tag{3.62}$$

For the case ϕ is the source for stress-energy at the boundary QFT (i.e. a perturbation of metric in the bulk gravity side), then $q(r) = 16\pi G_{d+1}$ and η is the transport coefficient for the shear viscosity (in the isotropic case),

$$\frac{\eta}{s} = \frac{1}{4\pi}. \tag{3.63}$$

This is the famous KSS bound conjecture (KOVTUN; SON; STARINETS, 2005), where all systems should satisfy the inequation $\eta/s \geq 1/4\pi$. Experimentally QGP and ultracold atomic Fermi gases have $\eta/s \gtrsim 1/4\pi$.

One possible violation of this happens in theories containing more then two derivatives of the metric such as Gauss-Bonnet (BRIGANTE et al., 2008b),

$$S = \frac{1}{16\pi G_5}\int \mathrm{d}^5x\sqrt{-g}\left[R - \frac{12}{L^2} - \frac{L^2}{2}\lambda\left(R^2 - 4R_{\mu\nu}R^{\mu\nu} + R_{\mu\nu\sigma\rho}R^{\mu\nu\sigma\rho}\right)\right], \tag{3.64}$$

which leads to

$$\frac{\eta}{s} = \frac{1-4\lambda}{4\pi}, \tag{3.65}$$

violating the KSS bound viscosity when $\lambda > 0$.

Another possibility is when homogeneity is broken, or even isotropy (as will be the case in this work).

Part II

Results

4 Anisotropic shear viscosity of a strongly coupled non-Abelian plasma from magnetic branes

This chapter directly follows the first article published during my PhD (CRITELLI et al., 2014). In section 4.1 we review the thermodynamics of the magnetic brane solution found in D'Hoker and Kraus (2009). We also introduce our notation and discuss the numerical procedure used to solve the Einstein-Maxwell coupled equations. In section 4.2, after a preliminary discussion about the computation of η/s (where η is the shear viscosity and s is the entropy density) using the membrane paradigm in isotropic theories, we show that metric fluctuations around the magnetic brane background (i.e. around an anisotropic theory) on directions parallel and transverse to an external magnetic field result in scalar field fluctuations with two different couplings which, in the context of the membrane paradigm, are the shear viscosity coefficients $\eta_\perp$ and $\eta_\parallel$. Finally we discuss how our results violate the Kovtun-Son-Starinets viscosity limit $\eta/s \geq 1/4\pi$.

4.1 Magnetic brane background

We consider in the bulk a simple Einstein-Maxwell system and look for solutions corresponding to the deformation of the AdS_5-Schwarzschild geometry due to a U(1) Abelian gauge field which is chosen to give a constant and homogeneous magnetic field. This magnetic field in the bulk is then taken as an external magnetic field at the boundary gauge theory which is a strongly coupled $\mathcal{N} = 4$ SYM theory (D'HOKER; KRAUS, 2009). Clearly, the adjoint fermions in SYM feel directly the effects of the magnetic field but, due to fermion loops, the gluon sector is also affected by the field. This is why the thermodynamic properties of this *magnetic* SYM plasma considerably differ from those found in SYM in the absence of external fields.

Let us review this background and its thermodynamic properties. The action of the 5-dimensional gravitational bulk theory is given by the Einstein-Hilbert action coupled with a Maxwell field

$$S = \frac{1}{16\pi G_5}\int d^5x\,\sqrt{-g}\left(R + \frac{12}{L^2} - F^2\right) + S_{CS} + S_{GHY}, \tag{4.1}$$

where G_5 is the 5-dimensional gravitational constant, L is the asymptotic AdS_5 radius and F is the Maxwell field strength 2-form. The subscripts in the actions S_{CS} and S_{GHY} stand for Chern-Simons and Gibbons-Hawking-York, respectively. The latter action is necessary to define a well posed variational problem, but both terms will not play a role in

the calculation of shear viscosity coefficients[1]. From holographic renormalization point of view, other terms are also needed in Equation 4.1 but they do not affect the calculations performed in this thesis.

The resulting Einstein field equations are then given by

$$R_{\mu\nu} = -\frac{4}{L^2}g_{\mu\nu} - \frac{1}{3}F_{\rho\sigma}F^{\rho\sigma}g_{\mu\nu} + 2F_{\mu\rho}F_{\nu}{}^{\rho}, \tag{4.2}$$

and the Maxwell's field equations for the Abelian field,

$$\nabla_\mu F^{\mu\nu} = 0. \tag{4.3}$$

Following D'Hoker and Kraus (2009), the Ansatz for the magnetic brane geometry is

$$ds^2 = -U(r)dt^2 + \frac{dr^2}{U(r)} + f(r)(dx^2 + dy^2) + p(r)dz^2, \tag{4.4}$$

where $U(r)$, $f(r)$ and $p(r)$ are determined by solving the equations of motion. The holographic coordinate r is such that the boundary is located at $r \to \infty$. We want a black brane background and, thus, we require that at a given $r = r_h$ the function $U(r)$ has a simple zero. The Ansatz for the field strength F is given by

$$F = B\, dx \wedge dy, \tag{4.5}$$

where the constant and homogeneous B is the bulk magnetic field oriented along the z-direction. It can be checked that the Equation 4.3 is trivially satisfied by this Ansatz.

In the absence of a magnetic field (i.e. $B = 0$) we must obtain $f = p$, which reflects the spatial SO(3) invariance of the boundary gauge theory. However, since the magnetic field ($B \neq 0$) establishes a preferred direction in space, it breaks SO(3) to a SO(2) symmetry in the (x, y)-directions. In the bulk theory this is taken into account by the fact that in this case $f \neq p$.

The Equation 4.2 together with the ansatz of Equation 4.4 result in the following equations of motion,

$$\begin{aligned}
U(V'' - W'') + (U' + U(2V' + W'))\,(V' - W') &= -2B^2 e^{-4V}, \\
2V'' + W'' + 2(V')^2 + (W')^2 &= 0, \\
\frac{1}{2}U'' + \frac{1}{2}U'(2V' + W') &= 4 + \frac{2}{3}B^2 e^{-4V}, \\
2U'V' + U'W' + 2U(V')^2 + 4UV'W' &= 12 - 2B^2 e^{-4V},
\end{aligned} \tag{4.6}$$

where we defined V and W by $f = e^{2V}$ and $p = e^{2W}$. The derivative with respect to r of the fourth equation is the same to a non-linear combination of the four equations in Equation 4.6 and, thus, the fourth equation can be taken as a constraint on initial data.

[1] We note that our definition for the Riemann tensor possesses an overall minus sign in comparison to the one used by D'Hoker and Kraus (2009).

It is well-known that charged systems undergo dimensional reduction in the presence of strong fields due to the projection towards the lowest Landau level (GUSYNIN; MIRANSKY; SHOVKOVY, 1994; GUSYNIN; MIRANSKY; SHOVKOVY, 1995; GUSYNIN; MIRANSKY; SHOVKOVY, 1996) (see the recent review in Shovkovy (2013)). Taking that into account, D'Hoker and Kraus (2009) proposed that the background described by Equation 4.4 satisfies two conditions. The first condition is that the geometry must be asymptotically AdS_5, i.e. when $r \to \infty$ then $U(r) \to r^2$, $p(r) \to r^2$ and $f(r) \to r^2$ because in the UV we must recover the dynamics of $\mathcal{N} = 4$ SYM without the influence of the magnetic field. The second condition is that in the asymptotic IR the geometry becomes a BTZ black hole (BANADOS; TEITELBOIM; ZANELLI, 1992) for coordinates in time, holographic and spatial direction parallel to the magnetic field; and a two dimensional torus T^2 for coordinates in spatial directions orthogonal to the magnetic field. In fact, deep in the IR, $r \sim r_h$, the geometry of the black brane is given by

$$ds^2 = \left[-3(r^2 - r_h^2)dt^2 + 3r^2dz^2 + \frac{dr^2}{3(r^2 - r_h^2)}\right] + \left[\frac{B}{\sqrt{3}}(dx^2 + dy^2)\right]. \tag{4.7}$$

This implies that in the IR the dynamics corresponds to a $(1+1)$-dimensional CFT. Thus, imposing that the background interpolates between the BTZ black hole for $r \sim r_h$ and AdS_5 for $r \to \infty$ and interpreting the flow along the r-direction as a renormalization group flow, this solution flows from a $(1+1)$-dimensional CFT in the IR to a 4-dimensional CFT in the UV (D'HOKER; KRAUS, 2009).

4.1.1 Numerical solution and thermodynamics

Unfortunately, no analytic solution interpolating between AdS_5 and the BTZ$\times T^2$ geometry is known and, thus, we must resort to numerics. In this subsection we briefly review the numerical procedure for solving the Equation 4.6 and the thermodynamics, first elaborated by D'Hoker and Kraus (2009). We do so since the same procedure will be used to determine $\eta_\parallel/\eta_\perp$ numerically in section 4.2.

The strategy is to first choose the scale for the t and r coordinates to fix the horizon position at $r_h = 1$ so that $\tilde{U}(1) = 0$, where the tilde indicates that we are in the rescaled coordinates $\tilde{t}$ and $\tilde{r}$. By using the fact that any physical quantity in this model should depend on the dimensionless ratio $T/\sqrt{B}$, we also fix the temperature at $T = 1/(4\pi)$ — this means that we must take $\tilde{U}'(1) = 1$. Also, we rescale the x, y, and z coordinates to have $\tilde{V}(1) = \tilde{W}(1) = 0$. In these new coordinates, the magnetic field is b. After these redefinitions, the first and fourth equations in Equation 4.6 yield

$$\tilde{V}'(1) = 4 - \frac{4}{3}b^2 \text{ and } \tilde{W}'(1) = 4 + \frac{2}{3}b^2. \tag{4.8}$$

This gives a well posed initial value problem for $\tilde{U}(\tilde{r})$, $\tilde{V}(\tilde{r})$, and $\tilde{W}(\tilde{r})$, which can be numerically integrated from near $\tilde{r} = 1$ to a large value of $\tilde{r}$. It can be checked that the

geometry has the asymptotic behavior

$$\tilde{U}(\tilde{r}) \to \tilde{r}^2, \; e^{2\tilde{V}(\tilde{r})} \to v\tilde{r}^2, \text{ and } e^{2\tilde{W}(\tilde{r})} \to w\tilde{r}^2, \tag{4.9}$$

where v and w are asymptotic coefficients that depend on the rescaled magnetic field b. This result implies that, apart from a coordinate rescaling, the geometry is asymptotically AdS_5. To go back to the original units and have the correct AdS_5 asymptotic behavior, we need to rescale back to our original coordinate system by doing $(\tilde{x}, \tilde{y}, \tilde{z}) \to (x/\sqrt{v}, y/\sqrt{v}, z/\sqrt{w})$. The metric (in coordinates that are asymptotically AdS_5) then becomes

$$ds^2 = -\tilde{U}(r)dt^2 + \frac{dr^2}{\tilde{U}(r)} + \frac{e^{2\tilde{V}(r)}}{v}(dx^2 + dy^2) + \frac{e^{2\tilde{W}(r)}}{w}dz^2, \tag{4.10}$$

where we note that we have taken $r = \tilde{r}$. By the same token, the field strength is now written as

$$F = \frac{b}{v}dx \wedge dy. \tag{4.11}$$

Therefore, the rescaled magnetic field is related to the physical field at the boundary by $B = b/v$. Also, if we take $b > \sqrt{3}$ in Equation 4.8 then we have $V'(1) < 0$, which means that the geometry will not be asymptotically AdS_5. Thus, the rescaled field b is bounded to $b < \sqrt{3}$.

From Equation 4.10 one can obtain the thermodynamics of the gauge theory. The physical field is $\mathcal{B} = \sqrt{3}B$, as argued in D'Hoker and Kraus (2009) by comparing the Chern-Simons term in Equation 4.1 with the $\mathcal{N} = 4$ SYM chiral anomaly. The dimensionless ratio $T/\sqrt{\mathcal{B}}$ is given by

$$\frac{T}{\sqrt{\mathcal{B}}} = \frac{1}{4\pi\, 3^{1/4}}\sqrt{\frac{v}{b}}. \tag{4.12}$$

while the dimensionless ratio of the entropy density s by $N^2\mathcal{B}^3$ (using that $G_5 = \pi/2N^2$) is

$$\frac{s}{N^2\mathcal{B}^{3/2}} = \frac{1}{2\pi 3^{3/4}}\sqrt{\frac{v}{b^3 w}}. \tag{4.13}$$

The numerical procedure for evaluating the thermodynamics can then be summarized as follows: one chooses a value of the rescaled magnetic field b, numerically solves the Equation 4.6 and obtains the asymptotic coefficients $v(b)$ and $w(b)$ as shown in Figure 6a by fitting the asymptotic behavior of $\tilde{V}(r)$ and $\tilde{W}(r)$ to the functions $v(b)r^2$ and $w(b)r^2$, respectively. Then using Equation 4.12 and Equation 4.13 one is able to evaluate $T/\sqrt{\mathcal{B}}$ versus $s/(N^2\mathcal{B}^{3/2})$ as shown in Figure 6b by using b as a parameter[2].

[2] We have checked that our results match those previously found in D'Hoker and Kraus (2009).

Figure 6 – (a) The asymptotic coefficients v (solid blue curve) and w (dashed black curve) as a function of $b/\sqrt{3}$; (b) The normalized entropy density $s/(N^2\mathcal{B}^{3/2})$ as a function of the dimensionless combination $T/\sqrt{\mathcal{B}}$.

(a) Asymptotic coefficients

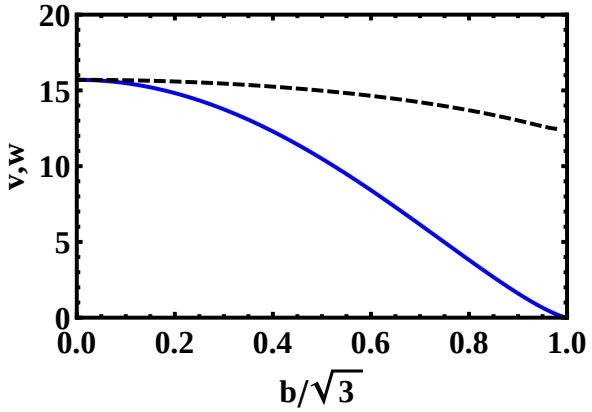

(b) Normalized entropy density

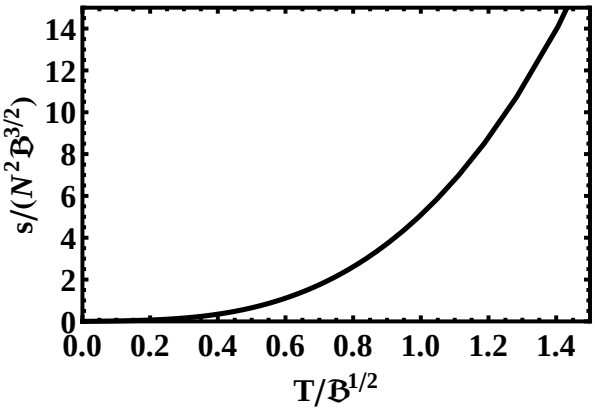

Source – Made by the authors.

4.2 Anisotropic shear viscosity due to an external magnetic field

We begin this section discussing the computation of the ratio between the shear viscosity and the entropy density from membrane paradigm in isotropic theories. Then we show that metric fluctuations around a magnetic brane background described by Equation 4.4 on directions parallel and transverse to the external magnetic field result in scalar field fluctuations yielding, in the context of the membrane paradigm, an anisotropic shear viscosity. Finally we show that this anisotropy violates the conjectured viscosity bound $\eta/s \geq 1/4\pi$.

4.2.1 Isotropic shear viscosity

From linear response theory (KAPUSTA; GALE, 2011), the viscosity tensor for an anisotropic theory is given by the Kubo formula

$$\eta_{ijkl} = -\lim_{\omega\to 0}\frac{1}{\omega}\text{Im}\; G^R_{ij,kl}(\omega,\vec{k}=0) \quad \text{with } i,j,k,l = x,y,z \tag{4.14}$$

where $G^R_{ij,kl}(\omega,\vec{k})$ is the retarded Green's function in momentum coordinates given by

$$G^R_{ij,kl}(\omega,\vec{k}) = -i\int d^4x\, e^{-ik\cdot x}\theta(t)\left\langle\left[\hat{T}_{ij}(x),\hat{T}_{kl}(0)\right]\right\rangle, \tag{4.15}$$

while $\hat{T}_{ij}$ is the stress-energy operator in the quantum field theory and $\theta(t)$ is the step function.

For an isotropic theory of hydrodynamics in the absence of other conserved currents, there are only two transport coefficients associated with energy and momentum at the

level of relativistic Navier-Stokes theory, namely the isotropic shear viscosity η and the bulk viscosity ζ. The computation of η in strongly coupled gauge theories using the gauge/gravity duality in the case of isotropic gauge theories with two derivative gravitational duals gives a universal value (POLICASTRO; SON; STARINETS, 2001; KOVTUN; SON; STARINETS, 2005)

$$\frac{\eta}{s} = \frac{1}{4\pi}. \tag{4.16}$$

A convenient method that can be used to derive this result is the membrane paradigm (IQBAL; LIU, 2009). In this framework, if we want to compute the transport coefficient χ of a scalar operator $\hat{O}$ given by the Kubo formula

$$\chi = -\lim_{\omega\to 0}\frac{1}{\omega}\text{Im } G^R(\omega, \vec{k}=0), \tag{4.17}$$

where G^R is the retarded correlator associated with the scalar operator $\hat{O}$

$$G^R(\omega,\vec{k}) = -i\int d^4x\, e^{-ik\cdot x}\theta(t)\langle\left[\hat{O}(x),\hat{O}(0)\right]\rangle, \tag{4.18}$$

one needs to look for fluctuations ϕ of the associated bulk field in dual gravity theory, in accordance with the gauge/gravity dictionary (GUBSER; KLEBANOV; POLYAKOV, 1998; SON; STARINETS, 2002). In the case that the action for the fluctuations is given by a massless scalar field with an r dependent coupling $\mathcal{Z}(r)$, i.e.

$$S_{fluc} = -\int d^5x\,\sqrt{-g}\frac{1}{2\mathcal{Z}(r)}(\partial\phi)^2, \tag{4.19}$$

then the transport coefficient χ is given by the corresponding transport coefficient χ_{mb} of the stretched membrane of the black brane horizon (IQBAL; LIU, 2009)

$$\chi = \chi_{mb} = \frac{1}{\mathcal{Z}(r_h)}. \tag{4.20}$$

In the case of the isotropic shear viscosity η, we must consider the fluctuations h_{xy} of the metric component g_{xy} since the energy-momentum tensor operator in the gauge theory $\hat{T}_{\mu\nu}$ is dual to the bulk metric $g_{\mu\nu}$ of the gravity dual[3]. Given that in isotropic backgrounds the mixed fluctuation h^y_x can be described by Equation 4.19 with $\mathcal{Z}(r) = 16\pi G_5$ (KOVTUN; SON; STARINETS, 2005), then Equation 4.20 guarantees that $\eta = 1/(16\pi G_5)$. The universal result in Equation 4.16 follows from identifying the entropy density with the area of the horizon via the Bekenstein formula.

4.2.2 Shear tensor in a magnetic field

Let us now consider metric fluctuations about the background Equation 4.4, which is a solution of the Einstein-Maxwell system in Equation 4.1. In a fluid with axial symmetry

[3] Since the background in this case is isotropic then one could have considered instead fluctuations of the metric components g_{xz} or g_{yz} without loss of generality.

due to an external magnetic field, we show how one can determine the form of the shear tensor — the detailed discussion can be found in Huang, Sedrakian and Rischke (2011). Here we will present an overview of how one can construct a rank-4 viscosity tensor $\eta^{\alpha\beta\mu\nu}$ defined in Equation 4.14, incorporate the anisotropy due to the magnetic field B, and then extract the shear viscosities η_{xzxz} and η_{xyxy} from Kubo formula[4]. To clarify the discussion, we define the dissipation function R,

$$R = \frac{1}{2}\eta^{\mu\nu\alpha\beta} w_{\mu\nu} w_{\alpha\beta}, \tag{4.21}$$

where $w_{\mu\nu} = \frac{1}{2}\left(\nabla_\mu u_\nu + \nabla_\nu u_\mu\right)$, with u^μ being the 4-velocity and $\nabla_\mu = \Delta_{\mu\nu}\partial^\nu$; the object $\Delta_{\mu\nu}$ is just a projector on the directions orthogonal to u^μ. Thus, the viscosity tensor gives us information about dissipation (i.e. generation of entropy) in the fluid. Taking the functional derivative of Equation 4.21 with respect to $w_{\mu\nu}$, we obtain the usual stress tensor $\Pi^{\mu\nu}$,

$$\Pi^{\mu\nu} = \eta^{\mu\nu\alpha\beta} w_{\alpha\beta}. \tag{4.22}$$

The construction of the viscosity tensor is based on its symmetry properties,

$$\eta^{\mu\nu\alpha\beta}(B) = \eta^{\nu\mu\alpha\beta}(B) = \eta^{\mu\nu\beta\alpha}(B) \tag{4.23}$$

and the Onsager principle (LIFSHITZ; PITAEVSKII, 1981; HUANG; SEDRAKIAN; RISCHKE, 2011),

$$\eta^{\mu\nu\alpha\beta}(B) = \eta^{\alpha\beta\mu\nu}(-B). \tag{4.24}$$

First, one writes down all the linear independent objects satisfying the above conditions of symmetry:

a) $\Delta^{\mu\nu}\Delta^{\alpha\beta}$;

b) $\Delta^{\mu\alpha}\Delta^{\nu\beta} + \Delta^{\mu\beta}\Delta^{\nu\alpha}$;

c) $\Delta^{\mu\nu}b^\alpha b^\beta + \Delta^{\alpha\beta}b^\mu b^\nu$;

d) $b^\mu b^\nu b^\alpha b^\beta$;

e) $\Delta^{\mu\alpha}b^\nu b^\beta + \Delta^{\mu\beta}b^\nu b^\alpha + \Delta^{\nu\alpha}b^\mu b^\beta + \Delta^{\nu\beta}b^\mu b^\alpha$;

f) $\Delta^{\mu\alpha}b^{\nu\beta} + \Delta^{\mu\beta}b^{\nu\alpha} + \Delta^{\nu\alpha}b^{\mu\beta} + \Delta^{\nu\beta}b^{\mu\alpha}$;

g) $b^{\mu\alpha}b^\nu b^\beta + b^{\mu\beta}b^\nu b^\alpha + b^{\nu\alpha}b^\mu b^\beta + b^{\nu\beta}b^\mu b^\alpha$.

Where b^μ is a spacelike vector orthogonal to the magnetic field, and $b^{\mu\nu} = \epsilon^{\mu\nu\alpha\beta}b^\alpha u^\beta$. This means that we have seven coefficients, five shear viscosities and two bulk viscosities. The shear viscosities are related to the traceless part of $\Pi^{\mu\nu}$ while the bulk viscosities are related to the trace of the stress tensor. We note that Onsager's condition in Equation 4.22

[4] For the sake of convenience, we will adopt the same conventions of those adopted in Huang, Sedrakian and Rischke (2011) and, thus, we will work in 4-dimensional Minkowski spacetime with mostly minus signature.

is responsible for the presence of the two last tensors, (f) and (g), involving the Levi-Civita symbol $\epsilon^{\mu\nu\alpha\beta}$. These structures may appear in magnetized plasmas (LIFSHITZ; PITAEVSKII, 1981; HUANG; SEDRAKIAN; RISCHKE, 2011) but they are not present in the case of anisotropic superfluids (LANDAU et al., 1986).

In fact, according to Erdmenger, Kerner and Zeller (2011), Erdmenger, Fernandez and Zeller (2013), Jain et al. (2015), for an anisotropic diagonal metric one can find only five linearly independent coefficients for the shear viscosity tensor due to metric fluctuations. This result is valid for the diagonal anisotropic background considered in this work (see Equation 4.4) and one can show using Kubo formulas that the two coefficients associated with (f) and (g) trivially vanish due to the general structure of the background metric.

For the sake of convenience, we will adopt the same combination of viscosity coefficients chosen in Huang, Sedrakian and Rischke (2011). Thus, using the general linear combination of the structures above, we find the most general form of the viscosity tensor in the presence of a constant magnetic field,

$$\begin{aligned}\eta^{\mu\nu\alpha\beta} &= (-2/3\eta_0 + 1/4\eta_1 + 3/2\zeta_\perp)(\mathrm{a}) + (\eta_0)(\mathrm{b}) + (3/4\eta_1 + 3/2\zeta_\perp)(\mathrm{c}) + \\ &+(9/4\eta_1 - 4\eta_2 + 3/2\zeta_\perp + 3\zeta_\parallel)(\mathrm{d}) + (-\eta_2)(\mathrm{e}) + (-\eta_4)(\mathrm{f}) + \\ &+(-\eta_3 + \eta_4)(\mathrm{g}),\end{aligned} \tag{4.25}$$

where the Kubo formulas for these coefficients are given by

$$\begin{aligned}\zeta_\perp &= -\frac{1}{3}\frac{\partial}{\partial\omega}\left[2G^R_{\tilde{P}_\perp\tilde{P}_\perp}(\omega,\vec{0}) + G^R_{\tilde{P}_\perp\tilde{P}_\parallel}(\omega,\vec{0})\right]\Big|_{\omega\to 0},\\ \zeta_\parallel &= -\frac{1}{3}\frac{\partial}{\partial\omega}\left[2G^R_{\tilde{P}_\perp\tilde{P}_\parallel}(\omega,\vec{0}) + G^R_{\tilde{P}_\parallel\tilde{P}_\parallel}(\omega,\vec{0})\right]\Big|_{\omega\to 0},\\ \eta_0 &= -\frac{\partial}{\partial\omega}\,\mathrm{Im}\,G^R_{\hat{T}^{12},\hat{T}^{12}}(\omega,\vec{0})\Big|_{\omega\to 0},\\ \eta_1 &= -\frac{4}{3}\eta_0 + 2\frac{\partial}{\partial\omega}G^R_{\tilde{P}_\perp\tilde{P}_\parallel}(\omega,\vec{0})\Big|_{\omega\to 0},\\ \eta_2 &= -\eta_0 - \frac{\partial}{\partial\omega}\,\mathrm{Im}\,G^R_{\hat{T}^{13},\hat{T}^{13}}(\omega,\vec{0})\Big|_{\omega\to 0},\\ \eta_3 &= -\frac{\partial}{\partial\omega}G^R_{\tilde{P}_\perp,\hat{T}^{23}}(\omega,\vec{0})\Big|_{\omega\to 0},\\ \eta_4 &= -\frac{\partial}{\partial\omega}G^R_{\hat{T}^{13},\hat{T}^{23}}(\omega,\vec{0})\Big|_{\omega\to 0},\end{aligned} \tag{4.26}$$

where $\tilde{P}_\perp = \hat{P}_\perp - (\theta_\beta - \Phi_\beta)\hat{\epsilon}$ and $\tilde{P}_\parallel = \hat{P}_\parallel - \theta_\beta\hat{\epsilon}$; with $\hat{P}_\perp = -\frac{1}{2}(\Delta_{\mu\nu} + b_\mu b_\nu)\hat{T}^{\mu\nu}$, $\hat{P}_\parallel = b_\mu b_\nu \hat{T}^{\mu\nu}$, $\theta_\beta = \left(\frac{\partial P}{\partial\epsilon}\right)_B$, $\Phi_\beta = -B\left(\frac{\partial M}{\partial\epsilon}\right)_B$, $\hat{\epsilon} = u_\mu u_\nu \hat{T}^{\mu\nu}$, and M is the magnetization of the plasma. Also, the retarded Green's function is defined as

$$G^R_{\hat{A}\hat{B}}(\omega,\vec{k}) = -i\int d^4x\, e^{-ik\cdot x}\theta(t)\left\langle\left[\hat{A}(x),\hat{B}(0)\right]\right\rangle. \tag{4.27}$$

The relation between these coefficients and the shear viscosities, $\eta_\perp$ and $\eta_\parallel$, calculated holographically, is

$$\begin{aligned} \eta_0 &= \eta_\perp, \\ \eta_0 + \eta_2 &= \eta_\parallel. \end{aligned} \tag{4.28}$$

Finally, one can see from Equation 4.26 that for the type of background considered in this work $\eta_3 = \eta_4 = 0$, because the components h_{xz}, h_{yz}, $(h_{yy} + h_{xx})$, and h_{xy} do not mix when one computes the action for the fluctuations. Thus, there are only five independents transport coefficients in this class of anisotropic backgrounds[5]. From now on, we will be especially interested in the following two components of η_{ijkl},

$$\eta_{xyxy} = \eta_\perp \text{ and } \eta_{yzyz} = \eta_{xzxz} = \eta_\parallel. \tag{4.29}$$

4.2.3 Anisotropic shear viscosity

The magnetic field breaks the SO(3) rotational invariance of background to only a SO(2) rotation invariance about the z-axis. Thus, as expected, it is possible to show that the fluctuation $\phi(t, r) = h^y_x(t, r)$ obeys

$$\delta S = -\frac{1}{32\pi G_5} \int d^5x \sqrt{-g}\, (\partial\phi)^2, \tag{4.30}$$

which means that the shear viscosity $\eta_{xyxy} \equiv \eta_\perp$ is still given by Equation 4.16 and this shear coefficient saturates the viscosity bound.

However, h_{zx} (or, equivalently, h_{zy}) fluctuations are not protected by the remaining rotation invariance of the background. In fact, in the context of the membrane paradigm, we must first show that the fluctuation $h_{zx}(t, r)$ obeys the equation of a massless scalar field in order to apply Equation 4.20. However, the coupling in the action may differ from Equation 4.30 and, thus, $\eta_\parallel \neq \eta_\perp$.

Consider then a fluctuation of the form $g_{zx} \to g_{zx} + h_{zx}$[6]. In order to have a scalar-like action with just the kinetic term (and possibly a r dependent coupling), we choose the mode $\psi(t, r) \equiv h^z_y(t, r)$, rather than $h^y_z(t, r)$ for example. Inserting this fluctuation into

[5] Incidentally, anisotropic superfluids also have 5 transport coefficients (LANDAU et al., 1986; ERDMENGER; KERNER; ZELLER, 2011)

[6] One can show that homogeneous fluctuations of the U(1) bulk field A_μ decouple from the corresponding fluctuations h_{xy} and h_{zx}.

the action and keeping only quadratic terms one can show that

$$\begin{aligned}\delta S &= \frac{1}{16\pi G_5}\int \mathrm{d}^5x\sqrt{-g}\left\{\psi^2\left(\frac{\Box p}{f}-\frac{p}{f^2}\Box f-\frac{3}{2f^2}\partial_\mu f\partial^\mu p+\frac{3p}{2f^3}(\partial f)^2\right)+\right.\\ &\quad+\frac{2p}{f}\psi\Box\psi-\frac{3p}{2f^2}\partial_\mu f\partial^\mu\psi^2+\frac{2}{f}\partial_\mu p\partial^\mu\psi^2+\\ &\quad-\frac{3p}{2f}\frac{(\partial_t\psi)^2}{U}+\frac{3p}{2f}U(\partial_r\psi)^2+\left(=\frac{3p}{2f}\partial_\mu\psi\partial^\mu\psi\right)\\ &\quad\left.-\left(R+\frac{12}{L^2}-F^2\right)\frac{p}{2f}\psi^2-\frac{p}{f}F^2\psi^2\right\},\end{aligned} \tag{4.31}$$

where the d'Alembertian is

$$\Box=-\frac{1}{U}\partial_t^2+U\partial_r^2+\left(U'+\frac{Uf'}{f}+\frac{Up'}{2p}\right)\partial_r. \tag{4.32}$$

The trace of Einstein field equations (i.e. Equation 4.2) gives $R+20/L^2=F^2/3$ and, integrating by parts the $\psi\Box\psi$ term, we rewrite the action in Equation 4.31 to

$$\begin{aligned}\delta S &= \frac{1}{16\pi G_5}\int d^5x\sqrt{-g}\left[-\frac{p}{2f}\partial_\mu\psi\partial^\mu\psi-\frac{p}{2f^2}\partial_\mu f\partial^\mu\psi^2+\frac{1}{f}\partial_\mu p\partial^\mu\psi^2+\right.\\ &\quad+\psi^2\left(\frac{\Box p}{f}-\frac{p}{f^2}\Box f-\frac{3}{2f^2}\partial_\mu f\partial^\mu p+\frac{3p}{2f^3}(\partial f)^2\right)+\\ &\quad\left.+\left(\frac{4p}{fL^2}\psi^2+\frac{F^2}{3}\frac{p}{f}\psi^2\right)-\frac{p}{f}F^2\psi^2\right].\end{aligned} \tag{4.33}$$

We now use Equation 4.2. One needs the zz equation,

$$\frac{4p}{fL^2}=\frac{\Box p}{2f}-\frac{(\partial p)^2}{2pf}-\frac{F^2}{3}\frac{p}{f}, \tag{4.34}$$

and also the yy equation,

$$-\frac{1}{2}\Box p+\frac{(\partial p)^2}{2p}=-\frac{4p}{L^2}-\frac{F^2}{3}p. \tag{4.35}$$

Using the Equation 4.34 in Equation 4.33 and integrating by parts once again, noting that

$$\frac{1}{f}\partial_\mu p\partial^\mu\psi^2=\nabla_\mu\left(\frac{\partial^\mu p}{f}\psi^2\right)+\frac{1}{f^2}\partial_\mu f\partial^\mu p\psi^2-\psi^2\frac{\Box p}{f}, \tag{4.36}$$

and

$$-\frac{p}{2f^2}\partial_\mu f\partial^\mu\psi^2=-\nabla_\mu\left(\psi^2\frac{p}{2f}\partial^\mu f\right)+\frac{\psi^2}{2f^2}\partial_\mu p\partial^\mu f-\frac{p}{f^3}\psi^2(\partial f)^2+\frac{p}{2f^2}\psi^2\Box f, \tag{4.37}$$

we arrive at

$$\begin{aligned}\delta S &= \frac{1}{16\pi G_5}\int d^5x\sqrt{-g}\left[-\frac{p}{2f}\partial_\mu\psi\partial^\mu\psi+\frac{p}{f}\psi^2+\right.\\ &\quad\left.+\frac{p}{f}\psi^2\left(\frac{1}{2}\frac{\Box p}{p}-\frac{1}{2f}\Box f+\frac{1}{2f^2}(\partial f)^2-\frac{(\partial p)^2}{2p^2}\right)-\frac{p}{f}F^2\psi^2\right].\end{aligned} \tag{4.38}$$

Finally, from Equation 4.34 and Equation 4.35

$$\frac{1}{2}\frac{\Box p}{p} - \frac{1}{2f}\Box f + \frac{1}{2f^2}(\partial f)^2 - \frac{(\partial p)^2}{2p^2} = F^2, \tag{4.39}$$

one can show that the action for the fluctuations Equation 4.38 becomes

$$\delta S = -\frac{1}{16\pi G_5}\int d^5x\,\sqrt{-g}\left(\frac{p(r)}{2f(r)}\partial_\mu\psi\partial^\mu\psi\right). \tag{4.40}$$

Therefore, we have a massless scalar field with a r dependent coupling $\mathcal{Z}(r) = 16\pi G_5 f/p$. These functions were found in the previous section to determine the thermodynamic properties of this system and, thus, in the next section we shall evaluate $\eta_\parallel$.

4.2.4 Viscosity bound violation due to an external magnetic field

From the result of the previous section, it follows that we can also apply the membrane paradigm to Equation 4.40 to evaluate $\eta_\parallel$, using Equation 4.20. We then have

$$\frac{\eta_\parallel}{s} = \frac{1}{4\pi}\frac{p(r_h)}{f(r_h)}. \tag{4.41}$$

In terms of the numerical, rescaled geometry described in Equation 4.10, we then obtain

$$\frac{\eta_\parallel}{s} = \frac{1}{4\pi}\frac{v}{w}. \tag{4.42}$$

Thus, the ratio $(\eta/s)_\parallel/(\eta/s)_\perp$ is given by v/w. Using this result, we can then evaluate the degree of anisotropy of the shear viscosities as a function of $\mathcal{B}/T^2$; see Figure 7. One can see that for $\mathcal{B}/T^2 \ll 1$, $\eta_\parallel \to \eta_\perp$, reflecting the fact that at high temperatures we recover the isotropic strongly coupled SYM plasma limit. The asymptotic behavior in the opposite limit, $\mathcal{B}/T^2 \gg 1$, can be understood by looking at the BTZ metric Equation 4.7, which is the relevant geometry in this case. Evaluating $\eta_\parallel$ in this limit, one obtains the asymptotic behavior

$$\frac{\eta_\parallel}{s} \sim \pi\frac{T^2}{\mathcal{B}} \text{ for } \mathcal{B} \gg T^2, \tag{4.43}$$

which is also shown in Figure 7.

We should note that in this model, $\eta_\parallel/s < 1/(4\pi)$ whenever $B > 0$. This gives another example in which the viscosity bound in a gravity dual is violated due to anisotropy. The formula above indicates that $\eta_\parallel/s$ can become much smaller than $1/(4\pi)$ for sufficiently strong fields. However, it is conceivable that in this limit other constraints must be imposed to obtain a well defined theory. In fact, it was found in Brigante et al. (2008b), Brigante et al. (2008a) that causality in the gauge theory constituted an important constraint that was used to set a lower value for η/s in that particular case involving higher order derivatives in the gravity dual. This matter deserves further study and we hope to address this question in the future.

Figure 7 – The ratio of shear viscosities $(\eta/s)_{\parallel}/(\eta/s)_{\perp}$ as a function of $\mathcal{B}/T^2$. The solid blue line is the numerical result from $(\eta/s)_{\parallel}/(\eta/s)_{\perp} = v/w$; the dashed red line is the asymptotic result valid only when $\mathcal{B} \gg T^2$ given by Equation 4.43.

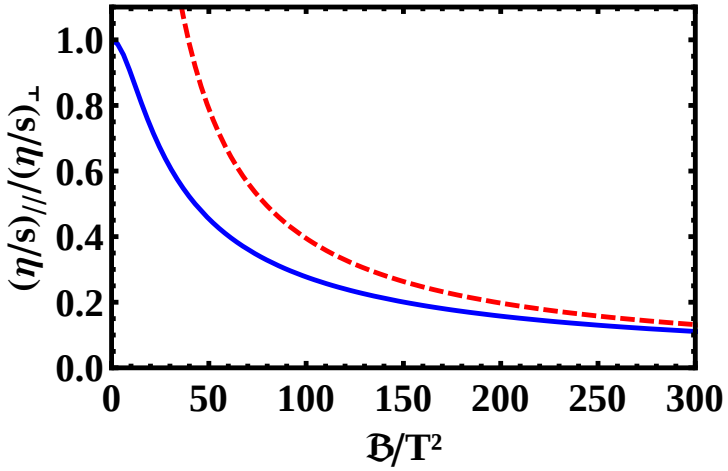

Source – Made by the authors.

4.3 Quasinormal modes for each scalar channels

We now analyze the near-equilibrium properties of the system encoded in its quasinormal modes as function of the magnetic field. In this section we calculate the QNM's for an external scalar perturbation on top of the magnetic brane background for each scalar channel, the parallel to the magnetic field $\phi_{\parallel}$ and the transversal to the magnetic field $\phi_{\perp}$. In each channel the field evaluated at the boundary act as a source for stress-energy tensor on the QFT side of the AdS/CFT correspondence. Each channel is described by corresponding the bulk action of a massless scalar field,

$$S = -\frac{1}{2}\int \mathrm{d}^5x\sqrt{-g}\frac{(\partial\phi)^2}{q(r)}, \tag{4.44}$$

where $\phi = \phi(t, \mathbf{x}, r)$ and $q(r)$ is the effective coupling. The perturbation of the metric transversal to the magnetic field is $\phi_{\perp} = h^y_x$, and the parallel is $\phi_{\parallel} = h^z_y$. The resulting equation of motion is

$$\partial_\mu\left(\frac{\sqrt{-g}}{q(r)}g^{\mu\nu}\partial_\nu\phi\right) = 0. \tag{4.45}$$

The numerical method used to obtain the QNM's in this section is direct numerical integration which is much less powerful and time consuming than the one recently used in section 5.2 called pseudospectral method. In order to make it less difficult to solve the following differential equations by numerical integration we consider just the hydrodynamical limit, i.e. when $\mathbf{k} \to \mathbf{0}$, which means the scalar function does not depend on position $\mathbf{x}$.

4.3.1 Transversal scalar channel

For the transversal perturbation of the metric, $\phi = h_x^y \equiv \phi_\perp(t,r)$, the effective coupling is $q_\perp(r) = 16\pi G_5$, and the equation of motion obeys

$$\phi_\perp'' + \left(\frac{U'}{U} + 2V' + W'\right)\phi_\perp' - \frac{\ddot{\phi}_\perp}{U^2} = 0, \tag{4.46}$$

where $\dot{\phi} \equiv \partial_t\phi$ and $\phi' \equiv \partial_r\phi$. Now we use the ansatz of plane wave functions propagating trough the bulk

$$\phi_\perp(t,r) = e^{-i\omega t}\tilde{\phi}_\perp(\omega,r). \tag{4.47}$$

As we will soon see, ω assumes only a discrete spectrum, then one cannot take Fourier transform in principle.

In addition to the plane wave solution we will simplify the differential equation in order to better manipulate the method of numerical integration, thus we rescale the holographic coordinate to $r \to r_H r$ so the event horizon is now located at $r = 1$, also the metric components are normalized to $U(r) \to r_H U_H' U(r)$, $V(r) \to V_H + V(r)$, and $W(r) \to W_H + W(r)$. The Hawking temperature is a scalar and takes the value

$$T = \frac{U_H'}{4\pi}. \tag{4.48}$$

The equation of motion reduces to

$$\tilde{\phi}_\perp'' + \left(\frac{U'}{U} + 2V' + W'\right)\tilde{\phi}_\perp' + \frac{(\omega/\pi T)^2}{16U^2}\tilde{\phi}_\perp = 0, \tag{4.49}$$

where $\omega/\pi T$ is an eigenvalue (that still needs well defined boundary conditions which we will soon offer). We choose the in-falling wave solution for the same reasons claimed in section 3.4, that is, to preserve causality in the gravity side so one identify a retarded Green function at the boundary QFT. One can compute the exponent α (for guidance see Equation 3.54) then

$$\tilde{\phi}_\perp(r) = (r-1)^{-i\frac{\omega}{\pi T}}P_\perp(r), \tag{4.50}$$

and we are free to choose a finite and nonzero value for $P_\perp$ at the horizon because the differential equation is homogeneous, then $P_\perp(1) = 1$.

Using this ansatz, the resulting differential equation becomes

$$\begin{aligned} P_\perp'' + \left(\frac{U'}{U} + 2V' + W' - \frac{i(\omega/\pi T)}{2(r-1)}\right)P_\perp' + \\ + \left(\frac{(\omega/\pi T)^2}{16U^2} - \frac{i(\omega/\pi T)(U' + U(2V'+W'))}{4U(r-1)} - \frac{(\omega/\pi T)(\omega/\pi T - 4i)}{16(r-1)^2}\right)P_\perp &= 0. \end{aligned} \tag{4.51}$$

To completely specify the eigenvalue problem to be solved in order to find the QNM spectra associated to this scalar channel, we still need to impose a Dirichlet boundary

condition. From the fact that $\tilde{\phi}$ is a scalar field defined on an asymptotically AdS_5 background, it follows that asymptotically close to the boundary it may be written as $\tilde{\phi}(r) = G(r) + \frac{F(r)}{r^4}$, with the leading, non-normalizable mode $\lim_{r\to\infty} G(r) = J(\omega)$ being the source for the QFT operator $\hat{O}$ dual to the scalar field ϕ, and the subleading, normalizable mode $\lim_{r\to\infty} F(r) = \langle\hat{O}(\omega)\rangle$ being its expectation value. According to the real time holographic dictionary (SON; STARINETS, 2002), the retarded propagator of the QFT operator $\hat{O}$ is given by the ratio between the normalizable and non-normalizable modes, $\mathcal{G}^R_{\hat{O}\hat{O}}(\omega) = -\langle\hat{O}(\omega)\rangle/J(\omega)$. Therefore, if we impose, as a Dirichlet boundary condition, the selection of the normalizable mode (i.e. no source for the QFT operator $\hat{O}$) by setting $\lim_{r\to\infty} G(r) = 0$ with $\lim_{r\to\infty} F(r) \neq 0$, we are left with an eigenvalue problem whose eigenfrequencies correspond to a dispersion relation where B/T^2 is the parameter, describing the poles of $\mathcal{G}^R_{\hat{O}\hat{O}}$, which are the QNM's we are looking for. This argument is mathematically summarized to

$$\lim_{r\to+\infty} P_\perp(r) = 0. \tag{4.52}$$

After one solves the Equation 4.51 with the Dirichlet boundary conditions one obtains the graphs below that show the evolution of the two lowest quasinormal modes as function of the physical magnetic field Figure 8, and also for each component in Figure 9.

Figure 8 – Flow direction of the lowest QNM's for the transversal scalar channel as the magnetic field B/T^2 increases.

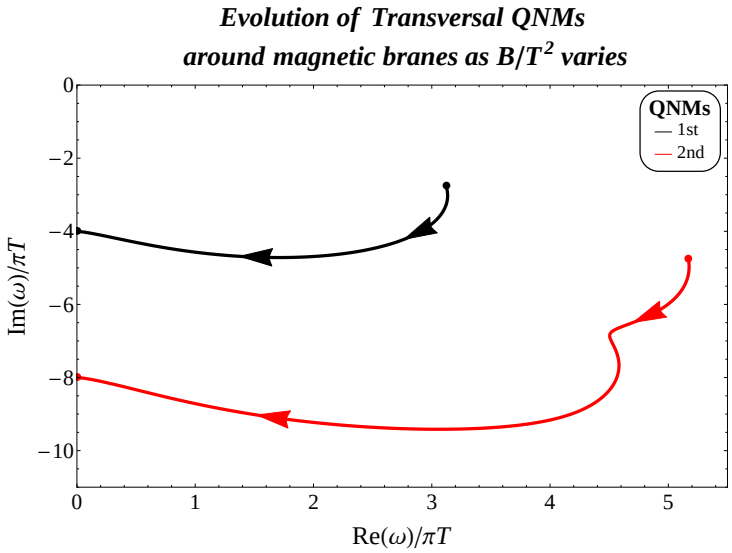

Source – Made by the authors.

Notice the QNM's becomes purely imaginary as the magnetic field goes to infinity.

Figure 9 – QNM's for the transversal scalar channel for a given value of the magnetic field B/T^2.

(a) Real part (b) Imaginary part

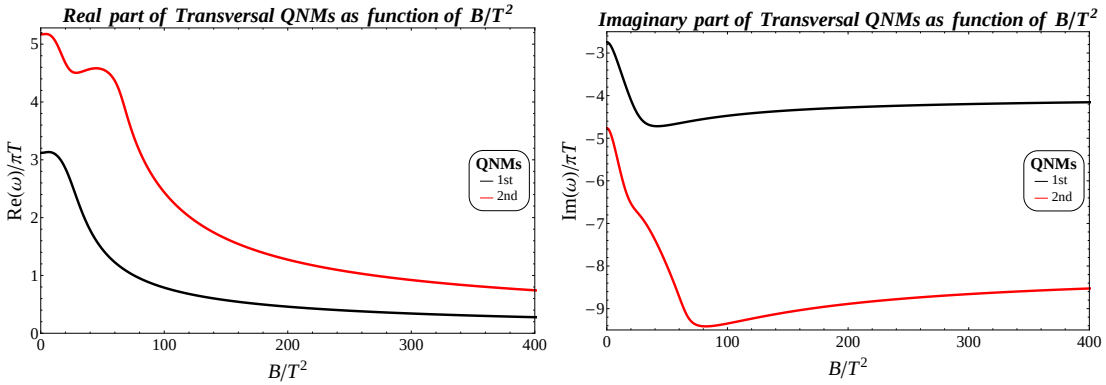

Source – Made by the authors.

4.3.2 Parallel scalar channel

For the case which $\phi = h_y^z \equiv \phi_\parallel(t,r)$ the effective coupling is $q_\parallel(r) = 16\pi G_5 e^{2(V-W)}$, and the equation of motion obey

$$\phi_\parallel'' + \left(\frac{U'}{U} + 3W'\right)\phi_\parallel' - \frac{\ddot{\phi}_\parallel}{U^2} = 0. \tag{4.53}$$

The resolution will be very similar as done for the transversal case. We use the ansatz of plane wave functions propagating trough the bulk

$$\phi_\parallel(t,r) = e^{-i\omega t}\tilde{\phi}_\parallel(\omega,r). \tag{4.54}$$

We also add the same rescaling for r and the components of the metric. The differential equation reduces to

$$\tilde{\phi}_\parallel'' + \left(\frac{U'}{U} + 3W'\right)\tilde{\phi}_\parallel' + \frac{(\omega/\pi T)^2}{16U^2}\tilde{\phi}_\parallel = 0 \tag{4.55}$$

Now we choose the in-falling wave solution with the same exponent as the transversal case

$$\tilde{\phi}_\parallel(r) = (r-1)^{-i\frac{\omega}{\pi T}}P_\parallel(r), \tag{4.56}$$

with $P_\parallel(1) = 1$.

Using this ansatz, the resulting differential equation is

$$\begin{aligned} P_\parallel'' + \left(\frac{U'}{U} + 3W' - \frac{i(\omega/\pi T)}{2(r-1)}\right)P_\parallel' + \\ + \left(\frac{(\omega/\pi T)^2}{16U^2} - \frac{i(\omega/\pi T)(U'+3UW')}{4U(r-1)} - \frac{(\omega/\pi T)(\omega/\pi T - 4i)}{16(r-1)^2}\right)P_\parallel \;=\; 0. \end{aligned} \tag{4.57}$$

Selecting the normalizable mode at the boundary is to impose

$$\lim_{r\to+\infty} P_{\parallel}(r) = 0. \tag{4.58}$$

Solving the eigenvalues above we obtain the graphs below that show the evolution of the two lowest quasinormal modes as function of the physical magnetic field Figure 10, and also for each component in Figure 11.

Figure 10 – Flow direction of the lowest QNM's for the parallel scalar channel as the magnetic field B/T^2 increases.

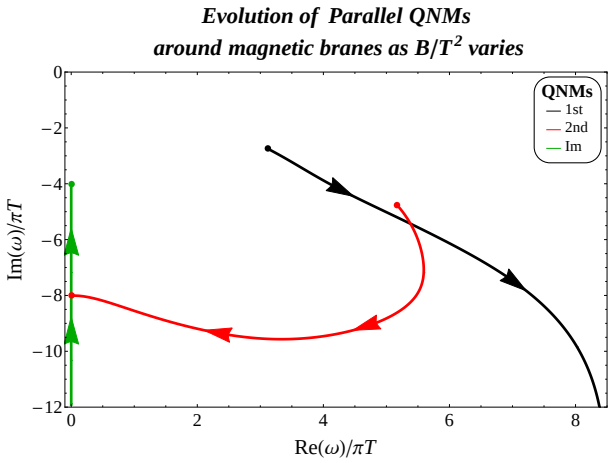

Source – Made by the authors.

Notice that only one of the QNM's becomes purely imaginary as the magnetic field goes to infinity, while the other increases both the real and imaginary part. There is a third quasinormal mode which is purely imaginary dominating the dynamics at finite magnetic field. This third mode was also observed by Janiszewski and Kaminski (2016).

Figure 11 – QNM's for the parallel scalar channel for a given value of the magnetic field B/T^2.

(a) Real part

(b) Imaginary part

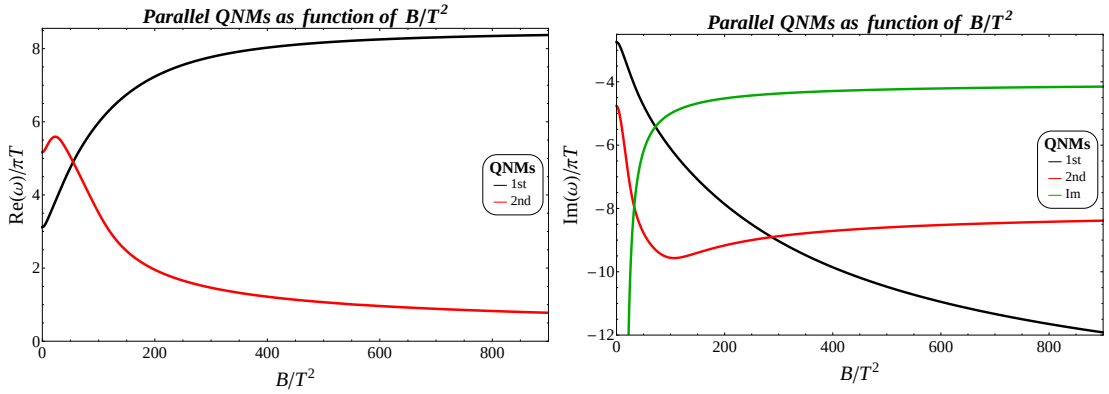

Source – Made by the authors.

5 Critical behavior of non-hydrodynamic quasinormal modes in a strongly coupled plasma

This chapter directly follows the second and last article published during my PhD (FINAZZO et al., 2017). This is the main chapter of this thesis. In section 5.1 we briefly review the 1RCBH model and its thermodynamics and phase diagram. Then we compute the QNM's for an external scalar perturbation in section 5.2 and for the vector diffusion channel in the limit of long wavelengths in section 5.3. This work is complemented by subsection 5.2.4, where we compute the spectral function in the external scalar channel. A discussion of the pseudo-spectral method, used in the numerical calculations done here, can also be found in this chapter.

5.1 1-R charge black hole model

For the sake of completeness, in this section we review the thermodynamics of the 1RCBH model (GUBSER, 1999; BEHRNDT; CVETIC; SABRA, 1999; KRAUS; LARSEN; TRIVEDI, 1999; CAI; SOH, 1999; CVETIC; GUBSER, 1999a; CVETIC; GUBSER, 1999b). We closely follow the discussion made in DeWolfe, Gubser and Rosen (2011b, chap. 4) and supplement it with additional plots to better illustrate the behavior of the thermodynamic properties of the model near the critical point.

5.1.1 Background

The 1RCBH model is described by an Einstein-Maxwell-dilaton (EMD) action,

$$S = \frac{1}{2\kappa_5^2}\int d^5x\sqrt{-g}\left[R - \frac{f(\phi)}{4}F_{\mu\nu}F^{\mu\nu} - \frac{1}{2}(\partial_\mu\phi)^2 - V(\phi)\right], \tag{5.1}$$

with the dilaton potential and the coupling between the dilaton and Maxwell fields given by, respectively,

$$V(\phi) = -\frac{1}{L^2}\left(8e^{\frac{\phi}{\sqrt{6}}} + 4e^{-\sqrt{\frac{2}{3}}\phi}\right) \text{ and } f(\phi) = e^{-2\sqrt{\frac{2}{3}}\phi}, \tag{5.2}$$

where κ_5^2 is the five dimensional Einstein's constant and L is the asymptotic AdS_5 radius. With these profiles for $V(\phi)$ and $f(\phi)$, one obtains a consistent truncation of maximally supersymmetric gauged supergravity in five dimensions, which is itself a consistent truncation of type IIB superstring theory on $AdS_5\times S^5$. This model is a *bona fide* top-down string theory construction, which is dual to a SYM plasma with a finite chemical potential

under a U(1) subgroup of the global SU(4) symmetry of R-charges. For simplicity, in the following we set $L = 1$ without loss of generality.

The 1RCBH line element has the following ansatz

$$ds^2 = e^{2A(r)}\left(-h(r)dt^2 + d\vec{x}^2\right) + \frac{e^{2B(r)}}{h(r)}dr^2, \tag{5.3}$$

where r is the holographic radial coordinate and the boundary of the asymptotically AdS_5 geometry is located at $r \to \infty$. The components of this metric have analytical solution,

$$\begin{aligned} A(r) &= \ln r + \frac{1}{6}\ln\left(1 + \frac{Q^2}{r^2}\right), \\ B(r) &= -\ln r - \frac{1}{3}\ln\left(1 + \frac{Q^2}{r^2}\right), \\ h(r) &= 1 - \frac{M^2}{r^2(r^2+Q^2)}, \end{aligned} \tag{5.4}$$

where Q is the charge and M is the mass of the black brane. The radial position of the black brane horizon may be written in terms of these two parameters as follows,

$$r_H = \sqrt{\frac{\sqrt{Q^4 + 4M^2} - Q^2}{2}}. \tag{5.5}$$

The 1RCBH background is, thus, completely characterized by two nonnegative[1] parameters, (Q, M) or, alternatively, (Q, r_H). This charge Q is responsible for the presence of an electrostatic potential described by the following electromagnetic potential vector,

$$\mathbf{A} = \Phi(r)dt = \left(-\frac{MQ}{r^2+Q^2} + \frac{MQ}{r_H^2+Q^2}\right)dt. \tag{5.6}$$

And, finally, the dilaton which couples to the Maxwell fields reads

$$\phi(r) = -\sqrt{\frac{2}{3}}\ln\left(1 + \frac{Q^2}{r^2}\right). \tag{5.7}$$

5.1.2 Phase diagram

The class of solutions corresponding to the 1RCBH model may be parametrized by different values of the dimensionless ratio Q/r_H which is the ratio between two extrinsic parameters of the black brane. In this subsection we show how to obtain the equivalent but thermodynamical parameter μ/T which, this time, is the ratio between two intrinsic parameters: the Hawking temperature T and the chemical potential μ. We will note that in this model any dimensionless ratio of thermodynamical quantities is always written in terms of μ/T, as expected

[1] For simplicity, the charge Q is considered nonnegative without loss of generality.

The Hawking temperature of the black brane horizon is given by

$$T = \left.\frac{\sqrt{-(g_{tt})'(g^{rr})'}}{4\pi}\right|_{r=r_H} = \frac{Q^2+2r_H^2}{2\pi\sqrt{Q^2+r_H^2}}, \tag{5.8}$$

where the prime symbol $'$ denotes a derivative with respect to r. On the other hand, the U(1) R-charge chemical potential reads

$$\mu = \lim_{r\to\infty}\Phi(r) = \frac{Qr_H}{\sqrt{Q^2+r_H^2}}. \tag{5.9}$$

Dividing the Equation 5.8 by Equation 5.9 and then solving for Q/r_H, one obtains

$$\frac{Q}{r_H} = \sqrt{2}\left(\frac{1\pm\sqrt{1-\left(\frac{\mu/T}{\pi/\sqrt{2}}\right)^2}}{\frac{\mu/T}{\pi/\sqrt{2}}}\right). \tag{5.10}$$

Since Q/r_H is nonnegative, Equation 5.10 implies that $\mu/T \in \left[0,\pi/\sqrt{2}\right]$. It also follows from Equation 5.10 that for every value of $\mu/T \in \left[0,\pi/\sqrt{2}\right)$, there are two different corresponding values of Q/r_H, which parametrize two different branches of solutions. As we are going to show in the next subsection, by analyzing the thermodynamics of the 1RCBH solutions one concludes that the point of the phase diagram where these two branches merge, $\mu/T = \pi/\sqrt{2}$ or, correspondingly, $Q/r_H = \sqrt{2}$, is a critical point of a second order phase transition.

In order to simplify the equations that lie ahead in this chapter, we define below a useful variable that smoothly connects these two branches of solutions,

$$y^2 + \left(\frac{\mu/T}{\pi/\sqrt{2}}\right)^2 = 1 \text{ with } y\in[-1,1], \tag{5.11}$$

where $y=0$ parametrizes the critical background geometry with $\mu/T = \pi/\sqrt{2}$, while $y=1$ parametrizes the AdS_5-Schwarzschild background, corresponding to $Q=0$ and $r_H \neq 0$, which implies $\mu/T = 0$. For $y=-1$ we also have $\mu/T=0$, but this time $r_H = 0$ and $Q\neq 0$, which corresponds to a supersymmetric BPS solution dubbed "superstar" (MYERS; TAFJORD, 2001) instead of a black hole.

As we are going to see in the next subsection, the thermodynamically stable branch corresponds to the lower sign in Equation 5.10 with $Q/r_H \in \left[0,\sqrt{2}\right)$ or $y\in\left(0,1\right]$, while the thermodynamically unstable branch corresponds to the upper sign in Equation 5.10 with $Q/r_H \in \left(\sqrt{2},\infty\right)$ or $y\in\left[-1,0\right)$, with both branches of solutions being smoothly connected at the critical point, $Q/r_H = \sqrt{2}$ or $y=0$. This is illustrated in Figure 12.

5.1.3 Thermodynamics: equation of state and susceptibilities

For a SYM plasma, it is known that (GUBSER; KLEBANOV; PEET, 1996)

$$\frac{1}{\kappa_5^2} = \frac{N_c^2}{4\pi^2}. \tag{5.12}$$

Figure 12 – Phase structure of the 1RCBH model (closely following the discussion in DeWolfe, Gubser and Rosen (2011b, chap. 4)): (a) the single dimensionless control parameter of the QFT phase diagram, μ/T, as a function of the corresponding dimensionless ratio Q/r_H on the gravity side for both stable and unstable branches (note that the superstar solution lies at $Q/r_H \to \infty$); (b) the same, now in terms of the alternative variable y defined in Equation 5.11.

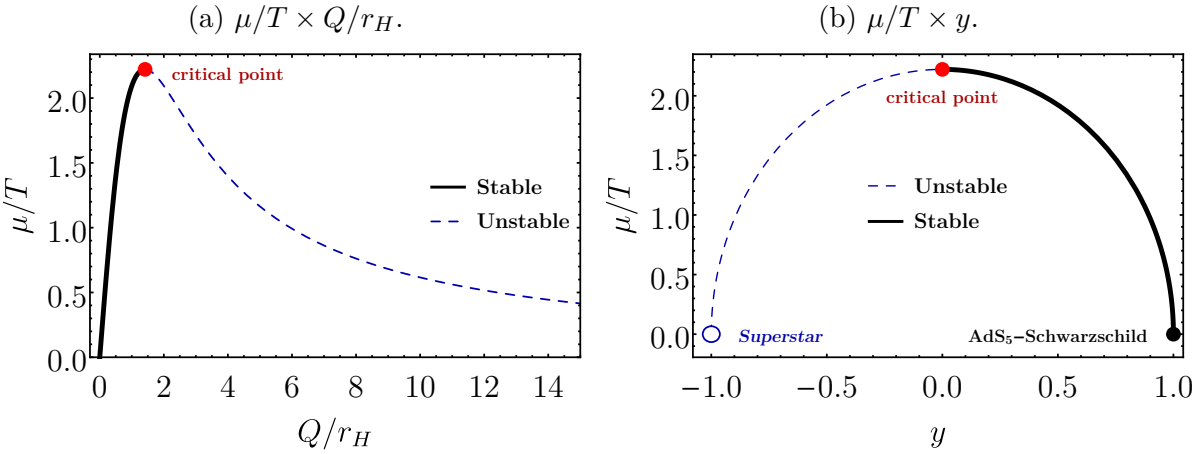

Source – Made by the authors.

By substituting the expression above in Bekenstein-Hawking's relation (BEKENSTEIN, 1973; HAWKING, 1975), one can write down the entropy density, $s = A_H/4G_5$ (see Table 1), as follows

$$\frac{s}{N_c^2 T^3} = \frac{\pi^2}{16}(3+y)^2(1-y). \tag{5.13}$$

The R-charge density, $\rho = \lim_{r\to\infty} \delta S/\delta\Phi'$, may be written as

$$\frac{\rho}{N_c^2 T^3} = \frac{\mu/T}{16}(3+y)^2. \tag{5.14}$$

From the Gibbs-Duhem relation, $dp = sdT + \rho d\mu$, one may compute the pressure,

$$\frac{p}{N_c^2 T^4} = \frac{\pi^2}{128}(3+y)^3(1-y). \tag{5.15}$$

Using the Equation 5.13, the Equation 5.14 and the Equation 5.15 one can readily evaluate the internal energy density, $\varepsilon = Ts - p + \mu\rho$, obtaining $\varepsilon = 3p$, as expected for a conformal QFT in four dimensions.

The heat capacity at fixed chemical potential is given by $C_\mu = (\partial s/\partial T)_\mu$, while the nth-order R-charge susceptibility is given by $\chi_n = (\partial^n p/\partial\mu^n)_T$ (note that $\chi_1 = \rho$). At the critical point the heat capacity C_μ and the higher order susceptibilities $\chi_{n\geq 2}$ diverge. In Figure 13 we show the equation of state and the heat capacity while in Figure 14 we display the susceptibilities for the stable and unstable branches of the 1RCBH model.

Figure 13 – Equation of state and heat capacity for the 1RCBH model (closely following the discussion in DeWolfe, Gubser and Rosen (2011b, chap. 4)).

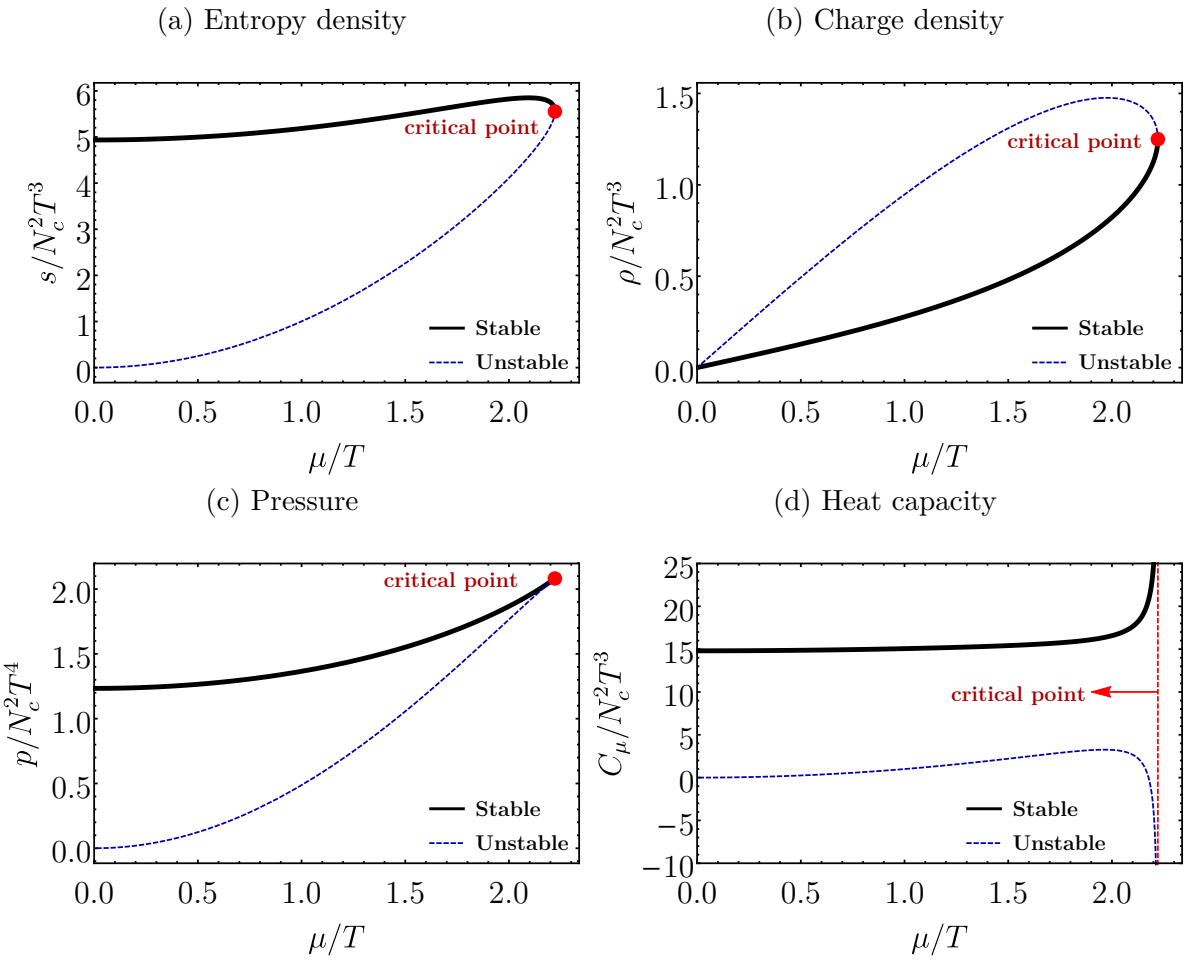

Source – Made by the authors.

In the 1RCBH model one obtains the Jacobian $\mathcal{J} = \partial(s,\rho)/\partial(T,\mu)$ to be

$$\frac{\mathcal{J}}{N_c^4 T^4} = \frac{3\pi^2}{256}(3-y)^4\left(1+\frac{1}{y}\right). \tag{5.16}$$

Thermodynamical stability is ensured if $\mathcal{J} > 0$, therefore, analyzing the Equation 5.16 we note that the quartic term is always positive while the expression in the last parenthesis becomes negative for $y \in \big(-1, 0\big)$, justifying the aforementioned classification of stable and unstable branches[2].

Finally, by analyzing the behavior of the R-charge density in Equation 5.14 near the critical point, one can obtain the static critical exponent $\delta = 2$ as discussed in Maeda, Natsuume and Okamura (2008), Buchel (2010), DeWolfe, Gubser and Rosen (2011b).

[2] Note that the superstar solution ($y = -1$) has $\mathcal{J} = 0$ and corresponds to a saddle point.

Figure 14 – nth-order susceptibilities for the 1RCBH model.

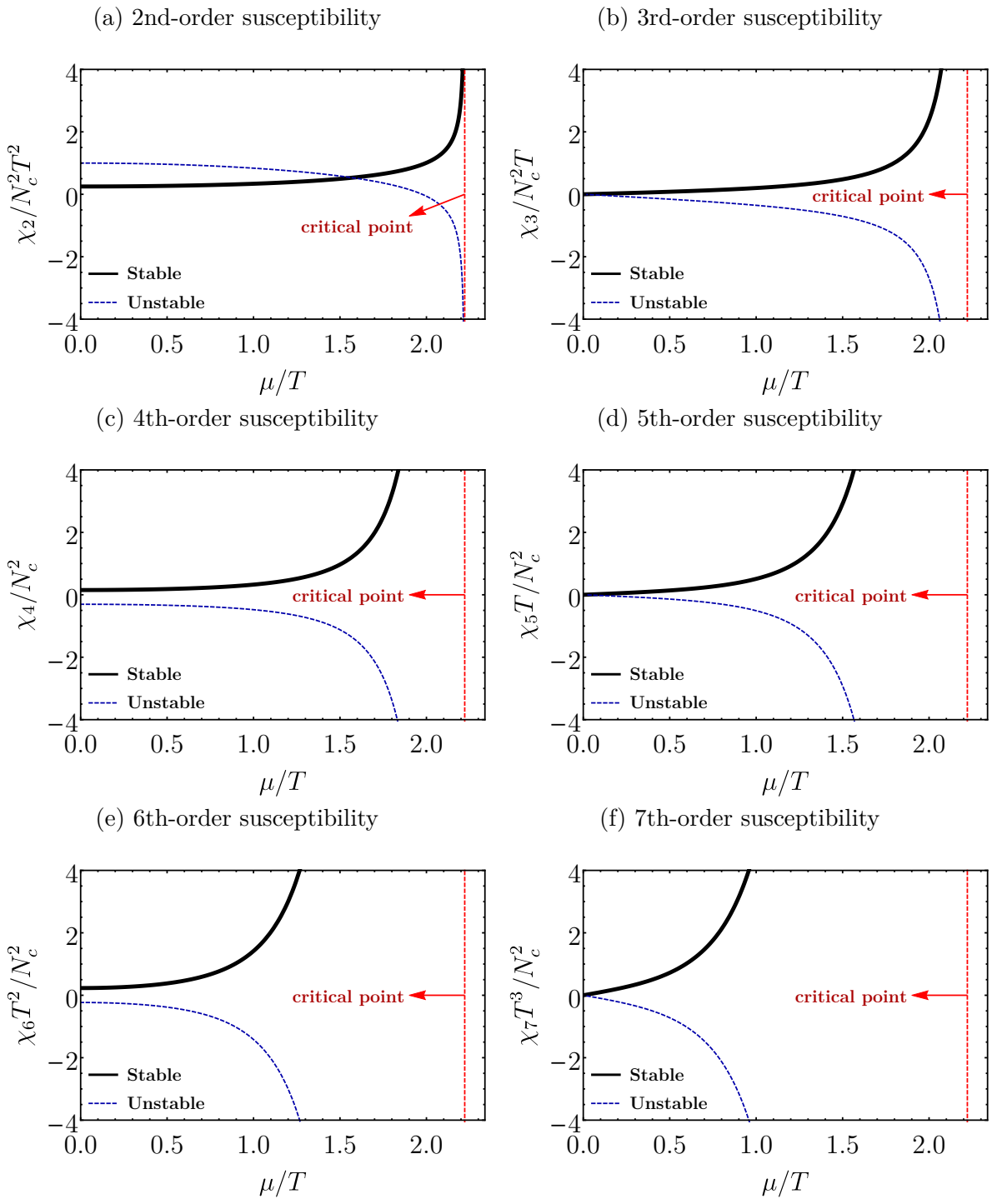

Source – Made by the authors.

5.2 QNM's for an external scalar fluctuation

In the previous section we reviewed the thermodynamical equilibrium properties of the 1RCBH plasma. We now analyze near-equilibrium properties of the system encoded in its quasinormal modes. In this section we calculate the QNM's for an external scalar perturbation φ on top of the 1RCBH backgrounds (which may be interpreted as the source

for stress-energy tensor on the QFT side of the AdS/CFT correspondence) described by the bulk action,

$$S = \frac{1}{2\kappa_5^2}\int d^5x\sqrt{-g}\left[-\frac{1}{2}(\partial_\mu\varphi)^2\right]. \tag{5.17}$$

In order to find these QNM's we will use the pseudospectral method and closely follow the procedure made by Yaffe (2014) that applied this method to a scalar channel on AdS_5-Schwarzschild background and compared the matching spectra to Starinets (2002, p. 9).

5.2.1 Equation of motion

The equation of motion following from Equation 5.17 is just the massless Klein-Gordon equation on top of the solution given by Equation 5.3. We take a plane-wave ansatz for the Fourier modes of the perturbation (it is not a completeness relation), $\varphi(t,\vec{x},r) = e^{-i\omega t+i\vec{k}\cdot\vec{x}}\tilde{\varphi}(\omega,\vec{k},r)$, which for brevity we write simply as $\tilde{\varphi}(\omega,\vec{k},r) \equiv \tilde{\varphi}(r)$ because the differential equations ahead have r as its variable while ω and $\vec{k}$ are treated as parameters. More precisely, the resulting equation of motion will depend on the frequency ω, the magnitude of the spatial 3-momentum $k \equiv |\vec{k}|$, and the background control parameter y.

In what follows we employ the in-falling Eddington-Finkelstein (EF) "time" coordinate defined by

$$dv = dt + \sqrt{-\frac{g_{rr}}{g_{tt}}}dr = dt + \frac{e^{B-A}}{h}dr, \tag{5.18}$$

in terms of which the line element in Equation 5.3 then becomes

$$ds^2 = e^{2A}\left(-hdv^2 + d\vec{x}^2\right) + 2e^{A+B}dvdr. \tag{5.19}$$

One of the main advantages of the EF coordinates is that the in-falling wave condition at the horizon, which is associated with the retarded Green's function, becomes automatically satisfied by just requiring regularity of the solutions there. In these coordinates, the equation of motion for $\tilde{\varphi}$ becomes

$$\tilde{\varphi}'' + \left(4A' - B' + \frac{h'}{h}\right)\tilde{\varphi}' - i\omega\frac{e^{B-A}}{h}(2\tilde{\varphi}' + 3A'\tilde{\varphi}) - k^2\frac{e^{2(B-A)}}{h}\tilde{\varphi} = 0. \tag{5.20}$$

We map the radial coordinate r, defined on the interval $r_H \leq r < \infty$, to a new dimensionless radial coordinate $u = r_H/r$, defined on the interval $0 \leq u \leq 1$, which is more suitable to be used in the pseudospectral method (BOYD, 2013) (to be briefly reviewed in subsection 5.2.2). In these new coordinates, the equation of motion for the external scalar

perturbation becomes

$$\begin{aligned}
&\tilde{\varphi}'' - \frac{\left(u^4(3-y)+2u^2(1-y)-3(1+y)\right)\tilde{\varphi}'}{u\left(1-u^2\right)\left(u^2(3-y)+1+y\right)} + \\
&-\frac{2i(\omega/T)}{\pi\left(1-u^2\right)\sqrt{3-y}\left(u^2(3-y)+1+y\right)}\left(\frac{\left(4u^2(1-y)+3(y+1)\right)\tilde{\varphi}}{u\sqrt{2u^2(1-y)+1+y}} + \right. \\
&\left. +2\sqrt{2u^2(1-y)+1+y}\,\tilde{\varphi}'\right) - \frac{4(k/T)^2\tilde{\varphi}}{\pi^2\left(1-u^2\right)(3-y)\left(u^2(3-y)+1+y\right)} = 0,
\end{aligned} \tag{5.21}$$

where the primes $'$ now denote derivatives with respect to the new radial coordinate u. From the discussion above, and from the definition of the background control parameter y in Equation 5.11, one concludes that the dimensionless quasinormal eigenfrequencies, ω/T, will depend only on the dimensionless ratios μ/T and k/T.

To completely specify the eigenvalue problem to be solved in order to find the QNM spectra associated to this external scalar perturbation, we still need to impose a Dirichlet boundary condition. From the fact that $\tilde{\varphi}$ is a scalar field defined on an asymptotically AdS_5 background, it follows that asymptotically close to the boundary it may be written as $\tilde{\varphi}(u) = G(u) + u^4 F(u)$, with the leading, non-normalizable mode $G(0) = J(\omega, \vec{k})$ being the source for the QFT operator $\hat{O}$ dual to the (external) scalar field φ, and the subleading, normalizable mode $F(0) = \langle\hat{O}(\omega, \vec{k})\rangle$ being its expectation value. According to the real time holographic dictionary (SON; STARINETS, 2002), the retarded propagator of the QFT operator $\hat{O}$ is given by the ratio between the normalizable and non-normalizable modes, $\mathcal{G}^R_{\hat{O}\hat{O}}(\omega, \vec{k}) = -\langle\hat{O}(\omega, \vec{k})\rangle/J(\omega, \vec{k})$. Therefore, if we impose, as a Dirichlet boundary condition, the selection of the normalizable mode (i.e. no source for the QFT operator $\hat{O}$) by setting $G(0) = 0$ with $F(0) \neq 0$, we are left with an eigenvalue problem whose eigenfrequencies correspond to the dispersion relation $\omega/T = \omega(k/T; \mu/T)/T$ describing the poles of $\mathcal{G}^R_{\hat{O}\hat{O}}$, which are the QNM's we are looking for. From Equation 5.21 we set $\tilde{\varphi}(u) = u^4 F(u)$ with $F(0) \neq 0$, then we obtain

$$\begin{aligned}
&16u\left(1-\frac{2}{u^2(3-y)+1+y}\right)F + \left(u^2\left(9-\frac{8}{u^2(3-y)+1+y}\right)-5\right)F' + \\
&-u\left(1-u^2\right)F'' + \frac{2i(\omega/T)}{\pi\sqrt{3-y}\left(u^2(3-y)+1+y\right)}\left(-\frac{\left(12u^2(1-y)+5(1+y)\right)F}{\sqrt{2u^2(1-y)+1+y}} + \right. \\
&\left. +2u\sqrt{2u^2(1-y)+1+y}\,F'\right) + \frac{4(k/T)^2 uF}{\pi^2(3-y)\left(u^2(3-y)+1+y\right)} = 0.
\end{aligned} \tag{5.22}$$

We now have a Generalized Eigenvalue Problem (GEP) for the eigenfunction $F(u)$ and the quasinormal eigenfrequency ω/T, which may be solved as functions of k/T and μ/T via pseudospectral method. Note that Equation 5.22 also reveals one of the greatest

virtues of the EF coordinates, namely, the fact that it reduces the QNM eigenvalue problem from a Quadratic Eigenvalue Problem (TISSEUR; MEERBERGEN, 2001) in the standard set of spacetime coordinates to a GEP, which requires far less computational cost when numerically evaluating the QNM spectra.

5.2.2 Brief overview of the pseudospectral method

The main numerical algorithm we employ in this work to find the QNM's is the pseudospectral method (BOYD, 2013). In this section, we briefly review the main steps required to tackle the problem. The main advantage of the pseudospectral method, when compared to other methods used in the literature to calculate QNM's, is the ease of numerical implementation and the accuracy — in general, it requires a modest number of collocation points and basis functions in order to compute several QNM's with high accuracy. The main disadvantage is the requirement of high numerical precision in the intermediate calculations, which still brings a drawback in terms of running time, since typical machine precision calculations result in spurious results for any but the lowest QNM's.

The general spectral method, of which the pseudospectral (or collocant) method is a particular case[3], aims to solve the following general non-homogeneous differential equation for a complex function $f(u)$,

$$\hat{L}f(u) = h(u), \tag{5.23}$$

where $\hat{L}$ is a general differential operator and $h(u)$ is the non-homogeneous term. One may consider, for instance, the basic interval $u \in [0, 1]$, which was used to define the radial holographic coordinate u in the main text (with the boundary at $u = 0$ and the horizon at $u = 1$). In finite difference methods one discretizes the basic interval using a finite grid and introduce finite difference approximations for the derivatives. In both spectral and pseudospectral methods, one instead introduces a subset $\{\phi_i(u)\}_{i=0}^{N}$ of a complete set $\{\phi_i(u)\}_{i=0}^{\infty}$ of orthogonal basis functions defined on the basic interval, approximating $f(u)$ by its truncated base expansion $f_N(u)$,

$$f(u) \approx f_N(u) = \sum_{i=0}^{N} a_i \phi_i(u). \tag{5.24}$$

[3] The main difference between spectral and pseudospectral methods regards the determination of the coefficients a_i to be specified in the sequel. As explained in Boyd (2013), the nomenclature used in the literature is a bit messy: both spectral and pseudospectral methods are known as spectral methods in a broad sense, due to the fact that they use a complete set of orthogonal functions. In the restricted sense, spectral methods (also called non-collocant methods) determine the generalized Fourier coefficients by exploiting the orthogonality of the basis, projecting down the unknown function $f(u)$. On the other hand, pseudospectral methods (also known as collocant methods) use a selected set of points on the function domain in order to build an interpolating polynomial. For the purposes of the present work, we will consider only pseudospectral (or collocant methods) in this restricted sense.

Now we consider the pseudospectral method in order to determine the coefficients a_i that best provide an approximation $f_N(u)$ for $f(u)$. First, one introduces the residual function $R\,(u;\{a_i\})$ defined by,

$$R\,(u;\{a_i\}) = \hat{L}f_N(u) - h(u) = \sum_{i=0}^{N} a_i \hat{L}\phi_i(u) - h(u). \tag{5.25}$$

The strategy is to suitably choose a set of points $\{u_j\}_{j=0}^{N}$ (the so-called collocation points) on the domain of the basis functions ϕ_i, and then fix a_i such that the residual function is zero at u_j, that is, $R(u_j;\{a_i\}) = 0$. This generates a system of N linear differential equations with N variables, $\{a_i\}$,

$$\sum_{i=0}^{N} a_i[\hat{L}\phi_i](u_j) = h(u_j). \tag{5.26}$$

By solving for $\{a_i\}$ one determines the approximate solution $f_N(u)$.

There are several possible choices for the basis functions ϕ_i and collocation points u_j, depending on the symmetries of the problem and boundary conditions. A generally proposed basis defined in the interval $x \in [-1,1]$ is given by the Chebyshev polynomials[4], $T_n(x)$. Since $u \in [0,1]$, we can relate these variables by $x = 2u-1$, then $\phi_i(u) = T_i(2u-1)$. A useful accompanying set of collocant points is given by the so-called Gauss-Lobatto grid, which for $u \in [0,1]$ can be written as,

$$u_j = \frac{1}{2}\left[1 - \cos\left(\frac{j\pi}{N}\right)\right], \text{ for } j = 0, 1, ..., N. \tag{5.27}$$

The Chebyshev polynomials along with the Gauss-Lobatto grid take the basis function at each collocant point to be[5]

$$\begin{aligned} \phi_i(u_j) = \cos\left(\frac{ij\pi}{N}\right),\ \phi_i'(u_j) = 2i\csc\left(\frac{j\pi}{N}\right)\sin\left(\frac{ij\pi}{N}\right), \\ \text{and } \phi_i''(u_j) = 4i\csc^2\left(\frac{j\pi}{N}\right)\left(\cot\left(\frac{j\pi}{N}\right)\sin\left(\frac{ij\pi}{N}\right) - i\cos\left(\frac{ij\pi}{N}\right)\right). \end{aligned} \tag{5.28}$$

Finally, we can solve the Generalized Eigenvalue Problem (GEP) which we are interested in by extending the operator $\hat{L}$ to include a dependence on a parameter λ, $\hat{L} \to \hat{L}(\lambda) = \hat{L}_0 + \lambda\hat{L}_1$, and then taking $h(u) = 0$, such as to search for eigenvalues $\lambda \equiv \omega/T$ satisfying $\hat{L}(\lambda)f(u) = 0$ with boundary values $f(0) = f_0$ and $f(1) = f_1$. The resulting matrix GEP is then,

$$(A_0 + A_1\lambda)\,a = 0, \tag{5.29}$$

where $a = \{a_i\}$ and $A_k = \{A_{k,ij}\} = \{[\hat{L}_k\phi_i](u_j)\}$ with $k \in \{0,1\}$.

[4] The Chebyshev polynomials are defined to be the set of polynomials satisfying $T_n(\cos\theta) = \cos(n\theta)$ for every angle $\theta \in [0,\pi]$ and $n \in \mathbb{N}$.

[5] The letters "i" in these equations are not the imaginary numbers.

In this work, we used a Chebyshev basis with N basis functions and collocant points, and then employed the Arnoldi method (via the built-in `Eigensystem[]` procedure in Wolfram... (2016)) to solve the resulting GEP[6] for ω/T. For higher order QNM's, one needs to use high numerical precision from the outset. Denoting the number of floating-point digits used in the calculations by M, the final error estimate of the numerical QNM's is mainly controlled by the number of basis functions N and the numerical precision parameter M. We have checked that using $M = 60$ and $N = 80$ yielded the 20 first QNM's with good accuracy — this was the setting used in most of the work. For higher order QNM's, such as the ones we are going to show in Figure 15 and Figure 23, we used $M = N = 100$. We verified the stability of the QNM spectra involving the desired modes by doubling the number of basis points N or the numerical precision parameter M, following the error control procedure discussed in Boyd (2013).

5.2.3 QNM spectra and equilibration time

In Figure 15 we show the evolution of the external scalar QNM spectra for the first 26 poles as we evolve k/T from 0 to 100, both for the AdS_5-Schwarzschild background (i.e. $\mu/T = 0$) and the critical geometry at $\mu/T = \pi/\sqrt{2}$. We observe the usual non-hydrodynamical QNM structure for the external scalar channel with an infinite series of QNM pairs with $\mathrm{Im}\,\omega < 0$ and $\mathrm{Re}\,\omega \neq 0$ symmetrically distributed with respect to the imaginary axis (KOVTUN; STARINETS, 2005). Keeping $k/T = 0$ as one increases μ/T enhances the magnitude of the Imaginary part of the pole which becomes more appreciable for higher order (faster varying) modes, while keeping the magnitude of the Real part almost unchanged. On the other hand, keeping μ/T fixed as one increases k/T enhances the magnitude of the Real part of the poles, while suppressing the magnitude of the Imaginary part. We see that by increasing the chemical potential one generally increases the damping of the quasinormal black hole oscillations, which qualitatively agrees with the result found previously in Rougemont et al. (2016) for a non-conformal, QCD-like bottom-up EMD model describing the physics of the QGP at finite baryon density.

Also, we note that the non-hydrodynamic modes in Figure 15 remain finite when evaluated at the critical point, even when $k = 0$. Thus, one can see that the timescales contained in the non-hydrodynamic modes are different than the usual equilibration time quantity $\tau_{\mathrm{eq}} \sim \xi^z$, where ξ is the correlation length (which diverges at the critical point) and z is the dynamical critical exponent, which becomes infinitely large at criticality describing the well-known phenomenon of critical slowing down. Nevertheless, in this strongly coupled model the microscopic scales defined by the non-hydrodynamic QNM's still display some critical behavior, as we show below.

[6] In the particular case of the AdS_5-Schwarzschild background, a didactic sample calculation of the QNM spectra using the pseudospectral method can be found in Yaffe (2014).

Figure 15 – First 26 QNM's trajectories in the external scalar channel evolved within the interval $0 \leq k/T \leq 100$ for $\mu/T = 0$ (beginning with a black dot for $k = 0$ and evolving into solid gray lines for $k > 0$) and for the critical point $\mu/T = \pi/\sqrt{2}$ (beginning with a red square for $k = 0$ and evolving into dashed pink lines for $k > 0$).

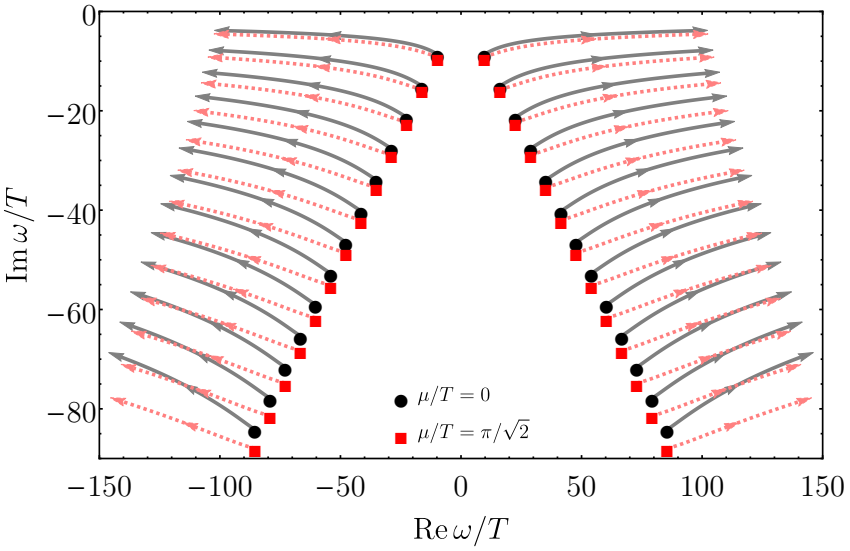

Source – Made by the authors.

In Figure 16 and Figure 17 we display the imaginary and real parts of the first four QNM's as functions of μ/T, for both stable and unstable branches, at $k/T = 0$ and $k/T = 1$. We see that at the critical point all the QNM's develop an infinite slope. Moreover, we also note that the effects on the non-hydrodynamic modes due to finite momentum are small for $k/T \sim 1$ (especially for the imaginary part), being more pronounced for the lowest QNM's, which seems to be a general holographic property of the dispersion relation of non-hydrodynamics QNM's known as "ultralocality" (HELLER et al., 2014; JANIK et al., 2015).

Following Horowitz and Hubeny (2000), one may define an upper bound for the equilibration time of the plasma, τ_{eq}, using the inverse of minus the imaginary part of the lowest non-hydrodynamical QNM evaluated at zero momentum, i.e.

$$\tau_{\text{eq}} = -\left.\frac{1}{\text{Im}\,\omega_1}\right|_{k=0}, \tag{5.30}$$

where $\omega_1 = \omega_1(k/T, \mu/T)$ is the lowest QNM. This is shown in Figure 18a, from which one can see that far from the critical point the equilibration time of the finite U(1) R-charge density SYM plasma decreases with increasing chemical potential, again in qualitative agreement with what was previously found in Rougemont et al. (2016) in the context of a phenomenologically realistic holographic model for the QGP at finite baryon chemical potential. However, for larger chemical potentials, as one approaches the critical point of the model, this behavior is modified and the equilibration time starts to increase, acquiring

Figure 16 – Imaginary part of the first four QNM's in the external scalar channel for $k/T = 0$ and $k/T = 1$, as a function μ/T, for both stable and unstable branches.

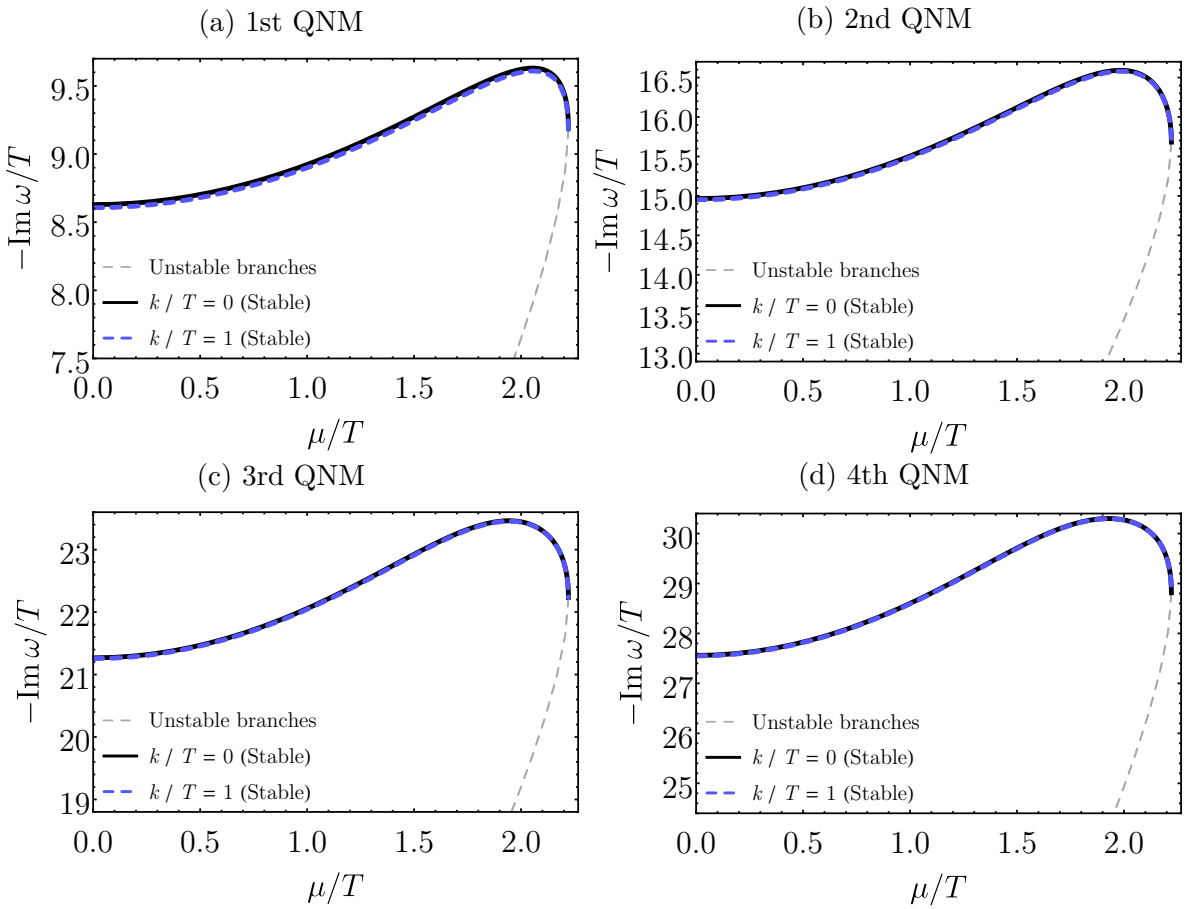

Source – Made by the authors.

an infinite slope at the critical point.

We may associate a new critical exponent with the derivative of the equilibration time, $d(T\tau_{\mathrm{eq}})/d(\mu/T)$, since it diverges at the critical point, as shown in Figure 18b. Close to the critical point,

$$\frac{d(T\tau_{\mathrm{eq}})}{d\,(\mu/T)} \sim \left(\frac{\pi}{\sqrt{2}} - \frac{\mu}{T}\right)^{-\theta} \quad \text{for} \quad \frac{\mu}{T} \sim \frac{\pi}{\sqrt{2}}, \tag{5.31}$$

where θ is the dynamical critical exponent which we want to calculate.

Let us now discuss the numerical procedure we followed in order to determine the critical exponent θ of the divergent quantities near the critical point $\mu/T = \pi/\sqrt{2}$, by performing fits of the asymptotic form given by Equation 5.31 as a function of μ/T.

We used a first order central difference formula with step size $h \equiv \Delta(\mu/T)$ in order to compute the required numerical derivatives. By varying h from 10^{-5} to 10^{-11}, and taking into account that we have an accuracy of several digits in the computed observables,

Figure 17 – Absolute value of the real part of the first four QNM's in the external scalar channel for $k/T = 0$ and $k/T = 1$, as a function μ/T, for both stable and unstable branches.

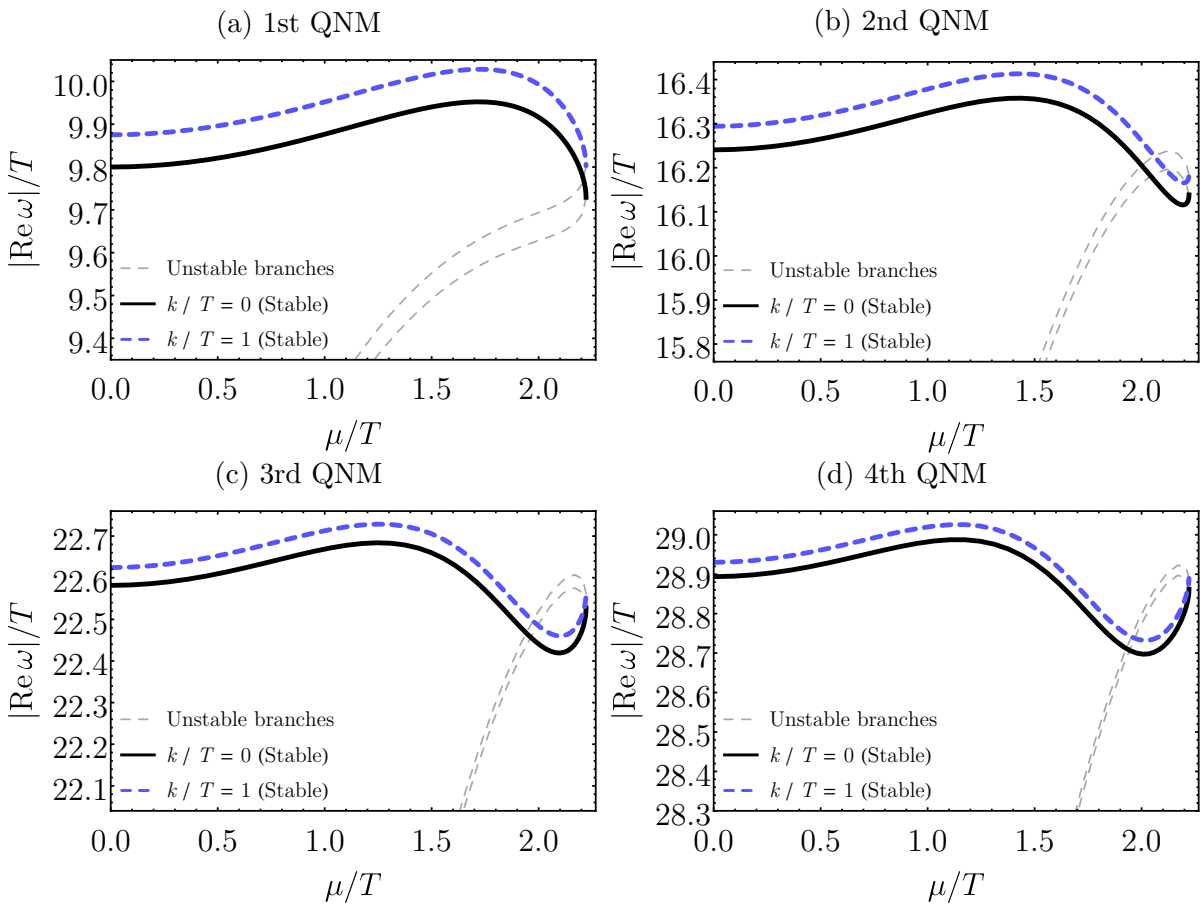

Source – Made by the authors.

we estimated the error introduced by the numerical differentiation to be of the order of 10^{-7}.

Taking as a specific example the calculation of the critical exponent for the equilibration time in the external scalar channel, in order to check that the asymptotic form in Equation 5.31 is valid close to the critical point $\mu/T = \pi/\sqrt{2}$, we split $d(T\tau_{\mathrm{eq}})/d(\mu/T)$ into 14 subintervals and then performed a least squares fit of Equation 5.31 to the resulting data within each subinterval, with each of them populated by 100 points evenly spaced in μ/T. In Table 2 we specify the subintervals used for the determination of the critical exponent of $d(T\tau_{\mathrm{eq}})/d(\mu/T)$ in the external scalar channel. In Figure 19 we display the convergence of the fitted critical exponent θ to the value 1/2. The estimate of the least squares standard error in the value of θ is of the order of 10^{-7} for the last interval.

More generally, one may consider different characteristic equilibration times of the medium associated with the different non-hydrodynamic QNM's, where equilibration times associated with higher order modes should be understood as estimates for how fast the

Figure 18 – Equilibration time (a) and its normalized derivative (b) in the external scalar channel as functions of μ/T at zero wavenumber.

(a) Equilibration time. (b) Normalized derivative.

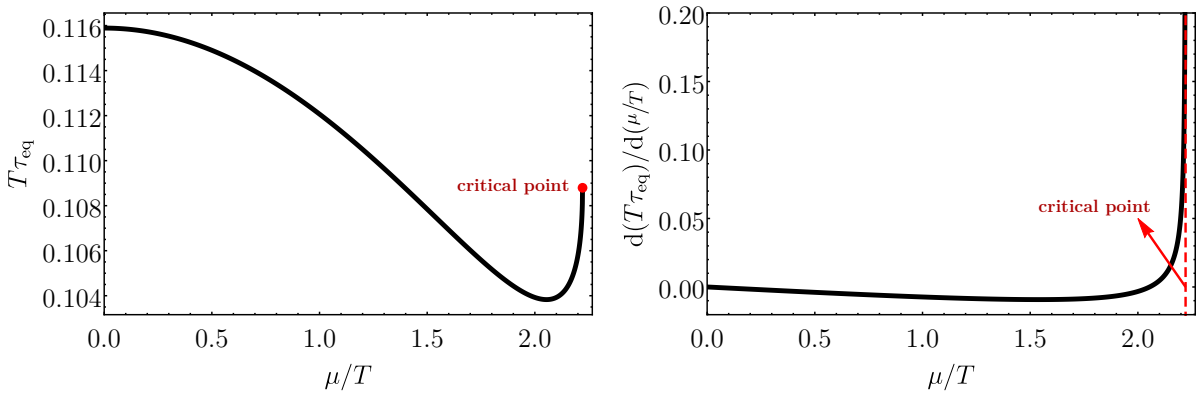

Source – Made by the authors.

Table 2 – Intervals for the derivative of equilibration time used for the fit procedure.

Interval	Starting – Ending points
1	0.05 – 0.10
2	0.10 – 0.15
3	0.15 – 0.20
4	0.20 – 0.25
5	0.25 – 0.30
6	0.30 – 0.50
7	0.50 – 1.0
8	1.0 – 5.0
9	5.0 – 15.0
10	15.0 – 40.0
11	40.0 – 70.0
12	70.0 – 150.0
13	150.0 – 250.0
14	250.0 – 530.0

Source – Made by the authors.

system relaxes to equilibrium depending on how rapidly varying are the perturbations to which it is subjected. Operationally, this amounts for computing the inverse of minus the imaginary part of the different non-hydrodynamic QNM's. By doing so, we obtain the same dynamical critical exponent $\theta = 1/2$ associated with all the different characteristic equilibration times of the plasma in the external scalar channel at zero wavenumber.

Figure 19 – Fit results for the critical exponent θ for each subinterval in $d(T\tau_{\rm eq})/d(\mu/T)$. The abscissas were chosen at the midpoint of the corresponding subinterval.

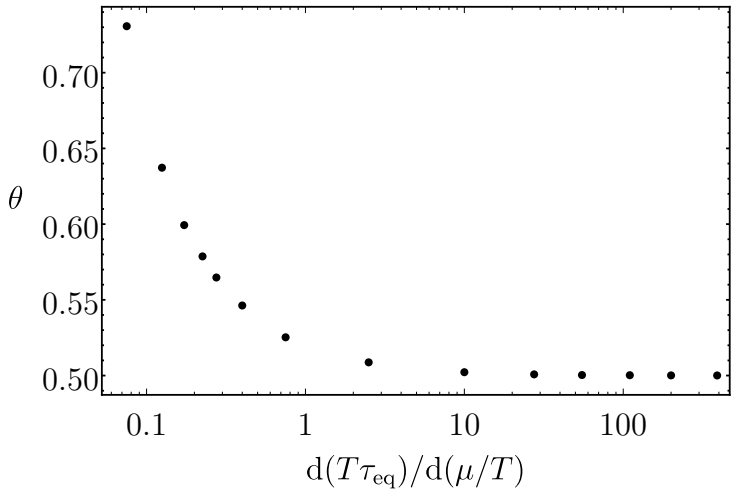

Source – Made by the authors.

5.2.4 Spectral function

In this subsection we study the spectral function associated with the external scalar fluctuation in the bulk. The motivation for this pursuit comes from the fact that QNM's are associated with poles of the retarded Green's function, whose imaginary part defines the spectral function. Therefore, one should expect that the critical behavior found for the QNM's leave somehow an imprint in the spectral function. Here we investigate this issue by considering the spectral function of the external scalar field fluctuation. Also, we note that due to the universal character of the δg^y_x fluctuation of the metric (KOVTUN; SON; STARINETS, 2005), the same calculation also gives the shear viscosity spectral function.

For the sake of completeness, let us briefly review here the holographic computation of the spectral function based on the real time holographic prescription (SON; STARINETS, 2002) recast using the holographic membrane paradigm (IQBAL; LIU, 2009). From linear response theory, the expectation value of the QFT operator $\hat{O}$ dual to the scalar perturbation is associated with the retarded correlator according to (see Ramallo (2015))[7],

$$\langle \hat{O}(\omega, \vec{k}) \rangle = -\mathcal{G}^R_{\hat{O}\hat{O}}(\omega, \vec{k}) J(\omega, \vec{k}), \tag{5.32}$$

where, as before, $J(\omega, \vec{k})$ denotes the leading mode of the scalar fluctuation at the boundary, which sources the QFT operator $\hat{O}$, while the expectation value is associated with the subleading mode, being given by

$$\langle \hat{O}(\omega, \vec{k}) \rangle = \lim_{r\to\infty} \Pi(r, \omega, \vec{k}) = \lim_{r\to\infty} \frac{\delta S}{\delta \tilde{\varphi}'}, \tag{5.33}$$

[7] Note that here in this chapter our definitions are such that there is a minus sign in the expression for the linear response result in comparison to that done in section 2.4.

where Π is the radial canonical momentum conjugate to the scalar perturbation $\tilde{\varphi}$. Once more, we impose that the scalar perturbation satisfies an in-falling wave condition at the horizon, which gives the retarded propagator.

Our goal here is to compute the spectral function defined by

$$F_s \equiv -\operatorname{Im} \mathcal{G}^R_{\hat{O}\hat{O}} = \lim_{r\to\infty} \operatorname{Im} \frac{\Pi}{\tilde{\varphi}}. \tag{5.34}$$

To do so, we have to first solve the equation of motion that follows from the action Equation 5.17 in the usual coordinates of Equation 5.3,

$$\tilde{\varphi}'' + \left(4A' - B' + \frac{h'}{h}\right)\tilde{\varphi}' + \frac{e^{2(B-A)}}{h^2}\left(\omega^2 - k^2 h\right)\tilde{\varphi} = 0, \tag{5.35}$$

with an in-falling horizon condition at $r = r_H$ and $\lim_{r\to\infty} \tilde{\varphi}(r, \omega, \vec{k}) = J(\omega, \vec{k})$.

We introduce a bulk response function[8] (IQBAL; LIU, 2009),

$$\zeta \equiv 2\kappa_5^2 \frac{\Pi}{\omega\tilde{\varphi}}, \tag{5.36}$$

which allows us to reduce the linear second order differential equation Equation 5.35 to a first order nonlinear Riccati equation,

$$\zeta' + \frac{\omega g_{rr}}{\sqrt{-g}}\left[\zeta^2 + g_{xx}^3\left(1 + \frac{g_{tt}}{g_{xx}}\frac{k^2}{\omega^2}\right)\right] = 0. \tag{5.37}$$

By requiring regularity at the horizon, one obtains the following horizon condition needed to solve the first order flow equation above,

$$\zeta(r = r_H, \omega, \vec{k}) = \pm i g_{xx}(r_H)^{3/2}, \tag{5.38}$$

where we choose the positive sign, which corresponds to the in-falling wave at the horizon. From the membrane paradigm (IQBAL; LIU, 2009), assuming that the scalar disturbance corresponds to the δg_x^y fluctuation of the metric, one recognizes this result as the shear viscosity,

$$\eta = \lim_{\omega\to 0}\lim_{\vec{k}\to 0} \frac{\operatorname{Im}\zeta(r_H, \omega, \vec{k})}{2\kappa_5^2}. \tag{5.39}$$

Then, one may write down the following dimensionless ratio,

$$\frac{F_s}{\omega\eta} = \frac{\operatorname{Im}\zeta(r\to\infty, \omega, \vec{k})}{g_{xx}(r_H)^{3/2}}. \tag{5.40}$$

One can now numerically integrate Equation 5.37 with the positive sign Equation 5.38 as the initial condition and then use Equation 5.40 to obtain the normalized spectral function.

[8] This response function should not be confused with the bulk viscosity, which is always zero in the conformal theory considered here.

The results are shown in Figure 20 for $\mu/T = 0$ (AdS_5-Schwarzschild) and $\mu/T = \pi/\sqrt{2}$ (critical point), both evaluated at $k = 0$. We see that, naively, an increase in μ/T seems to have only a small effect on the spectral function, even as one approaches the critical point. However, this is due to the fact that in the ultraviolet limit, $\omega/T \to \infty$, the dimensionless ratio $F_s/\omega\eta$ scales as $(\omega/T)^3$, which overwhelms any poles or fluctuations in the plot for the spectral function.

Figure 20 – Normalized spectral function as a function of ω/T for $\mu/T = 0$ and $\mu/T = \pi/\sqrt{2}$ (critical point). Both curves scale with $(\omega/T)^3$ as $\omega/T \to \infty$.

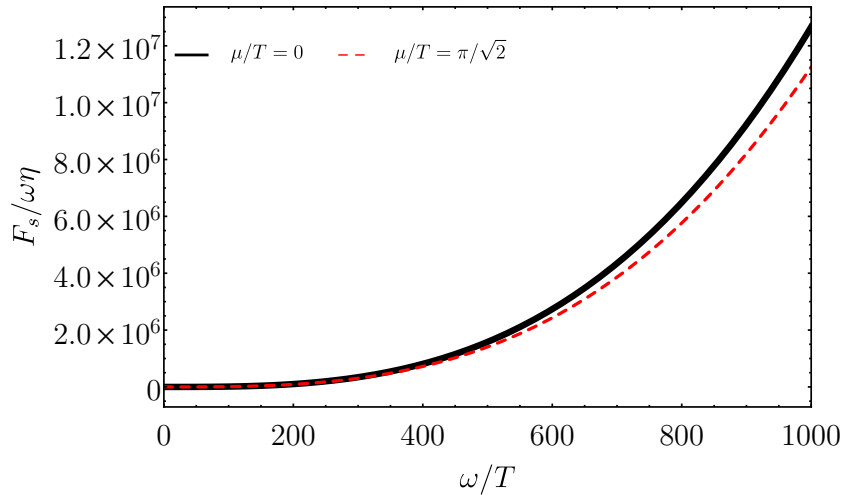

Source – Made by the authors.

Let us now consider a subtraction scheme which removes the scaling $(\omega/T)^3$ from the spectral function at some ultraviolet cutoff (CARON-HUOT et al., 2006; TEANEY, 2006; GÜRSOY et al., 2013),

$$\frac{\Delta F_s}{\omega\eta} \equiv \frac{F_s(\omega, k=0)}{\omega\eta} - a\left(\frac{\omega}{T}\right)^3, \tag{5.41}$$

where a is a constant defined by the asymptotic behavior of the spectral function,

$$a \equiv \lim_{\omega/T\to\infty} \frac{F_s/\omega\eta}{(\omega/T)^3}\bigg|_{k=0}. \tag{5.42}$$

We remark that in order to reliably perform the subtraction above, the flow equation Equation 5.37 must be solved with high numerical accuracy. This becomes more difficult for larger values of the ultraviolet cutoff in ω/T, which also requires one to increase the ultraviolet cutoff used to numerically parametrize the boundary in the radial coordinate. For the numerical evaluation of the first oscillations of the subtracted spectral function, one can safely take as the ultraviolet cutoff in the dimensionless frequency a value around $\omega/T \sim 40$.

In Figure 21 we display the behavior of $\Delta F_s/\omega\eta$ as a function of μ/T and ω/T at $k/T = 0$, while in Figure 22 we analyze the evolution of the height of its first peak as

a function of μ/T, which acquires an infinite slope at the critical point. By computing its derivative and fitting the numerical result close to the critical region using the same functional dependence as in Equation 5.31, one again obtains a critical exponent compatible with 1/2. Thus, we find that the critical behavior found in the QNM's can also be found, albeit in an indirect manner, in the spectral function.

Figure 21 – (a) Full surface profile of the subtracted normalized spectral function as a function of ω/T and μ/T, in the long wavelength limit, $k/T = 0$. (b) Details of $\Delta F_s/\omega\eta$ for $\mu/T = 0$ and $\mu/T = \pi/\sqrt{2}$ (critical point).

(a) Subtracted spectral function 3D.

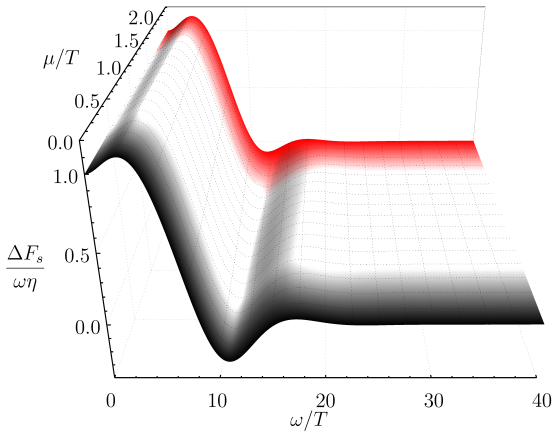

(b) Subtracted spectral function 2D.

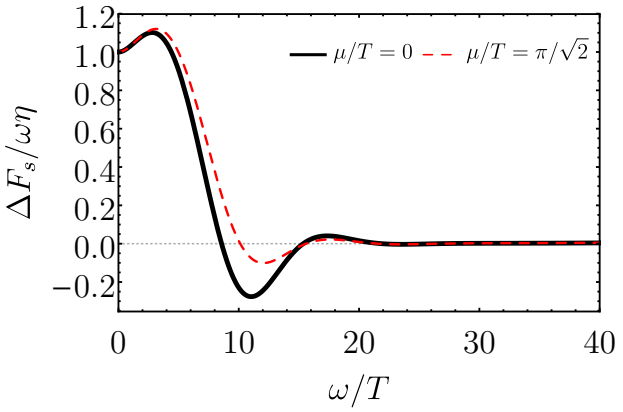

Source – Made by the authors.

Figure 22 – Height of the first peak of $\Delta F_s/\omega\eta$ as a function of μ/T in the long wavelength limit, $k/T = 0$.

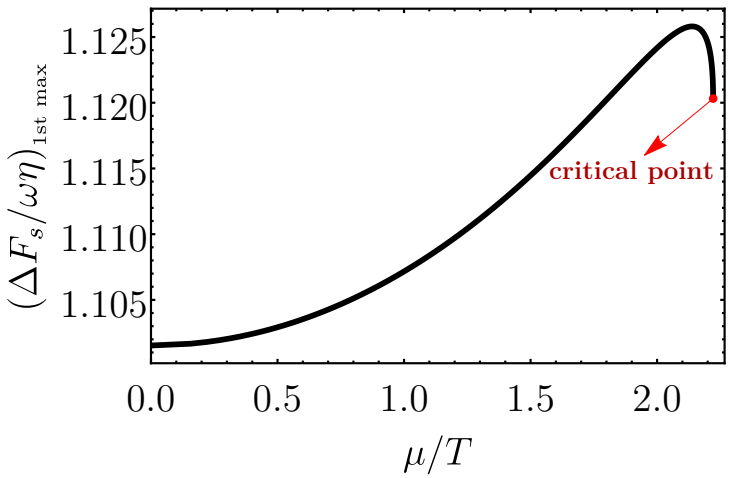

Source – Made by the authors.

5.3 QNM's in the vector diffusion channel

In this section we compute the QNM's of the vector diffusion channel in the long wavelength limit. Differently from what was done in the last section where we considered

an external scalar perturbation on top of the 1RCBH background, now we need to consider fluctuations of the Maxwell field A_μ which is already nonzero in the background and, therefore, we also need to consider disturbances in the background metric $g_{\mu\nu}$ and dilaton field ϕ.

5.3.1 Equation of motion

At zero spatial momentum the different channels for these fluctuations, at the linearized level, are classified by different representations of the SO(3) rotation group[9] (DEWOLFE; GUBSER; ROSEN, 2011b). By taking the fluctuation of the gauge field along the z-direction one finds that at the linearized level it only mixes with the fluctuation of g_t^z. Taking now the long wavelength limit, i.e. $k = 0$, we write down for the Fourier modes of these fluctuations,

$$\delta A_z = a(r)e^{-i\omega t} \text{ and } \delta g_t^z = s(r)e^{-i\omega t}. \tag{5.43}$$

Then, the linearized Maxwell's equations, $\nabla_\mu \left(f(\phi)F^{\mu\nu}\right) = 0$, expressed in Eddington-Finkelstein coordinates read,

$$-\Phi'' + \left(-2A' + B' - \frac{f'(\phi)\phi'}{f(\phi)}\right)\Phi' = 0, \tag{5.44}$$

$$\begin{aligned} a'' + \left(2A' - B' + \frac{h'}{h} - 2i\omega\frac{e^{A-B}}{h} + \frac{f'(\phi)\phi'}{f(\phi)}\right)a' - i\omega e^{B-A}\frac{f(\phi)A' + f'(\phi)\phi'}{f(\phi)h}a + \\ + \frac{\Phi'}{2h'}s' + \left[\frac{f'(\phi)\phi'\Phi' + f(\phi)\Big((2A' - B')\Phi' + \Phi''\Big)}{2f(\phi)h}\right]s \;=\; 0, \end{aligned} \tag{5.45}$$

where the Equation 5.44 is the equation of motion for the background Maxwell field, $\Phi(r)$, while Equation 5.45 is the equation of motion for the Maxwell perturbation, $a(r)$.

We may decouple the perturbations $a(r)$ and $s(r)$ by using Einstein field equations,

$$R_{\mu\nu} - \frac{g_{\mu\nu}}{3}\left(V(\phi) - \frac{f(\phi)}{4}F_{\alpha\beta}^2\right) - \frac{f(\phi)}{2}F_{\mu\alpha}F_\nu{}^\alpha - \frac{1}{2}\partial_\mu\phi\partial_\nu\phi = 0. \tag{5.46}$$

By taking the vz-component minus the rz-component of the above equation of motion, one obtains the constraint,

$$s' = -f(\phi)\Phi' e^{-2A}a. \tag{5.47}$$

By using the Equation 5.44 to eliminate the $s(r)$ term from Equation 5.45 and substituting Equation 5.47 into Equation 5.45, one obtains a decoupled equation of motion for the

[9] At nonzero k such classification is no longer valid and the corresponding fluctuations are organized in a more complicated way under a smaller SO(2) symmetry group. We are not going to pursue the investigation of this more involved case in the present work.

radial profile of the vector field perturbation, which is associated with the diffusion of the U(1) R-charge (KOVTUN; STARINETS, 2005; DEWOLFE; GUBSER; ROSEN, 2011b),

$$\begin{aligned} a'' + \left[2A' - B' + \frac{h'}{h} + \frac{f'(\phi)\phi'}{f(\phi)} - 2i\omega\frac{e^{B-A}}{h}\right]a' + \\ -\frac{e^{-2A}}{h}\left[i\omega e^{A+B}\left(A' + \phi'\frac{f'(\phi)}{f(\phi)}\right) + f(\phi)\Phi'^2\right]a \;=\; 0. \end{aligned} \tag{5.48}$$

Once again we apply the radial coordinate transformation $r \to r_H/u$, which yields,

$$\begin{aligned} a'' + \Bigg(-\frac{10u^6(y-3)(y-1) - 3u^4(5(y-2)y+1) + 4u^2\left(y^2-1\right) + (y+1)^2}{u\left(u^2-1\right)\left(u^2(y-3) - y - 1\right)\left(-2u^2(y-1) + y + 1\right)^2} + \\ -\frac{4i(\omega/T)\sqrt{(3-y)\left(-2u^2(y-1)+y+1\right)}}{\pi\left(u^2-1\right)(y-3)\left(u^2(y-3)-y-1\right)}\Bigg)a' + \\ + \Bigg(-\frac{8u^4(y-3)(y-1)(y+1)}{\left(u^2-1\right)\left(u^2(y-3)-y-1\right)\left(-2u^2(y-1)+y+1\right)^2} + \\ -\frac{2i(\omega/T)\left(4u^2(y-1)+y+1\right)}{\pi\left(u^2-1\right)u\left(u^2(y-3)-y-1\right)\sqrt{(y-3)\left(2u^2(y-1)-y-1\right)}}\Bigg)a \;=\; 0. \end{aligned} \tag{5.49}$$

For the vector perturbation the normalizable mode at the boundary corresponds to set $a(u) = u^2F(u)$, with $F(0) \neq 0$, from which one finally obtains,

$$\begin{aligned} F'' + \Bigg[-\frac{18u^6(y-3)(y-1) - 7u^4(5(y-2)y+1) + 20u^2\left(y^2-1\right) - 3(y+1)^2}{\left(u^2(y-3)-y-1\right)\left(-2u^2(y-1)+y+1\right)} + \\ -\frac{4iu(\omega/T)\sqrt{(3-y)\left(-2u^2(y-1)+y+1\right)}}{\pi(y-3)\left(u^2(y-3)-y-1\right)}\Bigg]\frac{1}{u(u^2-1)}F' + \\ + \frac{1}{u(u^2-1)}\Bigg[\frac{8u\left(6u^6(y-3)(y-1)^2 - 2u^4(y(7(y-3)y+9)+5)\right)}{\left(u^2(y-3)-y-1\right)\left(-2u^2(y-1)+y+1\right)^2} + \\ + \frac{8u\left(u^2(y+1)(3y-5)(3y-1) - 2(y-1)(y+1)^2\right)}{\left(u^2(y-3)-y-1\right)\left(-2u^2(y-1)+y+1\right)^2} + \\ -\frac{6i(\omega/T)\left(4u^2(y-1)-y-1\right)}{\pi\left(u^2(y-3)-y-1\right)\sqrt{(y-3)\left(2u^2(y-1)-y-1\right)}}\Bigg]F \;=\; 0. \end{aligned} \tag{5.50}$$

5.3.2 QNM spectra and equilibration time

With the QNM eigenvalue problem completely specified as discussed above, we can now apply the pseudospectral method (see subsection 5.2.2) to numerically solve it. In Figure 23 we display the QNM spectra for the first 30 symmetric poles in the vector diffusion channel in the limiting cases of $\mu/T = 0$ (AdS_5-Schwarzschild) and $\mu/T = \pi/\sqrt{2}$ (critical point).

Figure 23 – QNM spectra of the first 30 symmetric poles in the vector diffusion channel for $\mu/T = 0$ (black circles) and $\mu/T = \pi/\sqrt{2}$ (red squares) at $k/T = 0$. The hydrodynamical diffusive pole is depicted by the blue diamond. Note also the emergence of a new purely imaginary, non-hydrodynamical mode which comes from $-i\infty$ at $\mu/T = 0$ and remains at a finite distance from the origin at the critical point $\mu/T = \pi/\sqrt{2}$.

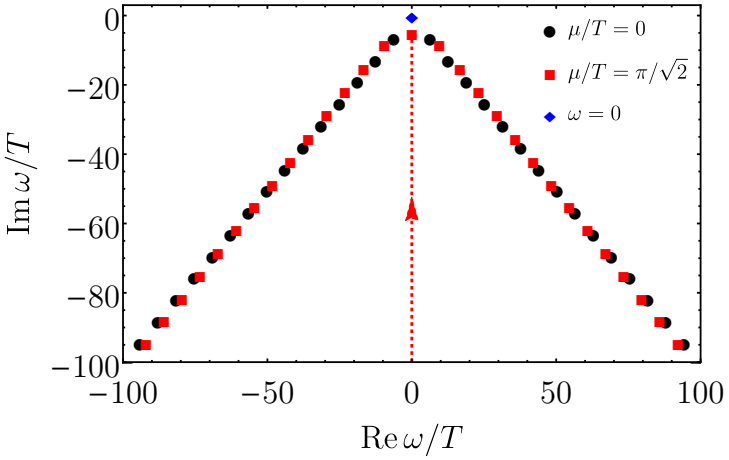

Source – Made by the authors.

In Figure 24 and Figure 25 we show the imaginary and real parts, respectively, of the first four QNM's as functions of μ/T, for both stable and unstable branches. We see that also in the vector diffusion channel both the real and imaginary parts of the QNM's develop an infinite slope at the critical point.

We remind the reader that at $k = \mu = 0$ the QNM spectra in the vector diffusion channel may be analytically calculated (KOVTUN; STARINETS, 2005),

$$\frac{\omega}{T} = 2\pi n(1 - i), \;\; n \in \mathbb{N} \text{ at } \mu = 0. \tag{5.51}$$

Our numerical calculations at $\mu/T = 0$ agree with this analytical result. The standard hydrodynamical mode $\omega(k = 0) = 0$ is depicted by the blue diamond in Figure 23. Since this is a hydrodynamical pole, it does not evolve with the chemical potential if we keep $k = 0$. This mode determines the R-charge conductivity of the model and the zero frequency limit of this transport coefficient was found in DeWolfe, Gubser and Rosen (2011b) to remain finite at the critical point, as expected for a type B dynamic universality class, while its derivative near the critical point has infinite slope described by an exponent equal to 1/2, which matches the exponent found in the previous section in the study of non-hydrodynamic modes of different nature corresponding to external scalar perturbations.

On the other hand, the main effect of the chemical potential on the symmetric non-hydrodynamical modes is to increase the magnitude of both the imaginary and real parts of these poles. Therefore, also in the vector diffusion channel one sees that the

Figure 24 – Imaginary part of the first 4 QNM's in the vector diffusion channel for $k/T = 0$, as a function of μ/T, for both stable and unstable branches.

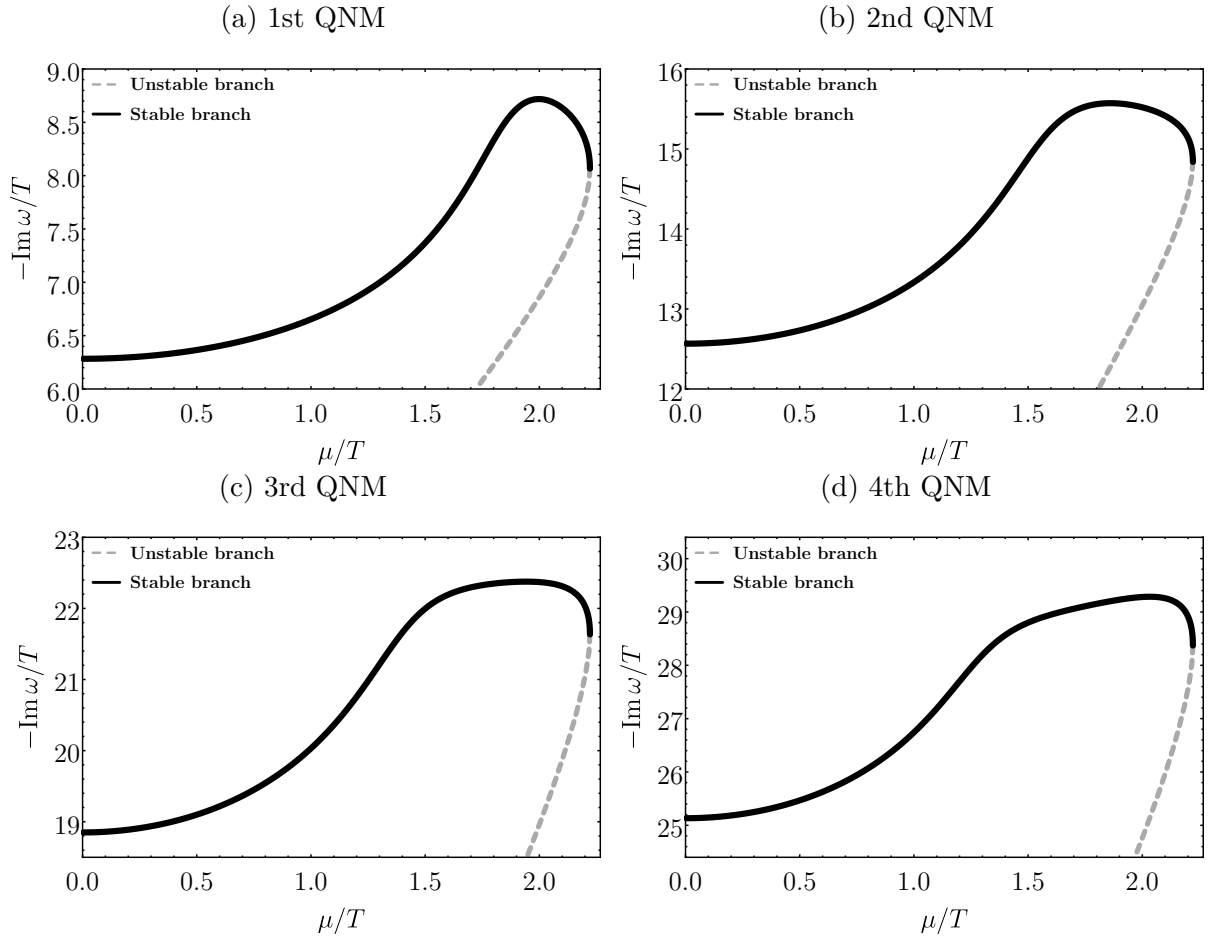

Source – Made by the authors.

inclusion of a chemical potential leads to additional damping for the quasinormal black hole oscillations.

A novel feature we observe in Figure 23 is the emergence of a new purely imaginary, non-hydrodynamical pole at finite chemical potential, which comes from $\omega/T \to -i\infty$ at $\mu/T = 0$ and lies at $\omega/T \approx -7.315i$ at the critical point $\mu/T = \pi/\sqrt{2}$. For $\mu/T \gtrsim 2$, this new purely imaginary pole becomes the lowest non-hydrodynamical mode, while for lower values of the chemical potential the lowest non-hydrodynamical mode is given by any of the first two symmetric poles with respect to the imaginary axis. Therefore, this new non-hydrodynamical imaginary mode plays a crucial role in the description of the equilibration time of the system in the vector diffusion channel when the chemical potential is large, specially at criticality, when it dominates the physics of the slowest varying perturbations. The appearance of such a purely imaginary mode is an interesting feature of this model that shows that the distinction between transient phenomena at weak and strong coupling, currently understood in terms of their different pattern of non-hydrodynamic modes at zero wavenumber (DENICOL et al., 2011) (see also Noronha

Figure 25 – Absolute value of the real part of the first 4 QNM's in the vector diffusion channel for $k/T = 0$, as a function μ/T, for both stable and unstable branches.

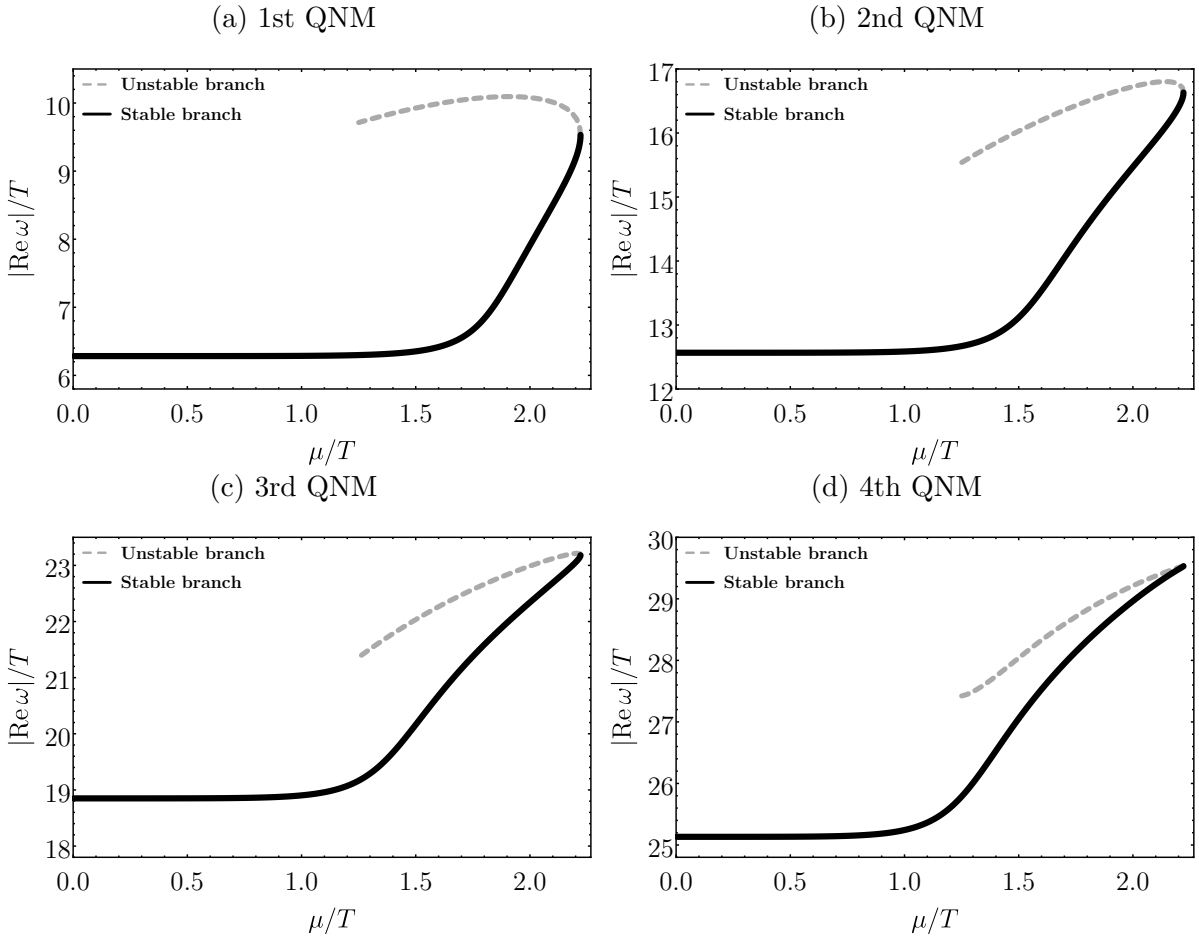

Source – Made by the authors.

and Denicol (2011)) corresponding to fluctuations around global equilibrium, can become more complicated near a critical point.

We define the upper bound for the equilibration time of the system in the vector diffusion channel as before by taking the inverse of minus the imaginary part of the lowest non-hydrodynamical QNM. The result is shown in Figure 26a. The kink observed in the equilibration time at $\mu/T \approx 2$ is due to the shift from the regime dominated by the first symmetric poles to the regime dominated by the new purely imaginary mode. This also causes a discontinuity in the derivative of the equilibration time, as seen in Figure 26b. As before, one can calculate the critical exponent associated with this derivative at the critical point and the result is once again compatible with $\theta = 1/2$. This shows that in this model both the hydrodynamic and the non-hydrodynamic modes in this vector diffusion channel have the same critical exponents.

Figure 26 – Equilibration time (a) and its normalized derivative (b) in the vector diffusion channel as functions of μ/T.

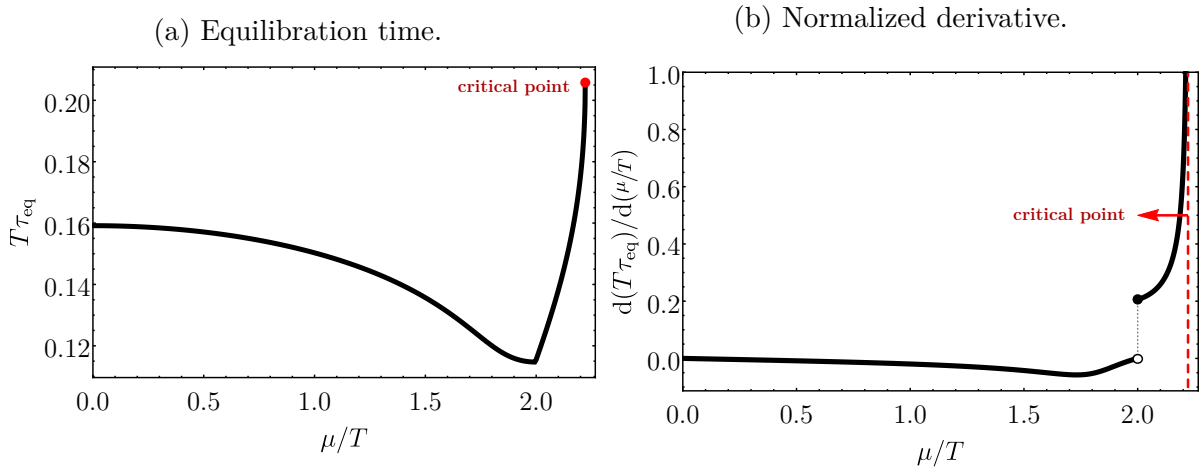

Source – Made by the authors.

Part III

Final remarks and bibliography

6 Conclusions and outlook

In this section we summarize the main results found in this thesis and present some other possible studies that can be performed later on.

Motivated by the recent studies involving the effects of electromagnetic fields on the strongly coupled plasma formed in heavy ion collisions, the holographic correspondence was used in chapter 4 to compute two anisotropic shear viscosity coefficients of a strongly coupled $\mathcal{N} = 4$ SYM plasma in the presence of a magnetic field. As expected, the shear viscosity that describes the dynamics in the plane transverse to the magnetic field, $\eta_\perp$, is not affected by the field and, thus, it still saturates the viscosity bound, i.e. $\eta_\perp/s = 1/(4\pi)$. On the other hand, the shear viscosity coefficient along the axis parallel to the external magnetic field, $\eta_\parallel$, violates the bound when $B > 0$, i.e. $\eta_\parallel/s < 1/(4\pi)$. These results are qualitatively similar to those found in Rebhan and Steineder (2012) for the case of an anisotropic plasma created by a spatial dependent axion profile (MATEOS; TRANCANELLI, 2011). However, the source of anisotropy in our case (the magnetic field) is arguably more directly connected to heavy ion phenomenology than the axion dependence.

Our results for the magnetic field dependence of $\eta_\parallel/s$ show that this ratio only deviates significantly from $1/(4\pi)$ when $\mathcal{B}/T^2 \gg 1$. Taking the typical temperature at the early stages of heavy ion collisions to be $T \sim 2m_\pi$, where m_π is the pion mass, we see that $4\pi\eta_\parallel/s \sim 0.9$ when $\mathcal{B} \sim 40m_\pi^2$. This value of magnetic field may be too large for heavy ion phenomenology and, thus, our results suggest that anisotropic shear viscosity effects in strongly coupled plasmas are minimal and the isotropic approximation is justified. It would be interesting to check if the same behavior is obtained in strongly coupled plasmas that are not conformal (such as the bottom-up models in Gürsoy and Kiritsis (2008), Gürsoy, Kiritsis and Nitti (2008), Gürsoy et al. (2008), Gubser and Nellore (2008), Noronha (2010)) to see if there is some nontrivial interplay between the confinement/deconfinement scale and the external magnetic field. The first study in this direction was done in (FINAZZO et al., 2016). Alternatively, one could also study the effects of strong magnetic fields on the weak coupling calculations of Arnold, Moore and Yaffe (2000), Arnold, Moore and Yaffe (2003) perhaps following the general procedure to compute transport coefficients of relativistic hydrodynamics from the Boltzmann equation proposed in Denicol et al. (2011).

Plasmas in the presence of magnetic fields usually experience instabilities and it would be interesting to investigate whether there are instabilities induced by strong magnetic fields in the strongly coupled plasma studied in chapter 4. In fact, one could compute the spectral functions and the quasi-normal modes associated with $\eta_\parallel$ and check if there is any sudden change in their behavior at strong fields. Part of this study has been done and this material is being prepared for publication. Also, instabilities in homogeneous

magnetic media can sometimes be resolved by the formation of magnetic domains and, thus, it would be interesting to investigate whether this is the case for the theory considered.

The behavior of the QNM's for the external scalar and vector diffusion channels of the 1RCBH model was analyzed in chapter 5, which is a top-down gauge/gravity construction dual to a SYM plasma at nonzero U(1) R-charge density. The phase diagram of the model displays a critical point at a second order phase transition and, except close to this critical point, by increasing the chemical potential one generally increases the damping of the quasinormal black hole oscillations, which leads to a reduction of the characteristic equilibration times of the dual plasma. However, as one approaches the critical point these equilibration times are enhanced and they acquire an infinite slope at the criticality. We found that the derivatives of all the characteristic equilibration times of the medium, obtained from the non-hydrodynamic QNM's at zero wavenumber, share the same critical exponent $\theta = 1/2$. Previously, the same value was also found for the critical exponent associated to the derivative of the DC conductivity extracted from the R-charge diffusive hydrodynamic mode in this model (DEWOLFE; GUBSER; ROSEN, 2011b). We also found a purely imaginary, non-hydrodynamical mode in the vector diffusion channel at nonzero chemical potential which dictates the critical behavior of the equilibration time in this channel.

The observation that the quasinormal black hole oscillations away from the critical region are additionally damped by a nonzero chemical potential, obtained here for a top-down conformal construction dual to a SYM plasma at finite R-charge density, is consistent with the behavior found previously in Rougemont et al. (2016) for a rather different holographic construction, which involves a bottom-up model with black brane solutions that are engineered to describe the realistic non-conformal physics of the QGP both at zero baryon density (FINAZZO et al., 2015) and also at finite density (ROUGEMONT; NORONHA; NORONHA-HOSTLER, 2015). This may indicate that this additional damping in the quasinormal black hole oscillations due to a nonzero chemical potential, and the consequent attenuation of the equilibration time of the dual plasma away from criticality, may be a general holographic property of strongly correlated quantum fluids.

Regarding the purely imaginary, non-hydrodynamical mode found in the diffusion channel at finite density, the common link between the 1RCBH model studied here and the Einstein-Maxwell model investigated in Janiszewski and Kaminski (2016) (where this mode was also found, although with no critical behavior, due to the lack of a phase transition) is the presence of bulk electromagnetic fields. Somehow, the Maxwell field changes qualitatively the dynamical response of the system to perturbations. From the point of view of the gravitational dynamics in five dimensions, what we see is that this purely imaginary non-hydrodynamic mode appears for electromagnetically charged asymptotically AdS black holes and that, when the charge of the black hole is large

enough, this new mode dominates the dynamics of relaxation towards equilibrium when the black hole is disturbed. From the point of view of the four dimensional dual quantum field theory at the boundary of the asymptotically AdS spacetime background, this new mode dominates the dynamics responsible for the characteristic equilibration time of the plasma at large enough densities in the diffusion channel. Since bulk electric fields map to boundary states at finite density, this may be a general feature of holographic models at finite density. Therefore, one could investigate if the behavior of non-hydrodynamic modes in other holographic models that display critical phenomena possess similar properties to those found in the present study, i.e. the corresponding equilibration times have infinite slope characterized by a single critical exponent θ. In particular, we intend to investigate in the near future these features in two bottom-up constructions of phenomenological relevance for the physics of the QGP: the EMD model at finite baryon chemical potential (ROUGEMONT et al., 2016; ROUGEMONT; NORONHA; NORONHA-HOSTLER, 2015) and the anisotropic EMD model at finite magnetic field from Rougemont, Critelli and Noronha (2016), Finazzo et al. (2016). Such studies may be relevant to understand how the presence of a critical endpoint in the QCD phase diagram may lead to new observables associated with, for instance, baryon transport in the baryon rich quark-gluon plasma produced in heavy ion collisions within the beam energy scan program at RHIC.

Bibliography

ADAMS, A. et al. Strongly Correlated Quantum Fluids: Ultracold Quantum Gases, Quantum Chromodynamic Plasmas, and Holographic Duality. **New J. Phys.**, v. 14, p. 115009, 2012. Cited on page 45.

ALANEN, J. et al. Mass spectrum and thermodynamics of quasi-conformal gauge theories from gauge/gravity duality. **Phys. Rev.**, D84, p. 086007, 2011. Cited on page 21.

AMMON, M.; ERDMENGER, J. **Gauge/gravity duality**. Cambridge, UK: Cambridge Univ. Pr., 2015. ISBN 9781107010345. Available at: <http://www.cambridge.org/de/academic/subjects/physics/theoretical-physics-and-mathematical-physics/gaugegravity-duality-foundations-and-applications>. Cited 2 times on pages 24 and 39.

AOKI, Y. et al. The Order of the quantum chromodynamics transition predicted by the standard model of particle physics. **Nature**, v. 443, p. 675–678, 2006. Cited on page 31.

ARNOLD, P. B.; MOORE, G. D.; YAFFE, L. G. Transport coefficients in high temperature gauge theories. 1. Leading log results. **JHEP**, v. 11, p. 001, 2000. Cited 3 times on pages 19, 32, and 101.

ARNOLD, P. B.; MOORE, G. D.; YAFFE, L. G. Transport coefficients in high temperature gauge theories. 2. Beyond leading log. **JHEP**, v. 05, p. 051, 2003. Cited 3 times on pages 19, 32, and 101.

ASAKAWA, M.; BASS, S. A.; MüLLER, B. Center domains and their phenomenological consequences. **Phys. Rev. Lett.**, v. 110, n. 20, p. 202301, 2013. Cited on page 19.

ASAKAWA, M.; BASS, S. A.; MULLER, B. Anomalous viscosity of an expanding quark-gluon plasma. **Phys. Rev. Lett.**, v. 96, p. 252301, 2006. Cited on page 19.

BALI, G. S. et al. The QCD equation of state in background magnetic fields. **JHEP**, v. 08, p. 177, 2014. Cited on page 20.

BALI, G. S. et al. The QCD phase diagram for external magnetic fields. **JHEP**, v. 02, p. 044, 2012. Cited on page 20.

BANADOS, M.; TEITELBOIM, C.; ZANELLI, J. The Black hole in three-dimensional space-time. **Phys. Rev. Lett.**, v. 69, p. 1849–1851, 1992. Cited on page 59.

BEHRNDT, K.; CVETIC, M.; SABRA, W. A. Nonextreme black holes of five-dimensional $\mathcal{N} = 2$ AdS supergravity. **Nucl. Phys.**, B553, p. 317–332, 1999. Cited 2 times on pages 23 and 73.

BEKENSTEIN, J. D. Black holes and entropy. **Phys. Rev.**, D7, p. 2333–2346, 1973. Cited on page 76.

BERTI, E.; CARDOSO, V.; STARINETS, A. O. Quasinormal modes of black holes and black branes. **Class. Quant. Grav.**, v. 26, p. 163001, 2009. Cited on page 21.

BLOCZYNSKI, J. et al. Azimuthally fluctuating magnetic field and its impacts on observables in heavy-ion collisions. **Phys. Lett.**, B718, p. 1529–1535, 2013. Cited on page 19.

BORSÁNYI, S. et al. The QCD equation of state with dynamical quarks. **JHEP**, v. 11, p. 077, 2010. Cited on page 32.

BOYD, J. **Chebyshev and Fourier Spectral Methods: Second Revised Edition**. Dover Publications, 2013. (Dover Books on Mathematics). ISBN 9780486141923. Available at: <https://books.google.com.br/books?id=b4TCAgAAQBAJ>. Cited 3 times on pages 79, 81, and 83.

BRAHMS COLLABORATION. Quark gluon plasma and color glass condensate at RHIC? The Perspective from the BRAHMS experiment. **Nucl. Phys.**, A757, p. 1–27, 2005. Cited on page 19.

BRIGANTE, M. et al. The Viscosity Bound and Causality Violation. **Phys. Rev. Lett.**, v. 100, p. 191601, 2008. Cited 2 times on pages 20 and 67.

BRIGANTE, M. et al. Viscosity Bound Violation in Higher Derivative Gravity. **Phys. Rev.**, D77, p. 126006, 2008. Cited 3 times on pages 20, 54, and 67.

BUCHEL, A. Relaxation time of non-conformal plasma. **Phys. Lett.**, B681, p. 200–203, 2009. Cited on page 23.

BUCHEL, A. Critical phenomena in $\mathcal{N} = 4$ SYM plasma. **Nucl. Phys.**, B841, p. 59–99, 2010. Cited 2 times on pages 23 and 77.

BUCHEL, A.; HELLER, M. P.; MYERS, R. C. Equilibration rates in a strongly coupled nonconformal quark-gluon plasma. **Phys. Rev. Lett.**, v. 114, n. 25, p. 251601, 2015. Cited on page 22.

BUCHEL, A.; HELLER, M. P.; NORONHA, J. Entropy Production, Hydrodynamics, and Resurgence in the Primordial Quark-Gluon Plasma from Holography. **Phys. Rev.**, D94, n. 10, p. 106011, 2016. Cited on page 21.

BUCHEL, A.; LIU, J. T. Universality of the shear viscosity in supergravity. **Phys. Rev. Lett.**, v. 93, p. 090602, 2004. Cited 3 times on pages 19, 20, and 32.

BUCHEL, A.; MYERS, R. C.; SINHA, A. Beyond $\eta/s = 1/4\pi$. **JHEP**, v. 03, p. 084, 2009. Cited on page 20.

BUCHEL, A.; PAGNUTTI, C. Transport at criticality. **Nucl. Phys.**, B834, p. 222–236, 2010. Cited on page 23.

BUCHEL, A.; PAGNUTTI, C. Critical phenomena in $\mathcal{N} = 2^*$ plasma. **Phys. Rev.**, D83, p. 046004, 2011. Cited on page 23.

CAI, R.-G.; HE, S.; LI, D. A hQCD model and its phase diagram in Einstein-Maxwell-Dilaton system. **JHEP**, v. 03, p. 033, 2012. Cited on page 23.

CAI, R.-G.; SOH, K.-S. Critical behavior in the rotating D-branes. **Mod. Phys. Lett.**, A14, p. 1895–1908, 1999. Cited 2 times on pages 23 and 73.

CARON-HUOT, S. et al. Photon and dilepton production in supersymmetric Yang-Mills plasma. **JHEP**, v. 12, p. 015, 2006. Cited on page 90.

CARROLL, S. M. **Spacetime and geometry: An introduction to general relativity**. [s.n.], 2004. ISBN 0805387323, 9780805387322. Available at: <http://www.slac.stanford.edu/spires/find/books/www?cl=QC6:C37:2004>. Cited on page 26.

CASALDERREY-SOLANA, J. et al. **Gauge/String Duality, Hot QCD and Heavy Ion Collisions**. [S.l.]: Cambridge University Press, 2014. Cited 3 times on pages 19, 32, and 49.

CONSEIL EUROPÉEN POUR LA RECHERCHE NUCLÉAIRE. **LHC Machine Outreach – Collisions**. 2008. Available at: <http://lhc-machine-outreach.web.cern.ch/lhc-machine-outreach/collisions.htm>. Cited on page 30.

CRITELLI, R. et al. Anisotropic shear viscosity of a strongly coupled non-Abelian plasma from magnetic branes. **Phys. Rev.**, D90, n. 6, p. 066006, 2014. Cited on page 57.

CVETIC, M.; GUBSER, S. S. Phases of R charged black holes, spinning branes and strongly coupled gauge theories. **JHEP**, v. 04, p. 024, 1999. Cited 2 times on pages 23 and 73.

CVETIC, M.; GUBSER, S. S. Thermodynamic stability and phases of general spinning branes. **JHEP**, v. 07, p. 010, 1999. Cited 2 times on pages 23 and 73.

DANIELEWICZ, P.; GYULASSY, M. Dissipative Phenomena in Quark Gluon Plasmas. **Phys. Rev.**, D31, p. 53–62, 1985. Cited on page 19.

DAVIS, M. et al. Gravitational radiation from a particle falling radially into a schwarzschild black hole. **Phys. Rev. Lett.**, v. 27, p. 1466–1469, 1971. Cited on page 21.

DENG, W.-T.; HUANG, X.-G. Event-by-event generation of electromagnetic fields in heavy-ion collisions. **Phys. Rev.**, C85, p. 044907, 2012. Cited on page 19.

DENICOL, G. S. et al. Derivation of transient relativistic fluid dynamics from the Boltzmann equation. **Phys. Rev.**, D85, p. 114047, 2012. [Erratum: Phys. Rev.D91,no.3,039902(2015)]. Cited on page 19.

DENICOL, G. S.; NORONHA, J. Divergence of the Chapman-Enskog expansion in relativistic kinetic theory. 2016. Available at: <https://arxiv.org/abs/1608.07869>. Cited on page 21.

DENICOL, G. S. et al. Origin of the Relaxation Time in Dissipative Fluid Dynamics. **Phys. Rev.**, D83, p. 074019, 2011. Cited 2 times on pages 95 and 101.

DEPARTMENT OF ENERGY/NATIONAL SCIENCE FOUNDATION – NUCLEAR SCIENCE ADVISORY COMMITTEE. **2007 Long Range Plans: The Frontier of Nuclear Science**. 2007. Available at: <https://science.energy.gov/np/nsac/>. Cited on page 31.

DEWOLFE, O.; GUBSER, S. S.; ROSEN, C. A holographic critical point. **Phys. Rev.**, D83, p. 086005, 2011. Cited on page 23.

DEWOLFE, O.; GUBSER, S. S.; ROSEN, C. Dynamic critical phenomena at a holographic critical point. **Phys. Rev.**, D84, p. 126014, 2011. Cited 7 times on pages 73, 76, 77, 92, 93, 94, and 102.

D'HOKER, E.; KRAUS, P. Magnetic Brane Solutions in AdS. **JHEP**, v. 10, p. 088, 2009. Cited 5 times on pages 20, 57, 58, 59, and 60.

D'HOKER, E.; KRAUS, P. Charged Magnetic Brane Solutions in AdS_5 and the fate of the third law of thermodynamics. **JHEP**, v. 03, p. 095, 2010. Cited on page 20.

D'HOKER, E.; KRAUS, P. Magnetic Field Induced Quantum Criticality via new Asymptotically AdS_5 Solutions. **Class. Quant. Grav.**, v. 27, p. 215022, 2010. Cited on page 20.

ERDMENGER, J.; FERNANDEZ, D.; ZELLER, H. New Transport Properties of Anisotropic Holographic Superfluids. **JHEP**, v. 04, p. 049, 2013. Cited 2 times on pages 20 and 64.

ERDMENGER, J.; KERNER, P.; ZELLER, H. Non-universal shear viscosity from Einstein gravity. **Phys. Lett.**, B699, p. 301–304, 2011. Cited 3 times on pages 20, 64, and 65.

FINAZZO, S. I. et al. Momentum transport in strongly coupled anisotropic plasmas in the presence of strong magnetic fields. **Phys. Rev.**, D94, n. 5, p. 054020, 2016. Cited 2 times on pages 101 and 103.

FINAZZO, S. I. et al. Hydrodynamic transport coefficients for the non-conformal quark-gluon plasma from holography. **JHEP**, v. 02, p. 051, 2015. Cited 2 times on pages 22 and 102.

FINAZZO, S. I. et al. Critical behavior of non-hydrodynamic quasinormal modes in a strongly coupled plasma. **JHEP**, v. 01, p. 137, 2017. Cited on page 73.

FLORKOWSKI, W.; RYBLEWSKI, R.; SPALIńSKI, M. Gradient expansion for anisotropic hydrodynamics. **Phys. Rev.**, D94, n. 11, p. 114025, 2016. Cited on page 21.

FUKUSHIMA, K.; KHARZEEV, D. E.; WARRINGA, H. J. The Chiral Magnetic Effect. **Phys. Rev.**, D78, p. 074033, 2008. Cited on page 19.

GATTRINGER, C.; LANG, C. B. Quantum chromodynamics on the lattice. **Lect. Notes Phys.**, v. 788, p. 1–343, 2010. Cited on page 30.

GUBSER, S. S. Thermodynamics of spinning D3-branes. **Nucl. Phys.**, B551, p. 667–684, 1999. Cited 2 times on pages 23 and 73.

GUBSER, S. S.; KLEBANOV, I. R.; PEET, A. W. Entropy and temperature of black 3-branes. **Phys. Rev.**, D54, p. 3915–3919, 1996. Cited on page 75.

GUBSER, S. S.; KLEBANOV, I. R.; POLYAKOV, A. M. Gauge theory correlators from noncritical string theory. **Phys. Lett.**, B428, p. 105–114, 1998. Cited 4 times on pages 19, 21, 32, and 62.

GUBSER, S. S.; NELLORE, A. Mimicking the QCD equation of state with a dual black hole. **Phys. Rev.**, D78, p. 086007, 2008. Cited 2 times on pages 22 and 101.

GUBSER, S. S. et al. Thermodynamics and bulk viscosity of approximate black hole duals to finite temperature quantum chromodynamics. **Phys. Rev. Lett.**, v. 101, p. 131601, 2008. Cited on page 22.

GÜRSOY, U. et al. The Chern-Simons Diffusion Rate in Improved Holographic QCD. **JHEP**, v. 02, p. 119, 2013. Cited on page 90.

GÜRSOY, U.; KIRITSIS, E. Exploring improved holographic theories for QCD: Part I. **JHEP**, v. 02, p. 032, 2008. Cited on page 101.

GÜRSOY, U. et al. Deconfinement and Gluon Plasma Dynamics in Improved Holographic QCD. **Phys. Rev. Lett.**, v. 101, p. 181601, 2008. Cited on page 101.

GÜRSOY, U. et al. Improved Holographic QCD. **Lect. Notes Phys.**, v. 828, p. 79–146, 2011. Cited on page 22.

GÜRSOY, U.; KIRITSIS, E.; NITTI, F. Exploring improved holographic theories for QCD: Part II. **JHEP**, v. 02, p. 019, 2008. Cited on page 101.

GUSYNIN, V. P.; MIRANSKY, V. A.; SHOVKOVY, I. A. Catalysis of dynamical flavor symmetry breaking by a magnetic field in $(2+1)$-dimensions. **Phys. Rev. Lett.**, v. 73, p. 3499–3502, 1994. [Erratum: Phys. Rev. Lett.76,1005(1996)]. Cited on page 59.

GUSYNIN, V. P.; MIRANSKY, V. A.; SHOVKOVY, I. A. Dimensional reduction and dynamical chiral symmetry breaking by a magnetic field in $(3+1)$-dimensions. **Phys. Lett.**, B349, p. 477–483, 1995. Cited on page 59.

GUSYNIN, V. P.; MIRANSKY, V. A.; SHOVKOVY, I. A. Dimensional reduction and catalysis of dynamical symmetry breaking by a magnetic field. **Nucl. Phys.**, B462, p. 249–290, 1996. Cited on page 59.

GYULASSY, M.; MCLERRAN, L. New forms of QCD matter discovered at RHIC. **Nucl. Phys.**, A750, p. 30–63, 2005. Cited on page 19.

HAWKING, S. W. Particle Creation by Black Holes. **Commun. Math. Phys.**, v. 43, p. 199–220, 1975. [,167(1975)]. Cited on page 76.

HAWKING, S. W.; ELLIS, G. F. R. **The Large Scale Structure of Space-Time**. [S.l.]: Cambridge University Press, 2011. (Cambridge Monographs on Mathematical Physics). ISBN 9780521200165, 9780521099066, 9780511826306, 9780521099066. Cited 2 times on pages 39 and 42.

HEINZ, U.; SNELLINGS, R. Collective flow and viscosity in relativistic heavy-ion collisions. **Ann. Rev. Nucl. Part. Sci.**, v. 63, p. 123–151, 2013. Cited 3 times on pages 19, 30, and 32.

HEINZ, U. W. Concepts of heavy ion physics. In: **2002 European School of high-energy physics, Pylos, Greece, 25 Aug-7 Sep 2002: Proceedings**. [s.n.], 2004. p. 165–238. Available at: <http://doc.cern.ch/yellowrep/CERN-2004-001>. Cited on page 31.

HELLER, M. P. et al. Coupling hydrodynamics to nonequilibrium degrees of freedom in strongly interacting quark-gluon plasma. **Phys. Rev. Lett.**, v. 113, n. 26, p. 261601, 2014. Cited on page 84.

HELLER, M. P.; JANIK, R. A.; WITASZCZYK, P. Hydrodynamic Gradient Expansion in Gauge Theory Plasmas. **Phys. Rev. Lett.**, v. 110, n. 21, p. 211602, 2013. Cited on page 21.

HELLER, M. P.; KURKELA, A.; SPALINSKI, M. Hydrodynamization and transient modes of expanding plasma in kinetic theory. 2016. Available at: <https://arxiv.org/abs/1609.04803>. Cited on page 21.

HIDAKA, Y.; PISARSKI, R. D. Suppression of the Shear Viscosity in a "semi" Quark Gluon Plasma. **Phys. Rev.**, D78, p. 071501, 2008. Cited on page 19.

HOHENBERG, P. C.; HALPERIN, B. I. Theory of dynamic critical phenomena. **Rev. Mod. Phys.**, American Physical Society, v. 49, p. 435–479, Jul 1977. Cited 2 times on pages 22 and 23.

HOROWITZ, G. T.; HUBENY, V. E. Quasinormal modes of AdS black holes and the approach to thermal equilibrium. **Phys. Rev.**, D62, p. 024027, 2000. Cited 2 times on pages 21 and 84.

HUANG, X.-G.; SEDRAKIAN, A.; RISCHKE, D. H. Kubo formulae for relativistic fluids in strong magnetic fields. **Annals Phys.**, v. 326, p. 3075–3094, 2011. Cited 3 times on pages 20, 63, and 64.

IQBAL, N.; LIU, H. Universality of the hydrodynamic limit in AdS/CFT and the membrane paradigm. **Phys. Rev.**, D79, p. 025023, 2009. Cited 4 times on pages 20, 62, 88, and 89.

JAIN, S. et al. A Strongly Coupled Anisotropic Fluid From Dilaton Driven Holography. **JHEP**, v. 01, p. 005, 2015. Cited 2 times on pages 20 and 64.

JANIK, R. A.; JANKOWSKI, J.; SOLTANPANAHI, H. Non-equilibrium dynamics and phase transitions. **Phys. Rev. Lett.**, v. 117, n. 9, p. 091603, 2016. Cited on page 21.

JANIK, R. A.; JANKOWSKI, J.; SOLTANPANAHI, H. Quasinormal modes and the phase structure of strongly coupled matter. **JHEP**, v. 06, p. 047, 2016. Cited on page 21.

JANIK, R. A. et al. Linearized nonequilibrium dynamics in nonconformal plasma. **Phys. Rev.**, D91, n. 12, p. 126013, 2015. Cited on page 84.

JANISZEWSKI, S.; KAMINSKI, M. Quasinormal modes of magnetic and electric black branes versus far from equilibrium anisotropic fluids. **Phys. Rev.**, D93, n. 2, p. 025006, 2016. Cited 3 times on pages 24, 72, and 102.

KAC, M. Can one hear the shape of a drum? **Am. Math. Mon.**, v. 73, p. 1–23, 1966. Cited on page 21.

KAPUSTA, J. I.; GALE, C. **Finite-temperature field theory: Principles and applications**. [S.l.]: Cambridge University Press, 2011. ISBN 9780521173223, 9780521820820, 9780511222801. Cited 2 times on pages 33 and 61.

KATS, Y.; PETROV, P. Effect of curvature squared corrections in AdS on the viscosity of the dual gauge theory. **JHEP**, v. 01, p. 044, 2009. Cited on page 20.

KHARZEEV, D. et al. Strongly Interacting Matter in Magnetic Fields. **Lect. Notes Phys.**, v. 871, p. pp.1–624, 2013. Cited on page 19.

KHARZEEV, D. E.; MCLERRAN, L. D.; WARRINGA, H. J. The Effects of topological charge change in heavy ion collisions: "Event by event P and CP violation". **Nucl. Phys.**, A803, p. 227–253, 2008. Cited on page 19.

KIRITSIS, E. **String theory in a nutshell**. [S.l.: s.n.], 2007. Cited 3 times on pages 39, 43, and 47.

KOKKOTAS, K. D.; SCHMIDT, B. G. Quasinormal modes of stars and black holes. **Living Rev. Rel.**, v. 2, p. 2, 1999. Cited on page 21.

KONOPLYA, R. A.; ZHIDENKO, A. Quasinormal modes of black holes: From astrophysics to string theory. **Rev. Mod. Phys.**, v. 83, p. 793–836, 2011. Cited on page 21.

KOVTUN, P.; SON, D. T.; STARINETS, A. O. Viscosity in strongly interacting quantum field theories from black hole physics. **Phys. Rev. Lett.**, v. 94, p. 111601, 2005. Cited 6 times on pages 19, 20, 32, 54, 62, and 88.

KOVTUN, P. K.; STARINETS, A. O. Quasinormal modes and holography. **Phys. Rev.**, D72, p. 086009, 2005. Cited 4 times on pages 21, 83, 93, and 94.

KRAUS, P.; LARSEN, F.; TRIVEDI, S. P. The Coulomb branch of gauge theory from rotating branes. **JHEP**, v. 03, p. 003, 1999. Cited 2 times on pages 23 and 73.

LANDAU, L. et al. **Course of Theoretical Physics: Theory of Elasticity**. Butterworth-Heinemann, 1986. v. 7. (Course of theoretical physics, v. 7). ISBN 9780750626330. Available at: <https://books.google.com.br/books?id=tpY-VkwCkAIC>. Cited 3 times on pages 20, 64, and 65.

LIFSHITZ, E.; PITAEVSKII, L. **Course of Theoretical Physics: Physical Kinetics**. Butterworth-Heinemann, 1981. v. 10. (Course of theoretical physics, v. 10). ISBN 9780750626354. Available at: <https://books.google.com.br/books?id=B2jGpmL5SxEC>. Cited 3 times on pages 20, 63, and 64.

LIGO SCIENTIFIC COLLABORATION AND VIRGO COLLABORATION. GW151226: Observation of Gravitational Waves from a 22-Solar-Mass Binary Black Hole Coalescence. **Phys. Rev. Lett.**, v. 116, n. 24, p. 241103, 2016. Cited on page 21.

LIGO SCIENTIFIC COLLABORATION AND VIRGO COLLABORATION. Observation of Gravitational Waves from a Binary Black Hole Merger. **Phys. Rev. Lett.**, v. 116, n. 6, p. 061102, 2016. Cited on page 21.

MAEDA, K.; NATSUUME, M.; OKAMURA, T. Dynamic critical phenomena in the AdS/CFT duality. **Phys. Rev.**, D78, p. 106007, 2008. Cited 2 times on pages 23 and 77.

MALDACENA, J. M. The Large N limit of superconformal field theories and supergravity. **Int. J. Theor. Phys.**, v. 38, p. 1113–1133, 1999. [Adv. Theor. Math. Phys.2,231(1998)]. Cited 3 times on pages 19, 21, and 32.

MATEOS, D.; TRANCANELLI, D. The anisotropic $\mathcal{N} = 4$ super Yang-Mills plasma and its instabilities. **Phys. Rev. Lett.**, v. 107, p. 101601, 2011. Cited 2 times on pages 20 and 101.

MEYER, H. B. A Calculation of the shear viscosity in SU(3) gluodynamics. **Phys. Rev.**, D76, p. 101701, 2007. Cited on page 19.

MEYER, H. B. Transport Properties of the Quark-Gluon Plasma: A Lattice QCD Perspective. **Eur. Phys. J.**, A47, p. 86, 2011. Cited on page 32.

MYERS, R. C.; TAFJORD, O. Superstars and giant gravitons. **JHEP**, v. 11, p. 009, 2001. Cited on page 75.

NASTASE, H. **Introduction to the ADS/CFT Correspondence**. Cambridge: Cambridge University Press, 2015. ISBN 9781107085855. Cited 2 times on pages 24 and 39.

NATIONAL AERONAUTICS AND SPACE ADMINISTRATION/WILKINSON MICROWAVE ANISOTROPY PROBE SCIENCE TEAM. **WMAP results**. 2013. Available at: <https://map.gsfc.nasa.gov/news/index.html>. Cited on page 25.

NATSUUME, M. AdS/CFT Duality User Guide. **Lect. Notes Phys.**, v. 903, p. pp.1–294, 2015. Cited on page 50.

NATSUUME, M.; OHTA, M. The Shear viscosity of holographic superfluids. **Prog. Theor. Phys.**, v. 124, p. 931–951, 2010. Cited on page 20.

NATSUUME, M.; OKAMURA, T. Dynamic universality class of large-N gauge theories. **Phys. Rev.**, D83, p. 046008, 2011. Cited on page 23.

NOLLERT, H.-P. TOPICAL REVIEW: Quasinormal modes: the characteristic "sound" of black holes and neutron stars. **Class. Quant. Grav.**, v. 16, p. R159–R216, 1999. Cited on page 21.

NORONHA-HOSTLER, J. et al. Bulk Viscosity Effects in Event-by-Event Relativistic Hydrodynamics. **Phys. Rev.**, C88, n. 4, p. 044916, 2013. Cited on page 19.

NORONHA-HOSTLER, J.; NORONHA, J.; GRASSI, F. Bulk viscosity-driven suppression of shear viscosity effects on the flow harmonics at energies available at the BNL Relativistic Heavy Ion Collider. **Phys. Rev.**, C90, n. 3, p. 034907, 2014. Cited on page 19.

NORONHA-HOSTLER, J.; NORONHA, J.; GREINER, C. Transport Coefficients of Hadronic Matter near T_c. **Phys. Rev. Lett.**, v. 103, p. 172302, 2009. Cited on page 19.

NORONHA-HOSTLER, J.; NORONHA, J.; GREINER, C. Hadron Mass Spectrum and the Shear Viscosity to Entropy Density Ratio of Hot Hadronic Matter. **Phys. Rev.**, C86, p. 024913, 2012. Cited on page 19.

NORONHA, J. Connecting Polyakov Loops to the Thermodynamics of SU(N_c) Gauge Theories Using the Gauge-String Duality. **Phys. Rev.**, D81, p. 045011, 2010. Cited on page 101.

NORONHA, J.; DENICOL, G. S. Transient Fluid Dynamics of the Quark-Gluon Plasma According to AdS/CFT. 2011. Available at: <https://arxiv.org/abs/1104.2415>. Cited on page 96.

OZVENCHUK, V. et al. Shear and bulk viscosities of strongly interacting "infinite" parton-hadron matter within the parton-hadron-string dynamics transport approach. **Phys. Rev.**, C87, n. 6, p. 064903, 2013. Cited on page 19.

PARTICLE DATA GROUP. Review of Particle Physics (RPP). **Phys. Rev.**, D86, p. 010001, 2012. Cited on page 27.

PESKIN, M. E.; SCHROEDER, D. V. **An Introduction to quantum field theory**. [s.n.], 1995. ISBN 9780201503975, 0201503972. Available at: <http://www.slac.stanford.edu/spires/find/books/www?cl=QC174.45%3AP4>. Cited 6 times on pages 25, 26, 27, 28, 29, and 37.

PHENIX COLLABORATION. Formation of dense partonic matter in relativistic nucleus-nucleus collisions at RHIC: Experimental evaluation by the PHENIX collaboration. **Nucl. Phys.**, A757, p. 184–283, 2005. Cited on page 19.

PHOBOS COLLABORATION. The PHOBOS perspective on discoveries at RHIC. **Nucl. Phys.**, A757, p. 28–101, 2005. Cited on page 19.

POLICASTRO, G.; SON, D. T.; STARINETS, A. O. The Shear viscosity of strongly coupled $\mathcal{N} = 4$ supersymmetric Yang-Mills plasma. **Phys. Rev. Lett.**, v. 87, p. 081601, 2001. Cited 3 times on pages 19, 32, and 62.

RAMALLO, A. V. Introduction to the AdS/CFT correspondence. **Springer Proc. Phys.**, v. 161, p. 411–474, 2015. Cited 3 times on pages 38, 49, and 88.

REBHAN, A.; STEINEDER, D. Violation of the Holographic Viscosity Bound in a Strongly Coupled Anisotropic Plasma. **Phys. Rev. Lett.**, v. 108, p. 021601, 2012. Cited 2 times on pages 20 and 101.

RISCHKE, D. H. The Quark gluon plasma in equilibrium. **Prog. Part. Nucl. Phys.**, v. 52, p. 197–296, 2004. Cited on page 31.

ROUGEMONT, R. Holographic black hole engineering at finite baryon chemical potential. In: **Hot Quarks 2016: Workshop for Young Scientists on the Physics of Ultrarelativistic Nucleus-Nucleus Collisions (HQ2016) South Padre Island, Texas, September 12-17, 2016**. [s.n.], 2016. Available at: <http://inspirehep.net/record/1492750/files/arXiv:1610.06124.pdf>. Cited on page 23.

ROUGEMONT, R.; CRITELLI, R.; NORONHA, J. Holographic calculation of the QCD crossover temperature in a magnetic field. **Phys. Rev.**, D93, n. 4, p. 045013, 2016. Cited on page 103.

ROUGEMONT, R. et al. Energy loss, equilibration, and thermodynamics of a baryon rich strongly coupled quark-gluon plasma. **JHEP**, v. 04, p. 102, 2016. Cited 6 times on pages 22, 23, 83, 84, 102, and 103.

ROUGEMONT, R.; NORONHA, J.; NORONHA-HOSTLER, J. Suppression of baryon diffusion and transport in a baryon rich strongly coupled quark-gluon plasma. **Phys. Rev. Lett.**, v. 115, n. 20, p. 202301, 2015. Cited 3 times on pages 23, 102, and 103.

RYU, S. et al. Importance of the Bulk Viscosity of QCD in Ultrarelativistic Heavy-Ion Collisions. **Phys. Rev. Lett.**, v. 115, n. 13, p. 132301, 2015. Cited on page 19.

SHOVKOVY, I. A. Magnetic Catalysis: A Review. **Lect. Notes Phys.**, v. 871, p. 13–49, 2013. Cited on page 59.

SKOKOV, V.; ILLARIONOV, A. Yu.; TONEEV, V. Estimate of the magnetic field strength in heavy-ion collisions. **Int. J. Mod. Phys.**, A24, p. 5925–5932, 2009. Cited on page 19.

SON, D. T.; STARINETS, A. O. Minkowski space correlators in AdS / CFT correspondence: Recipe and applications. **JHEP**, v. 09, p. 042, 2002. Cited 4 times on pages 62, 70, 80, and 88.

STAR COLLABORATION. Experimental and theoretical challenges in the search for the quark gluon plasma: The STAR Collaboration's critical assessment of the evidence from RHIC collisions. **Nucl. Phys.**, A757, p. 102–183, 2005. Cited on page 19.

STARINETS, A. O. Quasinormal modes of near extremal black branes. **Phys. Rev.**, D66, p. 124013, 2002. Cited 2 times on pages 21 and 79.

TEANEY, D. Finite temperature spectral densities of momentum and R-charge correlators in $\mathcal{N} = 4$ Yang Mills theory. **Phys. Rev.**, D74, p. 045025, 2006. Cited on page 90.

THORNE, K.; PRICE, R.; MACDONALD, D. **Black Holes: The Membrane Paradigm**. Yale University Press, 1986. (Silliman Memorial Lectures). ISBN 9780300037708. Available at: <https://books.google.com.br/books?id=T94hD5rR8oYC>. Cited 2 times on pages 20 and 49.

TISSEUR, F.; MEERBERGEN, K. The Quadratic Eigenvalue Problem. **SIAM Rev.**, v. 43(2), p. 235–286, 2001. Cited on page 81.

TUCHIN, K. On viscous flow and azimuthal anisotropy of quark-gluon plasma in strong magnetic field. **J. Phys.**, G39, p. 025010, 2012. Cited on page 20.

TUCHIN, K. Particle production in strong electromagnetic fields in relativistic heavy-ion collisions. **Adv. High Energy Phys.**, v. 2013, p. 490495, 2013. Cited on page 19.

VISHVESHWARA, C. V. Scattering of Gravitational Radiation by a Schwarzschild Black-hole. **Nature**, v. 227, p. 936–938, 1970. Cited on page 21.

WEINBERG, S. **Cosmology**. [s.n.], 2008. ISBN 9780198526827. Available at: <http://www.oup.com/uk/catalogue/?ci=9780198526827>. Cited 2 times on pages 25 and 30.

WIKIPEDIA. **Standard Model of Elementary Particles**. 2013. First version by user "MissMJ", 2006. Current version by user "Cush" — Own work by uploader, Public Domain. Available at: <https://commons.wikimedia.org/w/index.php?curid=4286964>. Cited on page 27.

WIKIPEDIA. **Elementary particle interactions in the Standard Model**. 2014. First version by user "Eric Drexler", 2014. Current version by user "Eric Drexler" — Own work, Public Domain. Available at: <https://commons.wikimedia.org/w/index.php?curid=32230766>. Cited on page 27.

WILKINSON MICROWAVE ANISOTROPY PROBE. Nine-year Wilkinson Microwave Anisotropy Probe (WMAP) observations: Final maps and results. **The Astrophysical Journal Supplement Series**, v. 208, n. 2, p. 20, 2013. Available at: <http://stacks.iop.org/0067-0049/208/i=2/a=20>. Cited on page 25.

WITTEN, E. Anti-de Sitter space and holography. **Adv. Theor. Math. Phys.**, v. 2, p. 253–291, 1998. Cited 3 times on pages 19, 21, and 32.

WITTEN, E. Anti-de Sitter space, thermal phase transition, and confinement in gauge theories. **Adv. Theor. Math. Phys.**, v. 2, p. 505–532, 1998. Cited on page 21.

WOLFRAM Mathematica, version 11. Wolfram Research, 2016. Available at: <https://www.wolfram.com/mathematica/>. Cited on page 83.

XU, Z.; GREINER, C. Shear viscosity in a gluon gas. **Phys. Rev. Lett.**, v. 100, p. 172301, 2008. Cited on page 19.

YAFFE, L. G. **Mathematica Summer School on Theoretical Physics**: Mathematica notebook for days 1-2. 2014. Available at: <http://msstp.org/?q=node/289>. Cited 2 times on pages 79 and 83.

ZAANEN, J. et al. **Holographic Duality in Condensed Matter Physics**. Cambridge Univ. Press, 2015. ISBN 9781107080089. Available at: <http://www.cambridge.org/mw/academic/subjects/physics/condensed-matter-physics-nanoscience-and-mesoscopic-physics/holographic-duality-condensed-matter-physics?format=HB>. Cited on page 49.